A Study on
Dynamical Properties of the Force Exerted by Lamellipodia and Filopodia using Optical Tweezers

Thesis submitted for the degree of
"*Doctor Philosophiæ*"

S.I.S.S.A. - I.S.A.S.

Neurobiology Sector

CANDIDATE
Mr. Rajesh Shahapure

SUPERVISOR
Prof. Vincent Torre

SISSA, Via Beirut 2-4, 34014 TRIESTE, ITALY

Dedicated to my Parents

This thesis led to following published and unpublished articles

1. Properties of the Force Exerted by Filopodia and Lamellipodia and the Involvement of Cytoskeletal Components
   Cojoc D*, Difato F*, Ferrari E*, Shahapure RB*, Laishram J, Righi M, Di Fabrizio E, Torre V.
   PLoS ONE 2(10), 24th October 2007.
   (***** Equally contributed)

2. Force Generation in Lamellipodia is a Probabilistic Process with Fast Growth and Retraction Events
   Shahapure R., Difato F., Laio, A., Cojoc D., Ferrari E. , Laishram J., Bisson G. & Torre V.
   (submitted)

3. Detection and Characterization of Discrete Events Underlying Force Generation in Lamellipodia of Dorsal Root Ganglia Neurons
   Shahapure R., Ercolini E., Amin L., Laio, A. Bisson G.1 & Torre V.
   (Draft in preparation)

1. Abstract 1

2. Introduction.....3

2.1. Neuronal growth cone.....3

2.1.1. Structure of growth cone…….……..3
2.1.2. Cytoskeleton function in growth cone guidance and advancement…….....6
2.1.3. Proteins regulating actin dynamics…….…....8

2.2. Force measurement in biological systems.....10

2.2.1. Force generation by actin polymerization 10
2.2.2. Theorotical models for generation by actin polymerization……..……11
2.2.2.1. Rachet models.....12
2.2.2.2. Autocatalytic models.....13
2.2.3. Force-Velocity (Fv) relationship.....14
2.2.4. Fv relationship *in vitro*.....15
References.....17

3. Material and methods.....20

3.1. Optical Tweezers.....20

3.1.1. An introduction to optical trapping.....20
3.1.2. Experimental set-up used in this project.....22
3.1.3. Position detection …….....24
3.1.4. Trapping Force calibration.....26
3.1.4.1. Equipartition method.....27
3.1.4.2. Power spectrum method.....27
3.1.4.3. Drag force method.....29
3.1.5. Biological applications of optical tweezers.....30
References.....32

4. Results.....35

4.1. Properties of the force exerted by filopodia and lamellipodia
and the involvement of cytoskeletal components ……..……..…..36
4.2. Force generation in lamellipodia is a probabilistic process
with fast growth and retraction events……..….44
4.3. Detection and Characterization of discrete events underlying
force generation in lamellipodia of Dorsal Root Ganglia Neurons…….……...65

5. Discussion and Conclusions.....84

References.....88

6. Acknowledgements…..…….....90

1 Abstract

During neuronal differentiation, lamellipodia and filopodia explore the environment in search for the correct path to the axon's final destination. Although the motion of lamellipodia and filopodia has been characterized to an extent, little is known about the force they exert. In this study, we used optical tweezers to measure the force exerted by filopodia and lamellipodia of dorsal root ganglia (DRG) neurons.

The first part of this thesis examines the properties of the force exerted by filopodia and lamellipodia and the involvement of cytoskeletal components. I have found that single filopodium exerts a maximum force of 3 pN, whereas lamellipodia can exert a force up to 20 pN. Using metabolic inhibitors, I have shown that no force is produced in the absence of actin polymerization and that development of forces larger than 3 pN requires microtubule polymerization. These results show that actin polymerization is necessary for force production and demonstrate that not only do neurons process information, but they also act on their environment exerting forces varying from tenths pN to tens of pN.

In the second part, dynamical properties of force generation in growth cone lamellipodia are presented. Using optical tweezers, the force-velocity (Fv) relationship and the power dissipated by lamellipodia, is measured with millisecond temporal resolution and piconewton sensitivity. When force and velocity are averaged over 3-5 s, the Fv relationships can be flat. On a finer time scale, random occurrence of fast growths and sub-second retractions become predominant. Maximal power dissipated by lamellipodia over a silica bead with a diameter of 1 μm is 10^{-16} W. The results clarify the dynamical properties of force generation: i) force generation is a probabilistic process; ii) underlying biological events have a bandwidth up to at least 10 Hz; iii) fast growths of lamellipodia leading edge alternate with local retractions.

The third part of my thesis presents preliminary results describing the molecular mechanisms by which lamellipodia generate a force on encountered obstacles such as silica beads. Optically trapped bead seals to the membrane of lamellipodium due to adhesion forces, leading to reduction in the amplitude of Brownian fluctuations often by more than 10 times. Under these conditions, when the lamellipodium grows and pushes

the bead, fluctuations of bead position increase, resulting in discrete jumps varying from ~5 to 50 nm. When the lamellipodium retracts, pulling the beads with it, no discrete events are observed. These discrete events are not observed in the presence of Latrunculin A, a blocker of actin polymerization. These jumps could be the elementary events underlying force generation in lamellipodia.

2 Introduction

Understanding the dynamics of force generation in growth cone is the main objective of the present work. In this chapter, initially I describe growth cone's structural elements and its molecular constitution. Then I discuss the role of growth cone's individual structural parts in the motility and in advancement of neurite. Finally, theoretical models proposed for force generation in biological systems are presented in the light of force measurements performed in vitro.

2.1 Neuronal growth cone

The growing tip of the neurite, the growth cone, plays a critical role in the formation of appropriate neuronal connections. Growth cone seeks out and connects to the potential target cells during development. Actively exploring tip of neurite explores the surroundings and respond to different chemical cues in the vicinity. Ramon y Cajal observed these expanded tips for the first time in Golgi preparations in 1890 and named it "cone d'accroissement" or growth cone. He later described its activities: "From the functional point of view, the growth cone may be regarded as a sort of club or battering ram, endowed with exquisite chemical sensitivity, with rapid ameboid movements and with certain impulsive force, thanks to which it is able to proceed forward and overcome obstacles met in its way, forcing cellular interstices until it arrives at its destination" (Landis, 1983).

2.1.1 Structure of growth cone

Structurally, the growth cone can be divided into three different domains namely peripheral, transition, and central domain (Figure 2.1).

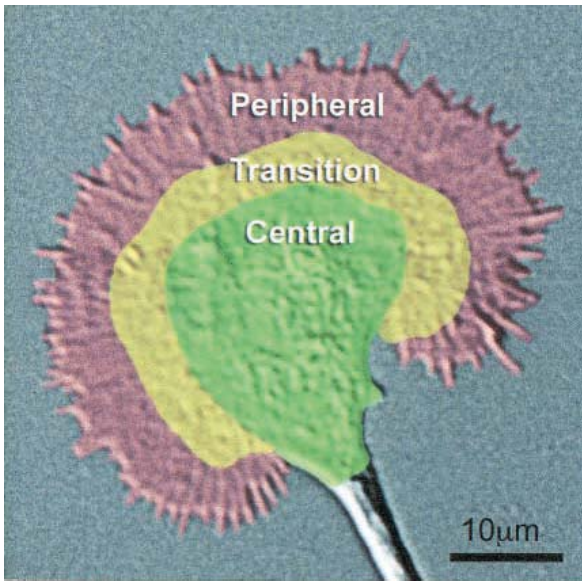

Figure 2.1. Large paused cortical growth cone imaged in differential interference contrast microscopy. The central, transition, and peripheral regions of the growth cone are indicated in green, yellow, and pink, respectively. Note the presence of organelles in the dense central region and the thin lamellipodial veil and spiky filopodia in the peripheral region. Adapted from (Dent et al., 2003).

At the peripheral domain, actin monomers are polymerized into filaments building the dense sheet-like actin meshwork called lamellipodium and small spike-like structures of actin bundles called as filopodia (Figure 2.2). Growth cone motility and guidance behaviors that cause the axon to advance, retract, turn and branch are regulated by reorganization and dynamics of the actin and microtubule cytoskeleton located in the growth cone (Dent and Gertler, 2003). The central region of the growth cone contains bundled microtubules, and the periphery is dominated by actin filaments that form both a meshwork in veil-like lamellipodia and bundles in fingerlike-like filopodia (Figure 2.2). Filopodia play an important role in sensing guidance cues and steering the growth cone while lamellipodia are responsible for the advancement of the growth cone.

Although actin filaments are primarily present in the peripheral region of growth cone and microtubules predominate in the central region, these two cytoskeletal elements extensively overlap in the transition region of the growth cone between the central domain and the periphery (Figure 2.1 and 2.2). Recent studies have shown that microtubules do not always remain confined to the central region but frequently penetrate

into the peripheral region of the growth cone and even invade filopodia, getting aligned with actin filament bundles (Dent and Kalil, 2001;Schaefer et al., 2002).

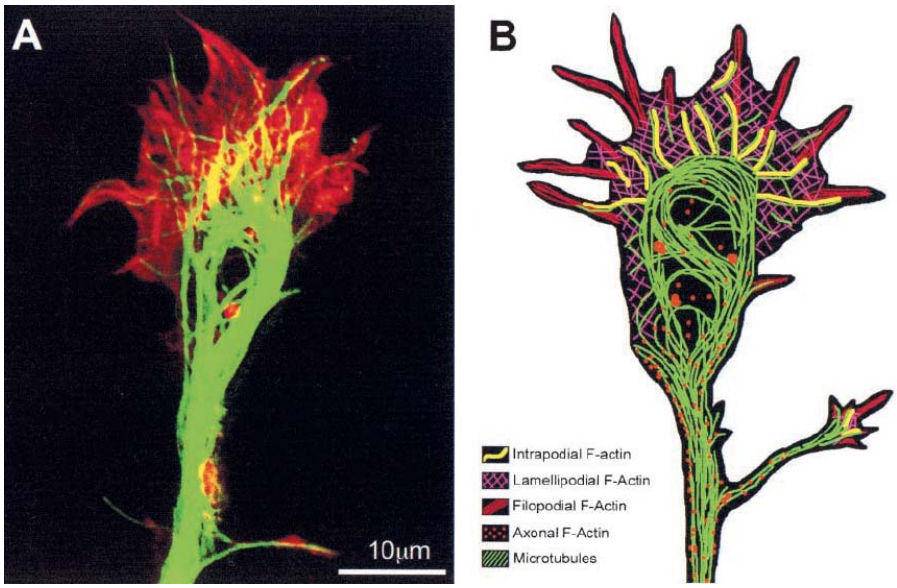

Figure 2.2. Actin filaments and microtubules localization in a large paused cortical growth cone. (A) A fixed growth cone has been stained with phalloidin and antibodies to tubulin in order to fluorescently label F-actin (pseudocolored red) and microtubules (pseudocolored green), respectively. Microtubules are bundled together in the axon shaft and form a prominent loop in the central region of the growth cone. They also extend out into the periphery where they overlap (pseudocolored yellow) with F-actin. (B) A sketch illustrates locations of different populations of actin filaments and microtubules. Microtubules (green) are located in the shaft of the axon and its branch and in the central region of the growth cone but also extend into the lamellipodium and Filopodia .F-actin forms dot-like structures in the axon shaft and central region of the growth cone, a meshwork in the lamellipodium, and straight bundles in filopodia. Adapted from (Dent and Kalil, 2001).

Both microtubules and actin filaments are highly dynamic structures in the growth cone. Through continuous polymerization and depolymerization processes they undergoing cycles of growth and shrinkage respectively. Moreover, actin filaments and microtubules can move and undergo dramatic changes in their organization and location within the growth cone. The actin filaments observed closely apposed to microtubules in the growth cone transition region (Figure 2.2 B) are also actin-based protrusive structures called as intrapodia, previously reported in growth cones of sympathetic neurons (Rochlin et al., 1999). Interactions between actin filaments and microtubules involve their coordinated polymerization and depolymerization (Dent and Kalil, 2001). Thus, proper

interplay between actin and microtubule is essential for initiating axon growth and navigation of growth cone leading axon to proper target.

2.1.2 Cytoskeleton function in growth cone guidance and advancement

In this work, by using optical tweezers, we have measured the force exerted by growth cone filopodia and lamellipodia with millisecond temporal resolution and Piconewton force sensitivity. Detailed analysis of these measurements enabled us to understand the dynamical properties of force generation. Also in order to understand the involvement of individual cytoskeletal components, we have studied the effect of different cytoskeleton blocking agents on force exerted by growth cone. In this section, the role of individual cytoskeletal element in growth cone motility and guidance is briefly discussed.

The cytoskeleton plays a major role in virtually every cell biological process in eukaryotes, from cell division and cell motility to the intracellular trafficking of organelles. In the nervous system, the cytoskeleton plays an important part in axon and dendrite formation, which allows neurons to establish their exquisite and complex morphology. The cytoskeleton also helps in the wiring of neural circuitry by driving both the guidance of neuronal processes and the formation of synapses, which are the sites of inter-neuronal communication.

Generally, cytoskeleton network is composed principally of three types of protein filaments- actin, microtubules, and intermediate filaments but, in peripheral domain of growth cones actin filaments and microtubules are predominantly present, each of which possesses unique biophysical and biochemical properties (Dent and Gertler, 2003).

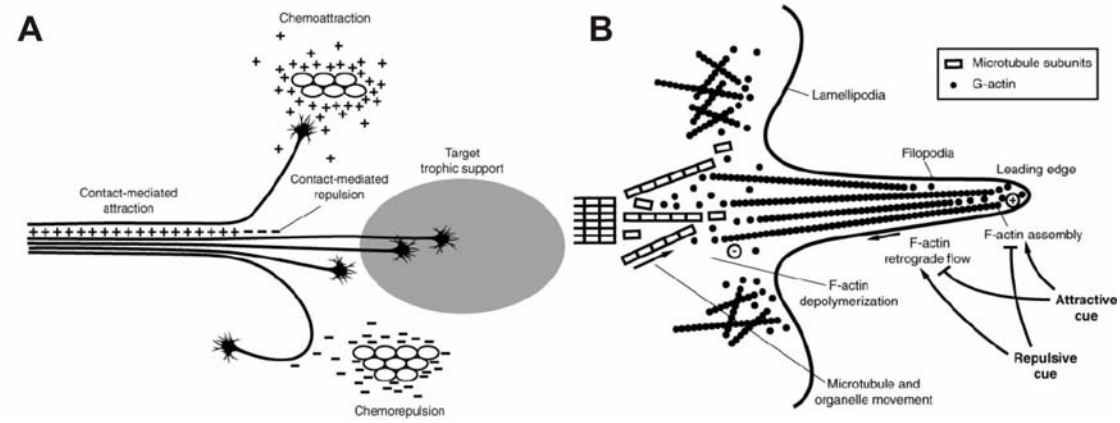

Figure 2.3. Growing axons respond to guidance cues in the extracellular milieu. **(A)** Axon growth, fasciculation, and steering are regulated by a wide range of attractive or repulsive axon guidance cues that can act over short or long distances. **(B)** The growth cone detects and responds to axon guidance cues. The lamellipodia contain cross-linked F-actin filaments. The filopodia extend and retract through regulation of the rates of actin polymerization and depolymerization at the plus (+) and minus (-) ends of actin filaments, respectively, and of F-actin retrograde flow. Repulsive and attractive cues influence growth cone morphology by regulating these processes. Adapted from (Huber et al., 2003).

Neurites form appropriate connections guided by variety of diffusible and surface-bound extracellular cues (Figure 2.3A). The motile growth cone present at the tip of neurites sense spatially and temporally distributed guidance signals that direct the growth cone to turn toward (attraction) or away from (repulsion) the guidance source to reach their targets (Figure 2.3B) (Tessier-Lavigne and Goodman, 1996). Receptors present on the growth cone surface are activated by guidance molecules, which induces a cascade of localized intracellular signaling events that steers the growth cone. In nerve growth cones, actin and microtubules are the cytoskeletal components responsible for locomotion and are the ultimate targets of signaling molecules.

At the leading edge kinetic force necessary for growth cone motility is generated as result of systematic interplay between various processes like actin-based protrusive activity coupled with retrograde actin flow from peripheral to central domain and attachment of the actin network to the membrane and substrate (Lin et al., 1994;Suter and Forscher, 2000). Microtubules are bundled together in the axonal shaft and central region (Figure 2.2) of the growth cone, whereas individual microtubules extend and occasionally invade the actin-rich peripheral area of growth cone, where they exhibit dynamic instability with characteristic rapid growth and shrinkage (Tanaka and Kirschner, 1991).

Although both cytoskeletal components are essential for growth cone motility, actin cytoskeleton is principally responsible for initiating and directing growth cone steering, whereas microtubules consolidate and support the new extension initiated by already protruded by actin (Smith, 1988;Mitchison and Kirschner, 1988).

Thus actin filaments play a central part in cell motility (Pollard and Borisy, 2003) and are well positioned at the leading edge of the growth cone to be the direct targets of guidance cues. Actin polymerization drives protrusion of the plasma membrane (Pantaloni et al., 2001;Pollard and Borisy, 2003), but how this leads to cell motility is still controversial. Different cell types have different strategies for moving and changing shape (Machesky, 2002) and accordingly they organize their actin filaments at leading edge (Bear et al., 2002). Actin filaments also draw the growth cone membrane rearward during retrograde actin flow and are involved in growth cone retraction. Steady state myosin-dependent retrograde flow occurs in both filopodia and lamellipodia (Lin and Forscher, 1995), and involves cycles of net assembly of actin filaments at the leading edge, retrograde movement of actin networks, and disassembly of filaments at their proximal end (Forscher and Smith, 1988). Retrograde actin flow regulate the rate of neurite outgrowth and avoid microtubules from entering into the peripheral domain of the growth cone (Zhou and Cohan, 2004).

2.1.3 Proteins regulating actin dynamics

Different proteins regulate actin dynamics at the leading edge of motile cells (Figure 2.4). In the case of growth cones, in response to external guidance cues, actin polymerization is stimulated by proteins such as profilin, Wasp, or Arp2/3, and actin crosslinking proteins such as filamin (Pollard and Borisy, 2003). Proteins such as cofilin and gelsolin depolymerize actin filament predominantly in the lamellipodium transition domain. In moving growth cones, the actin network moves centripetally backwards from the leading edge by retrograde flow (Forscher and Smith, 1988). Retrograde flow is driven by myosin motors and by actin assembly at the leading edge (Lin et al., 1996).

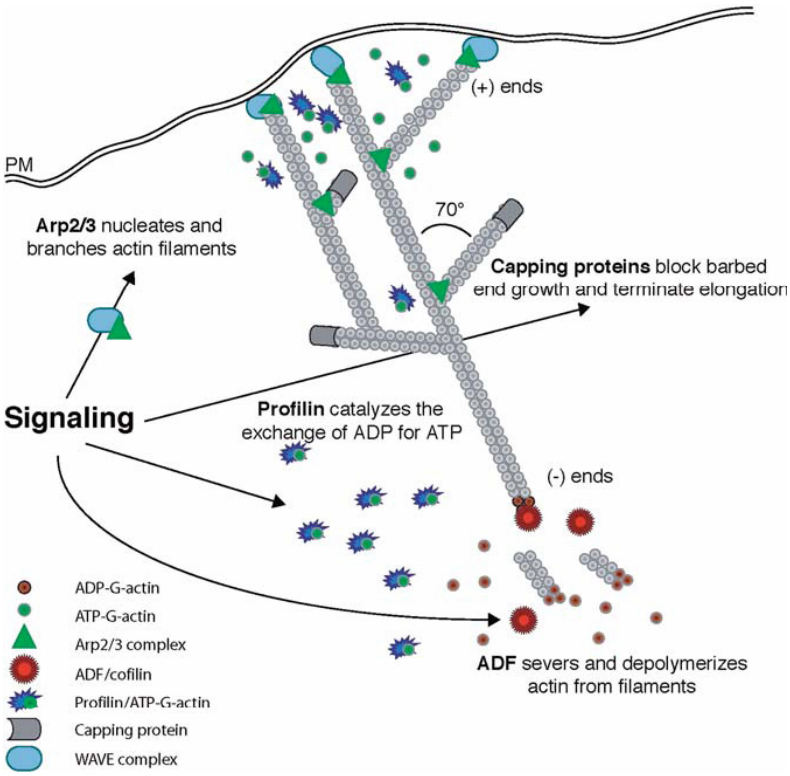

Figure 2.4. The actin polymerization machinery triggers dendritic nucleation for protrusion at the leading edge. The activated Arp2/3 complex nucleates and branches actin filaments at the leading edge, pushing the membrane forward. Capping proteins control the half-life of filaments, and by blocking a large fraction of barbed ends, promote site-directed elongation of uncapped filaments. ADF/cofilin promotes dissociation of ADP-actin from filament pointed ends and severs preexisting filaments, generating new barbed ends. Profilin catalyzes the exchange of ADP for ATP on monomeric actin molecules, which become available for new polymerization at barbed ends Adapted from (Disanza et al., 2005).

2.2 Force measurement in biological systems

In 1675 van Leeuwenhoek observed for the first time cells crawling across his microscope slide, but only recently the molecular mechanisms behind cell movement have become a scientific focus. Biophysical techniques like optical tweezers (which will be described in detail in next chapter), atomic force microscopy and magnetic tweezers helped identifying regions where different force generating proteins are located. There are reports in literature about, *in vitro* force measurements (Finer et al., 1994;Dogterom and Yurke, 1997;Theriot, 2000;Block et al., 2003;Parekh et al., 2005) and the forces associated with cell movement measured *in vivo* (Oliver et al., 1995;Brunner et al., 2006). Theoretical modeling is complementing experimental work and has helped quantifying how the proposed mechanisms and the forces generated at a molecular level are integrated to produce whole cell movement.

2.2.1 Force generation by actin polymerization

The propulsion of the leading edge is a multi-step, complex process (Pollard et al., 2000;Pollard and Borisy, 2003) but polymerization of actin filaments towards the cell membrane i.e. protrusion is a first step towards it. Polymerizing actin filaments alone, without any accompanying motors, can generate sufficient force to move leading edge of the cell.

Actin filaments are ~7 nm diameter, semi-flexible polymers with persistence length ~17 μm (Gittes et al., 1993). Actin filaments are made up of dimer pairs of globular actin monomers (length ~2.7 nm), and are functionally polar in nature (Figure 2.5). Each filament has two discrete ends: i -fast growing end called the plus end or barbed end and ii - slow growing end called the minus end or pointed end (Figure 2.5). Critical actin monomer concentration of the plus end of an actin filament is approximately six times less than that of minus end, when either of the ends is exposed to a concentration of monomeric actin that is greater than its critical concentration, the filament end binds monomers and grows by polymerization (Figure 2.5). On the contrary, while the monomer concentration is below the critical concentration, monomers detach from the filament end, and the filament depolymerizes (Figure 2.5). Basically by having

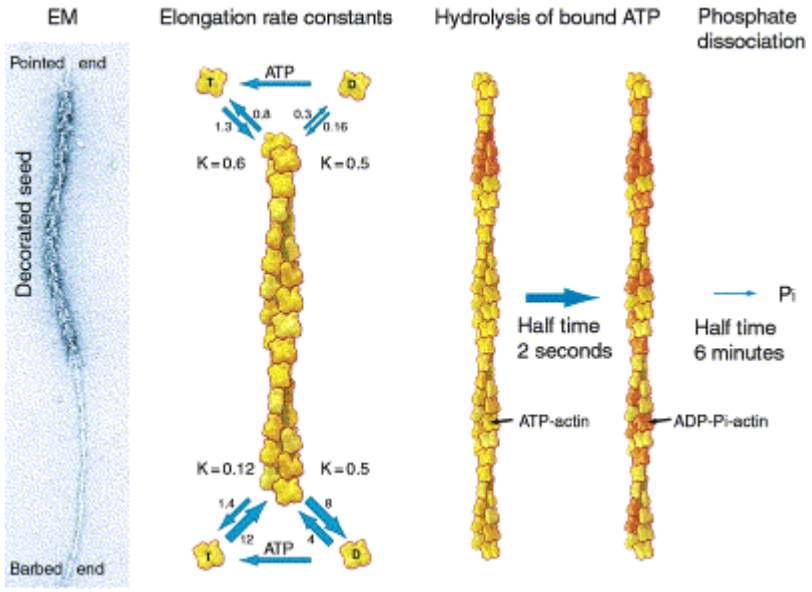

Figure 2.5. Actin Filament Elongation, ATP Hydrolysis, and Phosphate Dissociation The image shows an actin filament seed decorated with myosin heads and elongated with ATP-actin. The association rate constants have units of $\mu M^{-1}\ s^{-1}$. Dissociation rate constants have units of s^{-1}. The ratio of the dissociation rate constant to the association rate constant gives K, the dissociation equilibrium constant with units of μM. Note that the equilibrium constants for ATP-actin differ at the two ends, giving rise to slow steady state treadmilling. Hydrolysis of ATP bound to each subunit is fast, but dissociation of the γ phosphate is very slow. Adapted from (Pollard and Borisy, 2003).

these two different critical actin monomer concentrations at the opposing ends of the filament, actin filaments can grow asymmetrically, and when the concentration lies between the two values, only the plus end grows while the minus end shrinks. Thus, by the process of actin treadmilling length of the filament remains roughly constant and the net momentum is transferred forward to generate a force. Even though experimental progress towards quantifying these forces is quite slow, theoretical basis for understanding them is quite well developed.

2.2.2 Theoretical models for force generation by actin polymerization

Mainly two kinds of theoretical models have been proposed to explain force generation by actin polymerization: ratchet models (Figure 2.6) (Mogilner and Oster, 1996;Mogilner and Oster, 2003), and autocatalytic models (Carlsson, 2001;Carlsson, 2003).

2.2.2.1 Ratchet models

This model considers that cell membrane undergoes constant and random thermal fluctuations due to its microscopic size and relative flexibility. It assumes that, an actin filament is not an unbending rod that impedes growing once it reaches the membrane, but it is an elastic filament that can bend in response to the load. According to this model, if the bending of the filament away from the membrane is sufficiently large (angle > ~30°) and the filament is enough long (>~70 nm) but without buckling, an actin monomer (which is 2.7 nm in size) can easily insert itself between the filament and membrane (Mogilner and Oster, 1996;Mogilner and Oster, 2003). The extended filament consequently applies an elastic force on the membrane and moves it forward. Every addition of a monomer "ratchets" the membrane, preventing backward movement of the

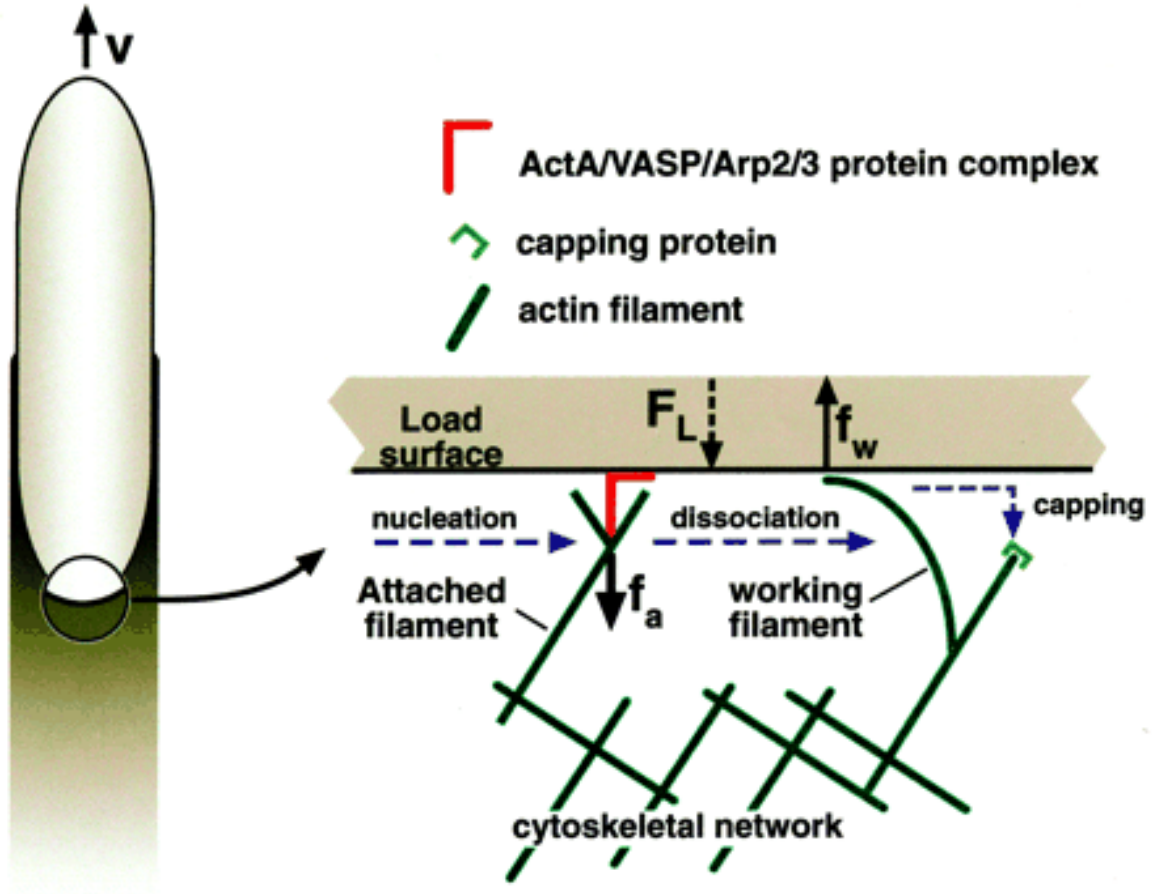

Figure 2.6. Sketch of the Ratchet model. Attached filaments (straight) are nucleated at rate n. They dissociate and become "working" filaments (bent). These, in turn, are capped at certain rate. The polymerization ratchet force generated by the working filaments is balanced by the force of attachment and load force. Adapted from (Mogilner and Oster, 2003).

membrane and only a net forward motion of the cell edge. This model, proposed to explain force generation by a single polymerizing actin filament, is called the elastic Brownian ratchet mode (Mogilner and Oster, 1996). An extension of this model is the tethered elastic Brownian ratchet model which includes the transient attachment of actin filaments to the membrane and considers two sets of filaments: working filaments, which are the filaments that are not attached to the membrane and can exert a force on it, and attached filaments, which cannot exert a force on the membrane (Figure 2.6) (Mogilner and Oster, 2003). Attached filaments could be converted into working filaments when they dissociate from the surface and working filaments could be converted to non working filaments when they are capped. Thu, tethered elastic Brownian ratchet model presume that new actin filaments/branches are generated independently of existing branches, and attempts to understand force generation from the group of actin filaments in the network.

2.2.2.2 Autocatalytic Models

Autocatalytic model also assumes that the load diffuses and that the probability of monomer addition to the tip of the polymer takes in to account Boltzmann factor (Carlsson, 2003). To understand the force generation by a network, two approaches have been used: stochastic simulations of an actin network growing against a load (Carlsson, 2003), and a deterministic approach that utilizes an explicit rate equation for filament orientation distribution (Carlsson, 2001). In both cases the main assumption that new actin branches are generated from existing branches, is different from the assumption made in the tethered elastic Brownian ratchet model. The transient attachment of actin filaments to the surface is not considered in either approaches of the autocatalytic model. The stochastic simulation predicts the dependence of growth velocity on capping rate and other parameters like, load force, and branching. The simulations show that, for a fixed actin concentration, the growth velocity has an inverse linear relation with the capping rate and equals zero when the number of branches is less than 1.5 (Carlsson, 2003). These simulations, however, could be performed only for a small parameter range that is computationally feasible. Hence, the deterministic model was developed to study a larger

parameter range and test the generality of the previous numerical results rigorously (Carlsson, 2001).

2.2.3 Force-Velocity (Fv) relationship

Experimentally verifiable and main prediction of above described models is the relation between the load (force) against which a polymerizing actin filament (or network) elongates and the filament's (or network's) resultant growth velocity.

For a single filament, the elastic Brownian ratchet model predicts an exponential force velocity relation (Mogilner and Oster, 1996):

$$V = V_{max}^{(-f\times\delta/k_BT)} - V_{dep},$$

Where V_{max} is the free polymerization velocity, f is the load force on a single filament, and V_{dep} is the depolymerization velocity. For a single filament, the autocatalytic model also predicts the same exponential force-velocity relation, given that the underlying basics of both models are the same (Carlsson, 2003).

Even if the single filament Fv relationships are similar for both type of models, the predicted Fv relationship for a network growing against a load are very different from the tethered elastic Brownian ratchet and the autocatalytic models. Probable reasons for these differences are:

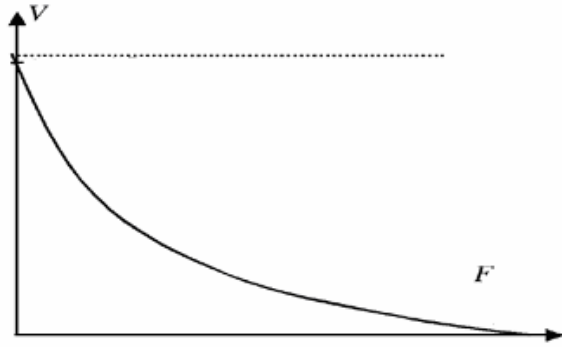

Figure 2.7. Fv relatioships predicted by the ratchet model (solid line) and autocatalytic branching model (dotted line).

1. In autocatalytic model all filaments are assumed to generate force to oppose the load force, whereas only the working filaments generate force (opposing the load

force and force from attached filaments) in the tethered elastic Brownian ratchet model.

2. New branches are generated only from existing branches in the autocatalytic model, while in case of tethered elastic Brownian ratchet model new branches are generated independent of existing branches.

The tethered elastic Brownian ratchet model predicts a biphasic force-velocity relation where the velocity decreases quickly for small forces and decreases gradually for high forces (Figure 2.7) (Mogilner and Oster, 1996). On the other hand, the autocatalytic model predicts that the actin network growth velocity is independent of the applied force (load), i.e $V=V_0$, the initial velocity, as explained in (Figure 2.7) (Carlsson, 2001;Carlsson, 2003). A qualitative explanation for the insensitivity of the velocity to the force in this model is that if the load increases, the number of filaments pushing the load also increases proportionately, leaving the force per filament and the growth velocity unchanged (Carlsson, 2001).

2.2.4 FV relationship *in vitro*

The FV relations for actin networks had been obtained *in vitro* with a pathogenic bacteria, *Listeria Monocytogens,* which is propelled by actin polymerization inside the host cell.

In the first study authors used increasing amounts of methylcellulose to slow *Listeria* velocity and computed the corresponding resistive force due to viscosity exerted on the body in each case with the Stokes Equation, knowing the viscosity of methylcelluose, the velocity of bacterial motion and the shape factor of the bacterium (McGrath et al., 2003). Quantitatively similar Fv relationship as proposed by the tethered elastic brownian ratchet model was obtained. In another similar study carried out with so called biomimetic system (spherical polystyrene bead coated with WASp on which an actin gel grows in the presence of other purified proteins) which also used varying amounts of methylcellulose to slow the bead velocity and computed the force acting on the bead with the Stokes Equation (Wiesner et al., 2003). In this case Fv relationship obtained supported the autocatalytic model. One reason for the different results of these

two similar in vitro experiments may be that only the analysis of Wiesner and coworkers (Wiesner et al., 2003) incorporates the impact of methylcellulose on the force-velocity curve other than due to its viscosity effect alone.

To better understand polymerization force, several other in vitro motility systems have also been designed. Neither model has been unambiguously favored as a result of these in vitro data. However, these studies still provide useful estimates of the polymerization forces such as the stall force of an actin filament, stall force of an actin network, the maximum propulsive force generated by an actin network in the given *in vitro* system and the contribution of each actin filament to the total force measured. They also help us begin understanding and investigating the polymerization mechanics operating *in vivo.*

References

1. Bear,J.E., T.M.Svitkina, M.Krause, D.A.Schafer, J.J.Loureiro, G.A.Strasser, I.V.Maly, O.Y.Chaga, J.A.Cooper, G.G.Borisy, and F.B.Gertler. 2002. Antagonism between Ena/VASP proteins and actin filament capping regulates fibroblast motility. *Cell* 109:509-521.

2. Block,S.M., C.L.Asbury, J.W.Shaevitz, and M.J.Lang. 2003. Probing the kinesin reaction cycle with a 2D optical force clamp. *Proceedings of the National Academy of Sciences of the United States of America* 100:2351-2356.

3. Brunner,C.A., A.Ehrlicher, B.Kohlstrunk, D.Knebel, J.A.Kas, and M.Goegler. 2006. Cell migration through small gaps. *European Biophysics Journal with Biophysics Letters* 35:713-719.

4. Carlsson,A.E. 2001. Growth of branched actin networks against obstacles. *Biophysical Journal* 81:1907-1923.

5. Carlsson,A.E. 2003. Growth velocities of branched actin networks. *Biophysical Journal* 84:2907-2918.

6. Dent,E.W. and F.B.Gertler. 2003. Cytoskeletal dynamics and transport in growth cone motility and axon guidance. *Neuron* 40:209-227.

7. Dent,E.W. and K.Kalil. 2001. Axon branching requires interactions between dynamic microtubules and actin filaments. *J. Neurosci.* 21:9757-9769.

8. Dent,E.W., F.J.Tang, and K.Kalil. 2003. Axon guidance by growth cones and branches: Common cytoskeletal and signaling mechanisms. *Neuroscientist* 9:343-353.

9. Disanza,A., A.Steffen, M.Hertzog, E.Frittoli, K.Rottner, and G.Scita. 2005. Actin polymerization machinery: the finish line of signaling networks, the starting point of cellular movement. *Cellular and Molecular Life Sciences* 62:955-970.

10. Dogterom,M. and B.Yurke. 1997. Measurement of the force-velocity relation for growing microtubules. *Science* 278:856-860.

11. Finer,J.T., R.M.Simmons, and J.A.Spudich. 1994. Single Myosin Molecule Mechanics - Piconewton Forces and Nanometer Steps. *Nature* 368:113-119.

12. Forscher,P. and S.J.Smith. 1988. Actions of Cytochalasins on the Organization of Actin-Filaments and Microtubules in A Neuronal Growth Cone. *Journal of Cell Biology* 107:1505-1516.

13. Gittes,F., B.Mickey, J.Nettleton, and J.Howard. 1993. Flexural Rigidity of Microtubules and Actin-Filaments Measured from Thermal Fluctuations in Shape. *Journal of Cell Biology* 120:923-934.

14. Huber,A.B., A.L.Kolodkin, D.D.Ginty, and J.F.Cloutier. 2003. Signaling at the growth cone: Ligand-receptor complexes and the control of axon growth and guidance. *Annual Review of Neuroscience* 26:509-563.

15. Landis,S.C. 1983. Neuronal growth cones. *Annu. Rev. Physiol* 45:567-580.

16. Lin,C.H., E.M.Espreafico, M.S.Mooseker, and P.Forscher. 1996. Myosin drives retrograde F-actin flow in neuronal growth cones. *Neuron* 16:769-782.

17. Lin,C.H. and P.Forscher. 1995. Growth Cone Advance Is Inversely Proportional to Retrograde F-Actin Flow. *Neuron* 14:763-771.

18. Lin,C.H., C.A.Thompson, and P.Forscher. 1994. Cytoskeletal reorganization underlying growth cone motility. *Curr. Opin. Neurobiol.* 4:640-647.

19. Machesky,L.M. 2002. Cell motility - Sharks' teeth and dunes. *Nature* 417:494-+.

20. McGrath,J.L., N.J.Eungdamrong, C.I.Fisher, F.Peng, L.Mahadevan, T.J.Mitchison, and S.C.Kuo. 2003. The force-velocity relationship for the actin-based motility of Listeria monocytogenes. *Current Biology* 13:329-332.

21. Mitchison,T. and M.Kirschner. 1988. Cytoskeletal dynamics and nerve growth. *Neuron* 1:761-772.

22. Mogilner,A. and G.Oster. 1996. Cell motility driven by actin polymerization. *Biophys. J.* 71:3030-3045.

23. Mogilner,A. and G.Oster. 2003. Force generation by actin polymerization II: the elastic ratchet and tethered filaments. *Biophys. J.* 84:1591-1605.

24. Oliver,T., M.Dembo, and K.Jacobson. 1995. Traction forces in locomoting cells. *Cell Motil. Cytoskeleton* 31:225-240.

25. Pantaloni,D., C.Le Clainche, and M.F.Carlier. 2001. Mechanism of actin-based motility. *Science* 292:1502-1506.

26. Parekh,S.H., O.Chaudhuri, J.A.Theriot, and D.A.Fletcher. 2005. Loading history determines the velocity of actin-network growth. *Nat. Cell Biol.* 7:1219-1223.

27. Pollard,T.D., L.Blanchoin, and R.D.Mullins. 2000. Molecular mechanisms controlling actin filament dynamics in nonmuscle cells. *Annu. Rev. Biophys. Biomol. Struct.* 29:545-576.

28. Pollard,T.D. and G.G.Borisy. 2003. Cellular motility driven by assembly and disassembly of actin filaments. *Cell* 112:453-465.

29. Rochlin,M.W., M.E.Dailey, and P.C.Bridgman. 1999. Polymerizing microtubules activate site-directed F-actin assembly in nerve growth cones. *Mol. Biol. Cell* 10:2309-2327.

30. Schaefer,A.W., N.Kabir, and P.Forscher. 2002. Filopodia and actin arcs guide the assembly and transport of two populations of microtubules with unique dynamic parameters in neuronal growth cones. *J. Cell Biol.* 158:139-152.

31. Smith,S.J. 1988. Neuronal Cytomechanics - the Actin-Based Motility of Growth Cones. *Science* 242:708-715.

32. Suter,D.M. and P.Forscher. 2000. Substrate-cytoskeletal coupling as a mechanism for the regulation of growth cone motility and guidance. *J. Neurobiol.* 44:97-113.

33. Tanaka,E.M. and M.W.Kirschner. 1991. Microtubule Behavior in the Growth Cones of Living Neurons During Axon Elongation. *Journal of Cell Biology* 115:345-363.

34. Tessier-Lavigne,M. and C.S.Goodman. 1996. The molecular biology of axon guidance. *Science* 274:1123-1133.

35. Theriot,J.A. 2000. The polymerization motor. *Traffic.* 1:19-28.

36. Wiesner,S., E.Helfer, D.Didry, G.Ducouret, F.Lafuma, M.F.Carlier, and D.Pantaloni. 2003. A biomimetic motility assay provides insight into the mechanism of actin-based motility. *J. Cell Biol.* 160:387-398.

37. Zhou,F.Q. and C.S.Cohan. 2004. How actin filaments and microtubules steer growth cones to their targets. *Journal of Neurobiology* 58:84-91.

3 Materials and methods

In this chapter the optical tweezers technique is described and the experimental setup utilized in this work is illustrated. Experimental methods to measure the position and force are reviewed. Finally biological applications of optical tweezers are overviewed.

3.1 Optical tweezers

Objects of microscopic size or smaller (such as microspheres or cells) can be trapped and manipulated by strongly focused laser beams (Ashkin et al., 1986). Optical tweezers is an easily controllable laser light-based technique which permits to measure, in real time, displacements in the sub-nanometer range and forces in the tenths to hundreds of piconewton with millisecond time-resolution. Radiation pressure imparted by photons is used to balance external force acting on the object. Based on this principle, optical tweezers is becoming the technique of choice for force measurement, force application and fine manipulation of micron sized objects.

3.1.1 An introduction to optical trapping

Optical tweezers were first demonstrated by Ashkin (Ashkin et al., 1986) and are based on the central observation that photons carry a momentum $p = h/\lambda$, where h is the Planck's constant and λ is the wave length of the light. Hence, if some microscopic object is placed in the path of photon flow, a force is exerted on the refractive interface of the object. On macroscopic objects, this force can be neglected, but on micrososcopic objects, such as micron-sized silica or polystyrene microspheres, the effect of this force can clearly be observed, if a high-intensity light source such as a laser is used. Two different optical forces are of importance to optical trapping: the gradient force and the scattering force. The gradient force on an object is pointed in the direction of highest light intensity (Figure 3.1A). The scattering force on an object is caused by backscattering of photons and acts in the direction of propagation of light beam (Figure 3.1 B).

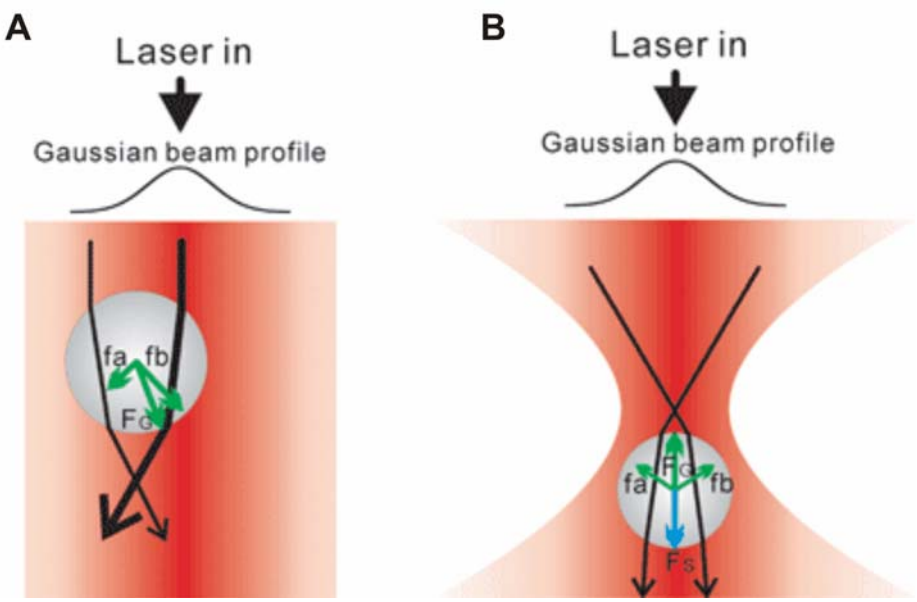

Figure 3.1. Schematics showing the principle of optical tweezers based on ray optics.The representative laser paths are shown as black lines with arrows indicating the direction of beam propagation. The thickness of the black lines indicates the intensity of the laser beam. The forces are shown as green and blue lines with arrows indicating the direction of forces. The length of the lines indicates the intensity of forces. **(A)** Gradient forces which are generated upon refraction (F_G, f_a and f_b, green lines). The beam is refracted on the surface of the bead, resulting in the change of momentum of the beam. Gradient forces (F_G) result to compensate the momentum changes on the surface of the bead. The gradient forces from the inner region (f_b) are larger than that from outer region (f_a) of the beam, due to Gaussian profile of the laser. Consequently, the net gradient force in the lateral direction directs particles to center of the beam (F_G). **(B)** Stable 3D trapping. The scattering forces (F_s, blue line) are in the direction of propagation of the laser beam (i.e., downward in this figure), while the gradient forces are directed toward the focused spot. Consequently, the bead is trapped slightly beyond the focused spot where the gradient force and scattering force are in equilibrium. Adapted from (Kimura and Bianco, 2006).

Although the concept of radiation pressure is well known, it is not trivial to provide a theoretical description of micron sized optical trapping by a strongly focused laser beam that is generally valid. To simplify this theoretical treatment, particles trapped by the optical tweezers can be divided into three regimes: Mie regime, when the radius of the particle, r, is much larger than the irradiation wavelength, λ, ($r>>\lambda$); Rayleigh regime ($r<<\lambda$); and a regime in between them ($r\sim\lambda$)(Ashkin and Dziedzic, 1987;Ashkin, 1997).

In the Mie regime, where the particle size is larger than the wavelength of the irradiation light, both the magnitude and the direction of the forces depend on the particle shape and trapping is generally restricted to spheres and ellipsoids. The conservation of momentum model (or ray optics) is applicable to this case (Ashkin, 1997). Any change of

momentum from individual rays of light when striking the particle results in an equal, opposite momentum change on the particle. A more intensive beam imparts a larger momentum change towards the centre of the trap than the less intensive beam. As shown in Figure 3.1 A, when the particle is out of trapping focus, the net momentum changes, and net force, can draw the particle back to the centre of the trap. When the particle is located in the centre of the trap, individual rays of light are refracting through the particle symmetrically, resulting in zero net lateral force and cancelling out the scattering force of the laser light (Ashkin and Dziedzic, 1987;Svoboda and Block, 1994).

If the particle size is substantially smaller than the wavelength, then the particle is in the Rayleigh regime. The direction of the force is independent of the particle shape and its magnitude varies with the particle orientation. The trapped particle can be considered as an induced dipole and the electromagnetic field of the light pulls the particle towards the brightest part of the beam, where the induced dipole minimizes its energy. In this case, the scattering force is proportional to the optical intensity and points towards the propagation of the laser light, while the gradient force is proportional to the gradient intensity and points in the direction of the intensity gradient. The gradient force attracts the particle into the region of the highest intensity, but the scattering force draws the particle into an equilibrium position that is slightly downstream of the maximum intensity. The competition between the two forces can result in stable trapping (Ashkin, 1992).

When the particle sizes are comparable with the wavelength of the trapping laser, neither the ray optic nor the dipole approach is valid. More complete electromagnetic theories are needed to explain optical trapping for particles in this intermediate size range. Majority of objects such as bacteria, yeast, organelles of larger cells and dielectric microspheres used alone or as handles to manipulate other biological objects, falls in this intermediate size range. Recently, a computational toolbox has been developed for a quantitative description of optical trapping in this size range (Nieminen et al., 2007).

3.1.2 Experimental set-up used in this project

Figure 3.2A shows a schematic drawing of the optical tweezers setup used in the experiments presented in this thesis. An inverted microscope (Olympus IX81) was used

to build this system (Figure 3.2C). As trapping laser, an Ytterbium Fiber laser (IPG Laser, λ = 1064 nm, P_{max}= 5W) was used. Infra-red (IR) laser was chosen as it is most suitable to work with living cells and absorption, and scattering in biological materials are minimized when using IR laser light (Neuman and Block, 2004). After emitting from the source, laser was passed through set of lenses (lens L1, L2, L3, and L4), so as to expand and collimate the laser to match the size of the entrance pupil of the microscope objective. In order to obtain stable trapping conditions, a high NA microscope objective (Olympus 100X, NA=1.4, oil immersion) was used to tightly focus the beam in the sample plane to the trap particles. A dichroic mirror (DM1) directs the laser beam to the microscope objective and let the upcoming illumination beam to pass in order to image the sample onto a CMOS camera (Epix, VCA1281 sensor)

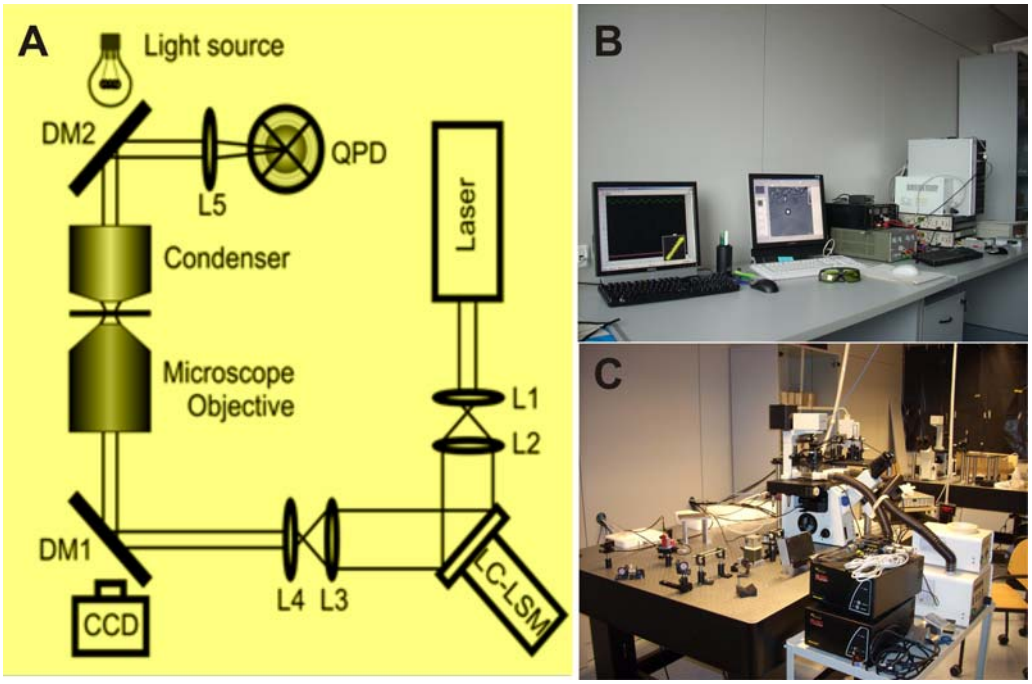

Figure 3.2. (A) Schematic diagram showing optical tweezers setup used in this work **(B)** Remote controls of the setup (To minimize all kinds of unintended noise due to external disturbances, the setup was operated from another room) **(C)** Actual set up.

The dish containing the differentiating dorsal root ganglia (DRG) neurons in nerobasal medium and 1µm in diameter silica beads functionalized with NH_2 group (PSI-1.0NH2; G.Kisker GbR, Steinfurt, Germany) was placed on the microscope stage, which could be moved by a 3-axis piezoelectric nanocube (17 MAX 301; Melles Griot Inc.,

USA). In our experiments beads were trapped very close to (1µm) the coverslip surface. We found that NH_2 coated silica beads were more suitable for our study as they settled down very fast and did not stick immediately to the surface of the coverslip. The temperature of the dish was maintained at 37^{o}c using a Peltier device and CO_2 level was maintained at 5% for live cell imaging and measurements. The bead position was determined by using back focal plane (BFP) detection (explained in detail in the next section). The BFP of the condenser was imaged onto a QPD using the dichroic mirror (DM2) and lens L5 (Figure 3.2A), and the light was converted to differential outputs, digitized, and low-pass filtered. All components were mounted on an actively-damped optical breadboard such that all beams were parallel to the table surface (beam height, 11 cm). The set up was controlled remotely from another room in order to avoid any kind of unintended noise due to external disturbances during experiments (Figure 3.2B).

Lateral bead displacement **d** = (dx,dy) from the equilibrium position inside the optical trap was also determined also using video tracking by correlation method with sub-pixel resolution so as to crosscheck the measurements obtained by QPD. The axial, lateral trap stiffness and the detector sensitivity were calibrated using the power spectrum method (explained below in 3.1.4.2 section).

In some experiments, multiple trapping was obtained by shaping the laser beam with a phase programmable modulator (PPM Hamamatsu X8267-11). This setup allows trapping multiple particles that can be organized in planar or volume arrays and manipulating the trapped particles independently in x-y-z directions.

3.1.3 Position detection

Accurate position detection and measurement are essential for a quantitative optical trapping. Different position detection methods, such as video-based position detection and laser-based position detection with a QPD, have been reviewed in (Neuman and Block, 2004). In this work we used QPD based position detection method, which can measure nanometer displacement at a rate of 10 kHz, which gives capability to measure small forces with a very high time resolution.

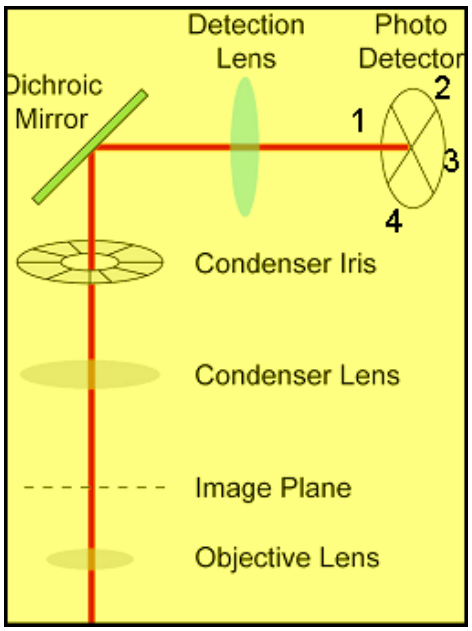

Figure 3.3. Diagram of back focal plane detection. The detection lens is positioned such that the back focal plane of the condenser is imaged onto a 2D photodetector. Rotations of the detection laser (red) cause translations in the back–focal plane which are read out at the detector. A dichroic mirror (green) reflects the detection laser (usually either red or infrared), but transmits the green light used for imaging. The voltage signal along diode quadrants are summed pairwise and differences are derived so as to obtain displacements along lateral (v_x,v_y) and axial (v_z) direction, $v_x=(v_1+v_4)-(v_2+v_3)$, $v_y=(v_1+v_2)-(v_3+v_4)$, $v_z=v_1+v_2+v_3+v_4$.

Displacements of a bead away from the equilibrium position cause rotations in the direction of laser propagation. These rotations occur in the image plane where the laser is focused, and hence cause translations in the back aperture of the condenser. Objective and condenser lenses are aligned in Koehler illumination. Like the objective, the back-aperture of the condenser lens is inaccessible in a microscope; hence a lens (L5 in Figure 3.2A) is used to image a photodetector into a plane conjugate to the back focal plane. Lateral translations of a bead in the laser focus cause translations of the detection laser in the back focal plane and are detected by a quadrant photodiode (QPD) (Lang et al., 2002). In our setup we adapted this method as shown in (Figure 3.3). More recently, (Shaevitz et al., 2003) reported a position sensitive detector, which is able to record the position of the center–of–intensity of the laser light in two dimensions and is more advantageous as detection is independent of the spot size falling on the detector. The detection lens is positioned such that the back focal plane of the condenser is imaged onto a photodetector. Rotations of the detection laser cause translations in the back focal plane

which are read out at the detector. A dichroic mirror reflects the detection laser (usually either red or infrared), but transmits the visible light used for imaging. Axial motion is also detected using an optical trap. Axial displacements of a bead through the laser focus change the collimation of the laser. As the laser light passes through the condenser iris, the outer most ring of light is blocked from the detector. When a bead moves through the laser focus axially, the relative amount of light that is blocked changes, and so the total amount of light impingent on the photodetector also changes. There is a trade off between the lateral and axial detection sensitivities. Because the axial detection relies on blockage of the outer edges of the detection beam, narrowing the condenser iris, effectively reducing the condenser numerical aperture, increases sensitivity to axial motions. In contrast, the lateral detection scheme monitors the rotation of the laser light in the image plane, which has a large contribution from the outer most rays. The diameter of the condenser iris was set such that the lateral and axial detection sensitivities fit the needs of the experiment at hand. The position detector is calibrated by moving a trapped or stuck bead while monitoring the x–, y–, and z–voltage signals from the photodetector (Lang et al., 2002), (Pralle et al., 1999) .

3.1.4 Trapping force calibration

The trapping forces depend on the intensity of the laser power, the shape of laser focus, the size and shape of the trapped particles, and the index of refraction of the trapped particles relative to the surrounding medium. It is difficult to measure the trapping forces directly, but there are several ways to calibrate them. The forces can be calibrated by a power spectrum of the Brownian motion of a trapped particle and the trapping stiffness can be determined (Sheetz, 1998;Berg-Sorensen and Flyvbjerg, 2004). Another way of calibration is based on the fact that the external forces applied to a single particle within an optical trapping can push a single particle away from the focal region, and the force from the optical tweezers usually draws the particle back to the centre of the trap. In the equilibrium position, the external force equals the force from the optical tweezers. For a small displacement, the force from the optical tweezers, termed as restoring force, can be estimated by:

$$F = -\alpha x,$$

where α is the trap stiffness and x is the displacement of the particle away from the centre of the trap, when displacements are smaller than half the radius of the particle within the focal region. Once the trap stiffness is determined or given, the external force applied on the particle can be determined by accurately monitoring the position of a particle in an optical trap. Optical tweezers, therefore, have been widely used as a passive force measurement tool.

Considerable effort has been made on measuring the trap stiffness with high accuracy. Many methods have been developed for this purpose, three of which will be described here.

3.1.4.1 Equipartition method

The easiest of these methods calculates the variance in the Brownian motion of a trapped bead (Neuman and Block, 2004). According to equipartition theorem, the energy in the Brownian motion of the trapped bead is equal to $\frac{1}{2} k_B T$, whereas the energy stored in the spring is equal to the one half times the spring constant, α, times the variance in the motion. Setting these two energies equal and solving for the stiffness, α, yields:

$$\alpha = \frac{\langle x^2 \rangle}{k_B T}.$$

Calculation of the variance in position is uncomplicated and easy way to estimate the trap stiffness although one needs a calibrated position detector.

3.1.4.2 Power spectrum method

An extensively used method and the one we used in the measurements presented in this thesis involves measuring the frequency spectrum of the Brownian noise exhibited by the bead. Typically, the mass of the bead is so small that the Reynolds number is very low and inertial forces are much weaker than those of hydrodynamic drag. In this regime, the equation of motion for the bead is that of a massless, damped oscillator driven by Brownian motion:

$$\beta \dot{x}(t) + \alpha x(t) = F(t),$$

where x is the position of the bead, $\beta = 6\pi\eta r$ is the drag coefficient of the bead, η is the viscosity of the surrounding fluid, and r is the bead radius. The Brownian noise source, $F(t)$, has zero mean, and is essentially white with amplitude:

$$\left|\tilde{F}(f)\right|^2 = 4\beta k_B T ,$$

The Fourier transform of the above equation is:

$$2\pi\beta\left(\frac{\alpha}{2\pi\beta} \quad if\right)\tilde{x}(f) = \tilde{F}(f) .$$

The power spectrum is given by:

$$\left|x(f)\right|^2 = \frac{k_B T}{\pi^2 \beta\left[\left(\frac{\alpha}{2\pi\beta}\right)^2 + f^2\right]} .$$

This equation is that of a Lorentzian with corner frequency $f_c = \alpha/2\pi\beta$. Therefore the stiffness of the trap is given by $\alpha = 2\pi\beta f_c$. Power spectra measurement and subsequent fitting of the corner frequency were done by a custom made program in MATLAB as shown in Figure 3.4. If the displacement of bead away from trapping center is relatively small (approximately 300nm) then the position to photodetector voltage calibration will be linear and the corner frequency can be found from the power spectrum of the voltage data (Neuman and Block, 2004).

Optical traps typically work around one micron above the coverslip, where the hydrodynamic drag coefficient of the bead is altered by the proximity of the surface. The viscous drag on a sphere of radius r whose center is a distance h above a surface is (Neuman and Block, 2004):

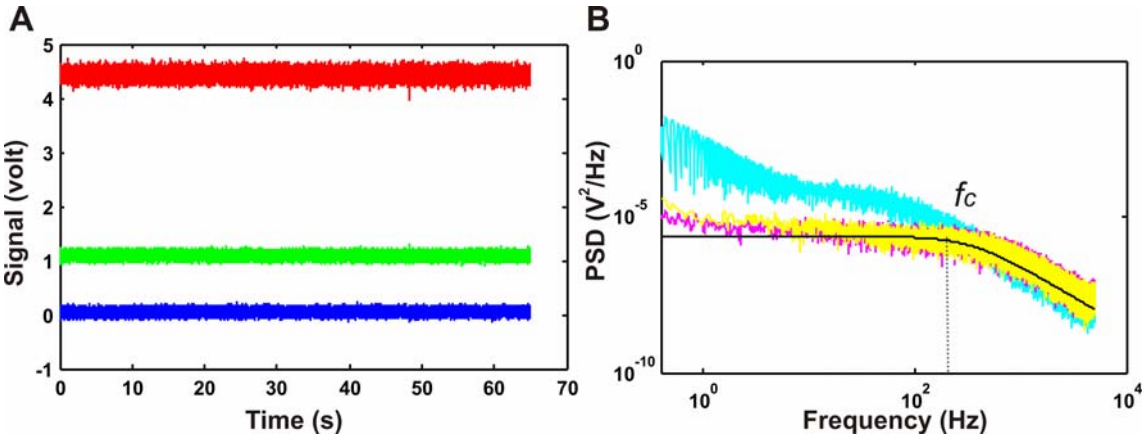

Figure 3.4. Typical calibration experiment recording of 1 μm silica bead trapped with 2 W laser power (at source). **(A)** QPD voltage signal along x, y, z axes in blue, green and red respectively (the signal along y is displaced by +1 volt for better visualization). **(B)** Power spectral densities calculated from the signal in volt along x, y and z axes in yellow, magenta and cyan respectively. Solid black line indicates Lorentzian fit corresponding to signal along x-axis (yellow) with corner frequency f_c = 230 Hz, which gives stiffness value of 0.015 pN.nm^{-1}.

$$\beta = \frac{6\pi\eta r}{1 - \frac{9}{16}\left(\frac{r}{h}\right) + \frac{1}{8}\left(\frac{r}{h}\right)^3 - \frac{45}{256}\left(\frac{r}{h}\right)^4 - \frac{1}{16}\left(\frac{r}{h}\right)^5}.$$

A useful table of correction values can be found in (Svoboda and Block, 1994). The height of the bead above the coverslip surface can be found by monitoring the axial detection signal as the surface is moving into contact with the bead (Lang et al., 2002).

3.1.4.3 Drag force method

A third method of stiffness calibration directly balances the trapping force with a drag force (Neuman and Block, 2004). The coverslip, attached to a piezo-controlled microscope stage, is moved at a constant velocity by nanopositioning devices. For a given velocity, the trap stiffness is given by:

$$\alpha = \frac{\beta v}{\Delta x},$$

where β is the drag coefficient corrected for the proximity to the surface, v is the stage velocity, and Δx is the measured displacement of the bead from the trap center. By measuring the displacement for a series of different stage velocities, one is able to use this method to probe the linearity of the optical trap, which cannot be done with the two

methods previously described. In practice, this calibration method is less straightforward than the others.

When all extra sources of noise and filtering are taken into account, the three different methods of calibrating trap stiffness usually agree to within 5–10%. It is a good idea to use all three methods when first calibrating an optical trap. However, on a daily basis, the power spectrum method was used as it affords the most information in the least amount of time.

3.1.5 Biological applications of optical tweezers

Optical tweezers have emerged as an important tool for manipulating single cell and performing sophisticated biophysical/biomechanical characterizations. Many proteins and enzymes, and their assemblies (constituting cell organelles), are true molecular motors whose mechanochemistry, as well as the elastic and mechanical properties of nucleic acids, are accessible to optical manipulation techniques (Bustamante et al., 2000). Biochemical processes investigated to date have revealed that forces developed by molecular motors are in the piconewton range, and, among different micromanipulation techniques, optical tweezers adapt better to this range. For instance magnetic tweezers normally cover forces up to 10 pN, and atomic force microscopy works well above some hundreds of piconewton (Bustamante et al., 2000).

The study of mechanics requires the measurement of a triad of independent magnitudes. Typically, for macroscopic purposes, these are time, distance and mass. At the molecule level, where chemical reactions are involved, energy is also very representative.

Optical tweezers constitute a technique that is successfully contributing to the explanation of the mechanistic models of protein and cell function. It is taking these approaches beyond the hypothesis. At the single-molecule level (Svoboda and Block, 1994;Bustamante et al., 2000), it is possible, for example, to measure in real time the concomitant forces generated during the conformational changes experienced by a protein in its folding/unfolding kinetic pathway (Kellermayer et al., 1997;Cecconi et al., 2005) or in the catalytic cycle of an enzyme (Bustamante et al., 2000;Stone et al., 2003;Abbondanzieri et al., 2005), DNA mechanics (Allemand et al., 1998;Bustamante et

al., 2003) and the behavior of molecular motors (Finer et al., 1994;Mehta et al., 1999;Smith et al., 2001;Asbury et al., 2003;Mallik et al., 2004;Pease et al., 2005;Dumont et al., 2006). Also, organelles, chromosomes or entire cells have been studied with optical tweezers in processes such as cell motility (Block et al., 1989) (Tadir et al., 1989) and mitosis (Berns et al., 1989). Cell-scale objects can be held directly in an optical trap and the specimen visualized by video microscopy. Molecules and aggregates, on the other hand, require their attachment to mechanical handles, usually in the form of silica or polystyrene microspheres. Finer attachments can be chemically engineered. For example, two dsDNA (double-stranded DNA) molecules could be used.

References

1. Abbondanzieri,E.A., W.J.Greenleaf, J.W.Shaevitz, R.Landick, and S.M.Block. 2005. Direct observation of base-pair stepping by RNA polymerase. *Nature* 438:460-465.

2. Allemand,J.F., D.Bensimon, R.Lavery, and V.Croquette. 1998. Stretched and overwound DNA forms a Pauling-like structure with exposed bases. *Proceedings of the National Academy of Sciences of the United States of America* 95:14152-14157.

3. Asbury,C.L., A.N.Fehr, and S.M.Block. 2003. Kinesin moves by an asymmetric hand-over-hand mechanism. *Science* 302:2130-2134.

4. Ashkin,A. 1992. Forces of A Single-Beam Gradient Laser Trap on A Dielectric Sphere in the Ray Optics Regime. *Biophysical Journal* 61:569-582.

5. Ashkin,A. 1997. Optical trapping and manipulation of neutral particles using lasers. *Proceedings of the National Academy of Sciences of the United States of America* 94:4853-4860.

6. Ashkin,A. and J.M.Dziedzic. 1987. Optical Trapping and Manipulation of Viruses and Bacteria. *Science* 235:1517-1520.

7. Ashkin,A., J.M.Dziedzic, J.E.Bjorkholm, and S.Chu. 1986. Observation of A Single-Beam Gradient Force Optical Trap for Dielectric Particles. *Optics Letters* 11:288-290.

8. Berg-Sorensen,K. and H.Flyvbjerg. 2004. Power spectrum analysis for optical tweezers. *Review of Scientific Instruments* 75:594-612.

9. Berns,M.W., W.H.Wright, B.J.Tromberg, G.A.Profeta, J.J.Andrews, and R.J.Walter. 1989. Use of a laser-induced optical force trap to study chromosome movement on the mitotic spindle. *Proc Natl Acad Sci U S A* 86:4539-4543.

10. Block,S.M., D.F.Blair, and H.C.Berg. 1989. Compliance of Bacterial Flagella Measured with Optical Tweezers. *Nature* 338:514-518.

11. Bustamante,C., Z.Bryant, and S.B.Smith. 2003. Ten years of tension: single-molecule DNA mechanics. *Nature* 421:423-427.

12. Bustamante,C., J.C.Macosko, and G.J.L.Wuite. 2000. Grabbing the cat by the tail: Manipulating molecules one by one. *Nat Rev Mol Cell Biol* 1:130-136.

13. Cecconi,C., E.A.Shank, C.Bustamante, and S.Marqusee. 2005. Direct observation of the three-state folding of a single protein molecule. *Science* 309:2057-2060.

14. Dumont,S., W.Cheng, V.Serebrov, R.K.Beran, I.Tinoco, Jr., A.M.Pyle, and C.Bustamante. 2006. RNA translocation and unwinding mechanism of HCV NS3 helicase and its coordination by ATP. *Nature* 439:105-108.

15. Finer,J.T., R.M.Simmons, and J.A.Spudich. 1994. Single Myosin Molecule Mechanics - Piconewton Forces and Nanometer Steps. *Nature* 368:113-119.

16. Kellermayer,M.S.Z., S.B.Smith, H.L.Granzier, and C.Bustamante. 1997. Folding-unfolding transitions in single titin molecules characterized with laser tweezers. *Science* 276:1112-1116.

17. Kimura,Y. and P.R.Bianco. 2006. Single molecule studies of DNA binding proteins using optical tweezers. *Analyst* 131:868-874.

18. Lang,M.J., C.L.Asbury, J.W.Shaevitz, and S.M.Block. 2002. An automated two-dimensional optical force clamp for single molecule studies. *Biophysical Journal* 83:491-501.

19. Mallik,R., B.C.Carter, S.A.Lex, S.J.King, and S.P.Gross. 2004. Cytoplasmic dynein functions as a gear in response to load. *Nature* 427:649-652.

20. Mehta,A.D., R.S.Rock, M.Rief, J.A.Spudich, M.S.Mooseker, and R.E.Cheney. 1999. Myosin-V is a processive actin-based motor. *Nature* 400:590-593.

21. Neuman,K.C. and S.M.Block. 2004. Optical trapping. *Review of Scientific Instruments* 75:2787-2809.

22. Nieminen,T.A., V.L.Y.Loke, A.B.Stilgoe, G.Knoner, A.M.Branczyk, N.R.Heckenberg, and H.Rubinsztein-Dunlop. 2007. Optical tweezers computational toolbox. *Journal of Optics A-Pure and Applied Optics* 9:S196-S203.

23. Pease,P.J., O.Levy, G.J.Cost, J.Gore, J.L.Ptacin, D.Sherratt, C.Bustamante, and N.R.Cozzarelli. 2005. Sequence-directed DNA translocation by purified FtsK. *Science* 307:586-590.

24. Pralle,A., M.Prummer, E.L.Florin, E.H.K.Stelzer, and J.K.H.Horber. 1999. Three-dimensional high-resolution particle tracking for optical tweezers by forward scattered light. *Microscopy Research and Technique* 44:378-386.

25. Shaevitz,J.W., E.A.Abbondanzieri, R.Landick, and S.M.Block. 2003. Backtracking by single RNA polymerase molecules observed at near-base-pair resolution. *Nature* 426:684-687.

26. Sheetz,M.P. 1998. Methods in cell biology. Academic Press, New York, NY.

27. Smith,D.E., S.J.Tans, S.B.Smith, S.Grimes, D.L.Anderson, and C.Bustamante. 2001. The bacteriophage straight phi29 portal motor can package DNA against a large internal force. *Nature* 413:748-752.

28. Stone,M.D., Z.Bryant, N.J.Crisona, S.B.Smith, A.Vologodskii, C.Bustamante, and N.R.Cozzarelli. 2003. Chirality sensing by Escherichia coli topoisomerase IV and the mechanism of type II topoisomerases. *Proceedings of the National Academy of Sciences of the United States of America* 100:8654-8659.

29. Svoboda,K. and S.M.Block. 1994. Biological Applications of Optical Forces. *Annual Review of Biophysics and Biomolecular Structure* 23:247-285.

30. Tadir,Y., W.H.Wright, O.Vafa, T.Ord, R.H.Asch, and M.W.Berns. 1989. Micromanipulation of Sperm by A Laser Generated Optical Trap. *Fertility and Sterility* 52:870-873.

4 Results

4.1

Properties of the Force Exerted by Filopodia and Lamellipodia and the Involvement of Cytoskeletal Components

Cojoc D[*], Difato F[*], Ferrari E[*], **Shahapure RB**[*], Laishram J, Righi M, Di Fabrizio E, Torre V.

PLoS ONE 2(10), 24th October 2007.
(***** Equally contributed)

OPEN ACCESS Freely available online

PLoS one

Properties of the Force Exerted by Filopodia and Lamellipodia and the Involvement of Cytoskeletal Components

Dan Cojoc[1,4,9]*, Francesco Difato[2,9], Enrico Ferrari[1,9], Rajesh B. Shahapure[2,9], Jummi Laishram[2], Massimo Righi[2], Enzo M. Di Fabrizio[1,3], Vincent Torre[2,5]*

1 Consiglio Nazionale delle Ricerche (CNR)-Istituto Nazionale per la Fisica della Materia (INFM), Laboratorio Nazionale Tecnologie Avanzate E Nanoscienza (TASC), Area Science Park Basovizza, Trieste, Italy, **2** International School for Advanced Studies (SISSA-ISAS), Trieste, Italy, **3** Università Magna Graecia di Catanzaro, Campus Germaneto, Catanzaro, Italy, **4** Centro per la Biomedicina Molecolare (CBM), LANADA Laboratory, Trieste, Italy, **5** Italian Institute of Technology, International School for Advanced Studies (ISAS) Unit, Italy

During neuronal differentiation, lamellipodia and filopodia explore the environment in search for the correct path to the axon's final destination. Although the motion of lamellipodia and filopodia has been characterized to an extent, little is known about the force they exert. In this study, we used optical tweezers to measure the force exerted by filopodia and lamellipodia with a millisecond temporal resolution. We found that a single filopodium exerts a force not exceeding 3 pN, whereas lamellipodia can exert a force up to 20 pN. Using metabolic inhibitors, we showed that no force is produced in the absence of actin polymerization and that development of forces larger than 3 pN requires microtubule polymerization. These results show that actin polymerization is necessary for force production and demonstrate that not only do neurons process information, but they also act on their environment exerting forces varying from tenths pN to tens of pN.

Citation: Cojoc D, Difato F, Ferrari E, Shahapure RB, Laishram J, et al (2007) Properties of the Force Exerted by Filopodia and Lamellipodia and the Involvement of Cytoskeletal Components. PLoS ONE 2(10): e1072. doi:10.1371/journal.pone.0001072

INTRODUCTION

During morphogenesis, neuronal precursor cells migrate from the zone where they are born to their final destination, which, in some cases, is at a distance of several millimeters[1,2]. After reaching their destination, neurons must establish appropriate synaptic connections by sending out from their soma projections called neurites. The motion of neurites is guided by growth cones located at their tips[3,4]. Growth cones contain a variety of chemical and mechanical receptors and sophisticated biochemical machinery that couples these receptors to the cytoskeleton[5–7]. Extruding from the tip of the growth cone are highly motile structures called filopodia and lamellipodia that are used to explore and probe the environment[3,6]. All these complex events, which are at the basis of neuronal development and differentiation, involve cell motility requiring a precise control of cellular and molecular motors. The motion of these structures has been analyzed and characterized to some extent by time-lapse microscopy[8–12].However, little is known about how neurons use these structures to sense the mechanical properties of their environment and about what range of forces these structures exert during their exploratory motion.

Analysis of the forces exerted by neurons has been limited to theoretical considerations; experimental analysis has been limited to samples of isolated filaments[13–17]or migrating cells[18,19]. Measured forces range from 1 or 2 pN in isolated actin filaments and microtubules to 1 nN in migrating keratocytes. Quantitative characterization of the force exerted by lamellipodia and filopodia during neuronal differentiation could help to elucidate how neurons sense the environment and process mechanical information. Precise description of the mechanical and dynamic events that occur during neuronal differentiation and migration would provide new insights regarding the molecular events controlling these biological functions. In addition, it would offer a more precise way for evaluating the role of molecular motors in cell motility under physiological conditions and in neurodegenerative disease.

In this study, we used optical tweezers[20–22] to measure the force exerted by filopodia and lamellipodia during neuronal differentiation. Unlike other force measurement methods, optical tweezers are non-invasive and provide direct high temporal resolution for position detection ($<$10 nm) and force measurement ($<$1 pN), highly relevant in biological systems[21]. We found that a single filopodium exerts a force not exceeding 3 pN. In contrast, lamellipodia exert forces of 20 pN or more lasting less than 1 s to approximately 30 s. Treatment of growth cones with the selective myosin light chain kinase (MLCK) inhibitor ML-7[23] or the microtubule depolymerizing agent nocodazole[24] drastically reduced the motion and force exerted by lamellipodia, while filopodia continued to move and exert forces up to 3 pN. Growth cones treated with the actin depolymerizing agent latrunculin A[24] did not exert any detectable force. These findings suggest that no force can be produced in the absence of actin polymerization and that development of forces larger than 3 pN requires microtubule polymerization. This study shows that not only do neurons process information, but also they act on the environment, exerting forces varying 1 to 2 orders of magnitude.

Academic Editor: Lin Mei, Medical College of Georgia, United States of America

Received July 6, 2007; **Accepted** October 4, 2007; **Published** October 24, 2007

Funding: This work was partially supported by the EU grants NEURO and BINASP, by a FIRB grant from the Italian Government and by the GRAND grant from CIPE/FVG.

Competing Interests: The authors have declared that no competing interests exist.

* **To whom correspondence should be addressed.** E-mail: cojoc@tasc.infm.it (DC); torre@sissa.it (VT)

9 These authors contributed equally to this work.

RESULTS

During neuronal differentiation and development, the growth cone of each neurite extends its filopodia and lamellipodia to explore the chemical nature of the environment and to probe the rigidity and composition of the extracellular matrix[23]. Under these circumstances, cell motility is strictly linked to the generation of forces. Therefore, we used optical tweezers[20–22] to measure the force exerted by the growth cones of differentiating neurons.

Force exerted by growth cones of differentiating neurons

Neurons from dorsal root ganglia (DRG) were isolated from P10-P12 rats and plated on poly-L-lysine-coated glass coverslips and positioned on the stage of an inverted microscope that was used for imaging and measurement of forces (see Methods). After incubation for 24 to 48 h, neurites could be seen emerging from the DRG soma. Their motion was analyzed with time-lapse differential interference contrast microscopy (Movie S1). Filopodia and lamellipodia moved rapidly, exploring the three-dimensional space in all directions, with velocities of up to 1.2 μm s-1 and reaching heights up to 1–3 μm.

Silica beads 1 μm in diameter were functionalized with amino groups to reduce sticking and trapped with 1064-nm infrared optical tweezers (laser power between 8 and 44 mW) close to the growth cones of the differentiating neurites (Fig. 1a and Movie S2). We verified that 50 mW laser power reaching the specimen plane and focused on the growth cone did not affect its motion for at least 1 h. Often we observed both lateral and axial displacement of the trapped bead by a growth cone. In several experiments, the growth cone moved the bead as much as 2–3 microns from its equilibrium position inside the trap (Fig. 1b). After the collision, the bead did not remain attached to the growth cone and could return to its original position in the trap (Fig. 1c). We measured the lateral force exerted by the growth cone Fneu = (Fx, Fy) by following the bead position with a quadrant photo diode (QPD)[22] and video tracking[25] (see Methods). When the bead was far from the growth cone, QPD recordings of Fx and Fy were

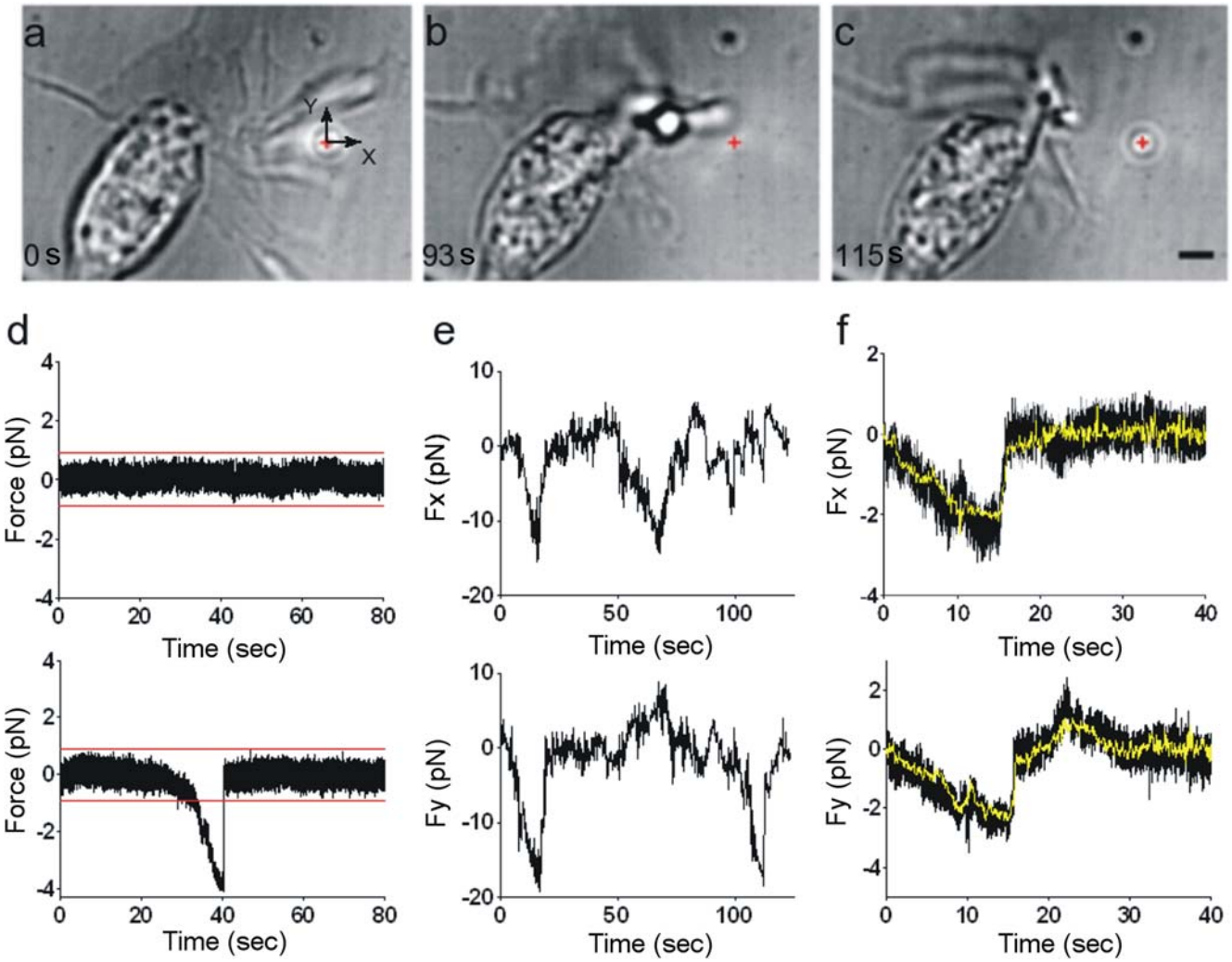

Figure 1. Collisions between a growth cone and a trapped bead. **(a–c)** A growth cone displacing a bead from the optical trap. The red cross indicates the bead's equilibrium position inside the optical trap. Scale bar, 2 μm. **(d)** Example of a force component obtained with QPD when the bead was distant from the growth cone (upper trace) and when the bead was in contact with the growth cone (lower trace). Red lines are drawn 5 σ from the 0 mark. σ, s.d. of force fluctuations. When the QPD trace crossed the red lines for at least 100 ms and a lamellipodium or filopodium was seen hitting the bead, a reliable collision was detected. **(e)** Example of F_x and F_y during repetitive collisions between a moving lamellipodium and a trapped bead. Trap stiffness was 0.05 pN nm^{-1}. **(f)** Comparison of F_x and F_y determined with a QPD (black traces) and video tracking (yellow traces).
doi:10.1371/journal.pone.0001072.g001

quiet, with a s.d. σ of approximately 0.18 pN (Fig. 1d, upper trace), but when the bead was moved close to the growth cone, collisions producing a force greater than 5 σ were observed (Fig. 1d, lower trace). On several occasions, Fx and Fy increased within 1–10 s, reaching values of 20 pN (Fig. 1e), and when the growth cone stopped pushing, the bead rapidly returned to its equilibrium position, often in less than 1 ms.

The presence of floating debris and wandering filopodia near the bead could affect the light pattern impinging on the QPD. Therefore, a collision was considered reliable when the bead displacement obtained with the QPD and video tracking were in agreement (black and yellow traces, respectively, in Fig. 1f) and the presence of a colliding filopodium or lamellipodium was verified by visual inspection of the movie. We analyzed collisions between growth cones and trapped beads in more than 200 experiments. Each experiment lasted 2 min, and in many experiments there were several collisions that could be used for statistical analysis (see Methods). These collisions produced maximal forces ranging from less than 1 pN to at least 20 pN, with a maximal rate of increase of 10 pN s-1. They lasted for less than 1 s to approximately 60 s. Typically, larger forces were observed during longer lasting collisions. As these forces extended over a wide range of intensities and durations, we took the further step of characterizing the force developed by each major component of growth cones, filopodia and lamellipodia.

Force exerted by filopodia

Filopodia have an elongated and well defined shape with diameters varying from 100 to 500 nm and an average length of approximately 15 μm[26]. Filopodia can exert force during both exploratory motion and growth. During their exploratory motion often filopodia pivot and push beads aside, possibly as a consequence of shearing movements of the lamellipodial actin network where the filopodial shaft emerges. We refer to the first case as lateral collisions and to the latter case, where the filopodium pushes the bead, as protrusion. An isolated filopodium, after wandering around the bead (Fig. 2a), sometimes collided with it (Fig. 2b and Movie S3), exerting a maximal force of up to 1 pN (Fig. 2c). The force measured during lateral collisions depends on the exact geometry of the collision: a moving filopodium can strike a trapped bead at its center or just lightly touch its surface. Results from 42 experiments show that filopodia never exerted a force larger than 2 pN (Fig. 2g), which is a reliable upper boundary for the maximal force exerted during a lateral collision. Some lateral collisions lasted less than 1 s, but on several occasions we observed filopodia pushing beads for 15 s.

The force exerted by a filopodium is generated by its elastic properties[19] and a variety of molecular processes[27], including polymerization of actin filaments[28,29], which generates a protrusion force counterbalanced by the membrane resistance force[30–32], leading to a net force Ftip. To measure forces produced during protrusion, beads were trapped in front of filopodia tips (Fig. 2d). In 33 experiments, we observed protruding filopodia displacing beads, often repeatedly (Fig. 2e and Movie S4; see also Figure S1 and Movie S5). The measured force was approximately 1 pN, and it developed within 30 ms (Fig. 2f). Ftip did not exceed 3 pN (Fig. 2h). These collisions rarely lasted more than 30 s.

When a filopodium collides with an encountered obstacle, it senses the object's chemical properties and also probes its mechanical resistance and size. Therefore, we investigated whether the force exerted by filopodia varies with the stiffness of the optical trap. We conducted several experiments in which we increased the trap stiffness from 0.006 pN nm-1 to 0.01 pN nm-1 and analyzed the collisions that occurred between the same growth cone and trapped beads. Under the two conditions of trap stiffness, collisions produced forces similar in magnitude (Fig. 3a, b), but collisions with beads trapped with a higher stiffness appeared to be shorter in duration. Data from 18 experiments show a similar distribution of measured forces under the two conditions but more frequent longer lasting collisions with the lower trap stiffness (Fig. 3c, d).

As shown in Figure 3, filopodia appeared to modulate their mechanical response by decreasing the duration of the collision when encountering a stiffer obstacle. Thus, they appear to be able to communicate the mechanical properties of the environment to the internal biochemical machinery that powers the cytoskeleton.

Force exerted by lamellipodia

We often observed that a lamellipodium repeatedly pushes a trapped bead (Fig. 4a,b and Movie S6), exerting a force of 3–4 pN (Fig. 4c). Lamellipodia could displace beads from the trap when the maximum trapping force was 20 pN. In 6 experiments, we observed lamellipodium increasing the exerted force in well resolved steps of approximately 0.2 pN, corresponding to displacements of approximately 18 nm (Fig. 4d). These steps have properties very similar to those observed during microtubule assembly, where discrete jumps of approximately 20–30 nm are observed[16]. In 65 experiments, lamellipodia exerted a force ranging from less than 1 pN to at least 20 pN, with a variable duration (Fig. 4e, f).

An isolated filopodium is complex from a molecular point of view, but it has a defined structure, and the force it exerts is well localized in space. In contrast, lamellipodia have a more differentiated structure and are thought to exert a force with variable direction in space. Therefore, we attempted to characterize the force field generated by lamellipodia by trapping multiple beads in front of a lamellipodium. Traps were separated by 3–6 μm and located on the same plane. In several experiments, 3 beads were displaced simultaneously by the lamellipodium (Fig. 5a), and we determined their trajectory with video imaging. The direction of forces at the three locations changed during the experiment and could span a large fraction of the free space surrounding the moving lamellipodium (Fig. 5b).

The force simultaneously exerted at the two locations separated by 3 μm was sometimes in opposite directions, and often the direction of force exerted at one location reversed within 10 s. This confirms that the force field generated by a lamellipodium is complex and dynamic over a short time scale.

Effects of metabolic inhibitors on force exertion

In order to identify the molecular mechanisms of force production, we analyzed the effect of metabolic inhibitors at concentrations known to be effective[23,24]. Within 5 min after addition of 50 nM latrunculin A, an inhibitor of actin polymerization[24], the exploratory motion of growth cones was drastically reduced; under this condition, the force exerted by filopodia and lamellipodia did not exceed 3 or 4 pN, and collisions were shorter (black symbols in Fig. 6d). When the concentration of latrunculin A was increased to 100 nM, moving filopodia collapsed (Fig. 6a–c), and no detectable motion or force was observed in filopodia or lamellipodia (red symbols in Fig. 6d). In contrast, addition of 50 nM nocodazole, an inhibitor of microtubule polymerization[24], had a more specific effect. It reduced the motion of lamellipodia but not of filopodia, which continued to move (Fig. 6e–g), exerting a force of up to 3 pN (Fig. 6e). Upon addition of 4 μM of the myosin II inhibitor ML-7[23], a fast retraction of moving filopodia was observed (Fig. 6i–j), but within 2–5 min new filopodia emerged from the growth cone (Fig. 6k), which exerted a force in the pN range (Fig. 6l).

These results suggest the existence of two distinct but coupled molecular motors within growth cones. Actin polymerization

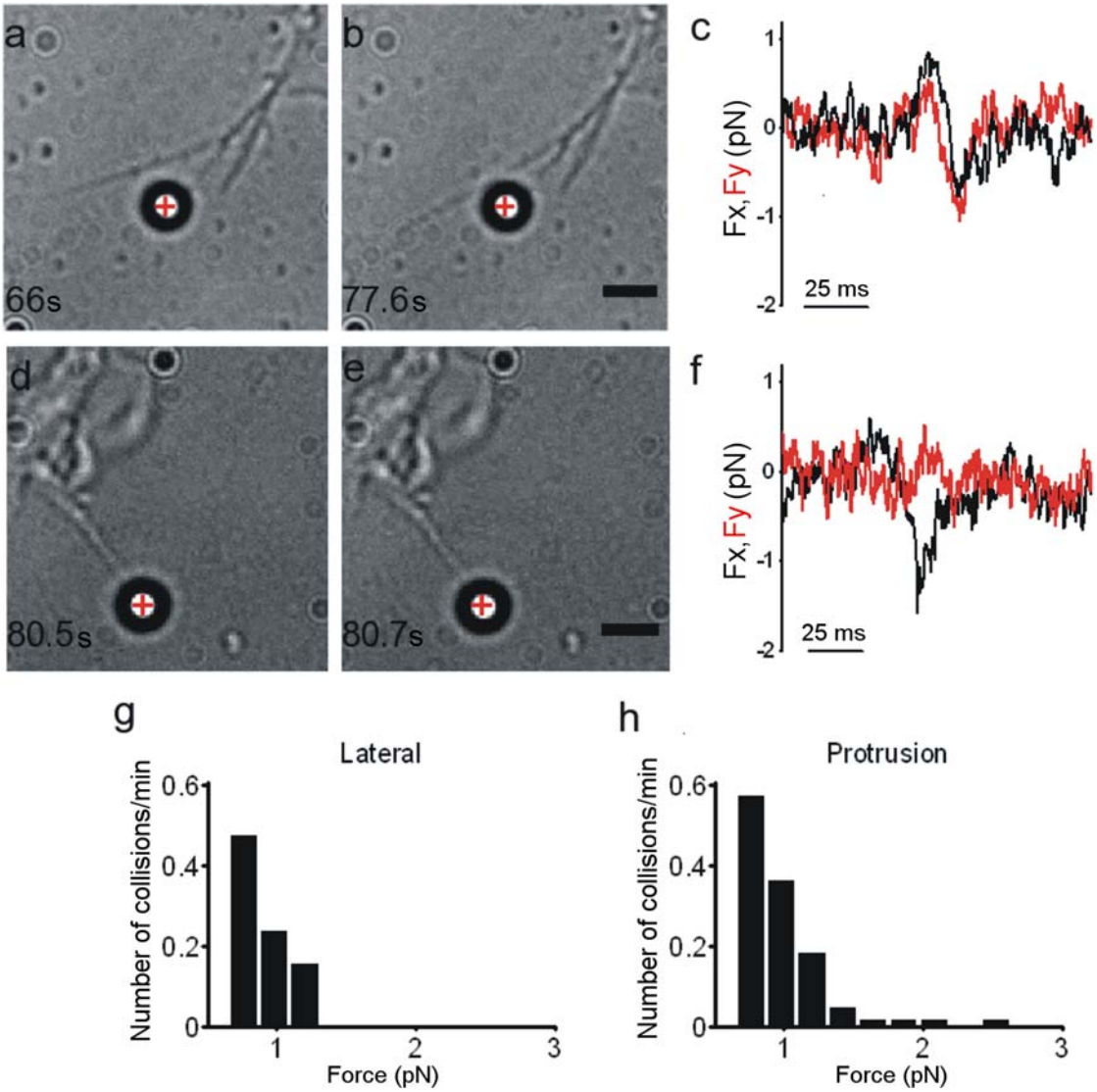

Figure 2. Force exerted by Filopodia. (a–b) Lateral collision between a filopodium and a trapped bead. Trap stiffness was 0.008 pN nm^{-1}. The red cross indicates the bead's equilibrium position inside the optical trap. **(c)** F_x and F_y from the QPD during the lateral collision shown in (a–b). **(d–e)** Collision between a protruding filopodium and a trapped bead. **(f)** F_x and F_y from the QPD during the filopodial protrusion shown in (d–e). Trap stiffness was 0.008 pN nm^{-1}. **(g–h)** Histograms of forces measured during lateral collisions and protrusions. Data were collected from 75 experiments, each lasting 2 min. Scale bar, 2 μm.
doi:10.1371/journal.pone.0001072.g002

seems necessary for the development of any significant motion and force in filopodia and lamellipodia. Microtubule polymerization is not essential for filopodia motion or for the generation of weak forces, but it is necessary for lamellipodia motion and generation of forces larger than 3 pN.

DISCUSSION

A typical growth cone can be divided into two regions: the central region and the peripheral region. The latter consists of filopodia and a lamellipodia[33–36]; the motion of these structures is a major component of neuronal differentiation. This is the first report of a quantitative determination with a millisecond temporal resolution of the force exerted by filopodia and lamellipodia in differentiating neurons. The force developed over time, with a maximal rate of increase of 10 pN s-1. Thin filopodia, during a protrusion or lateral collision (Fig. 2), exerted a force not exceeding 3 pN. In contrast, lamellipodia exerted a force of up to 20 pN and possibly more, which could increase in discrete steps of approximately 0.2 pN (Fig. 4d). These steps had properties very similar to those observed during the assembly of isolated microtubules[16]. The measured forces were smaller than forces involved in cellular traction force or measured in migrating keratocytes[15,18]. Measured forces here reported, may not fully represent the ability that lamellipodia have because, at least in some cases, only a fraction of the forces exerted is picked up by the beads and therefore the value of 20 pN here reported for lamellipodia is the maximal force that was measured. Indeed we expect lamellipodia to exert larger forces, possibly up to hundreds of pN, as in migrating epithelial cells[37]. The diameter of filopodia tips is approximately 100 nm, i.e. 10 times smaller than the diameter of the used beads, therefore the maximal force measured for filopodia is expected to be a reliable estimate of the force exerted by these structures.

Force measurements with optical tweezers require test beads to be in the harmonic potential well of the trapping optical force and

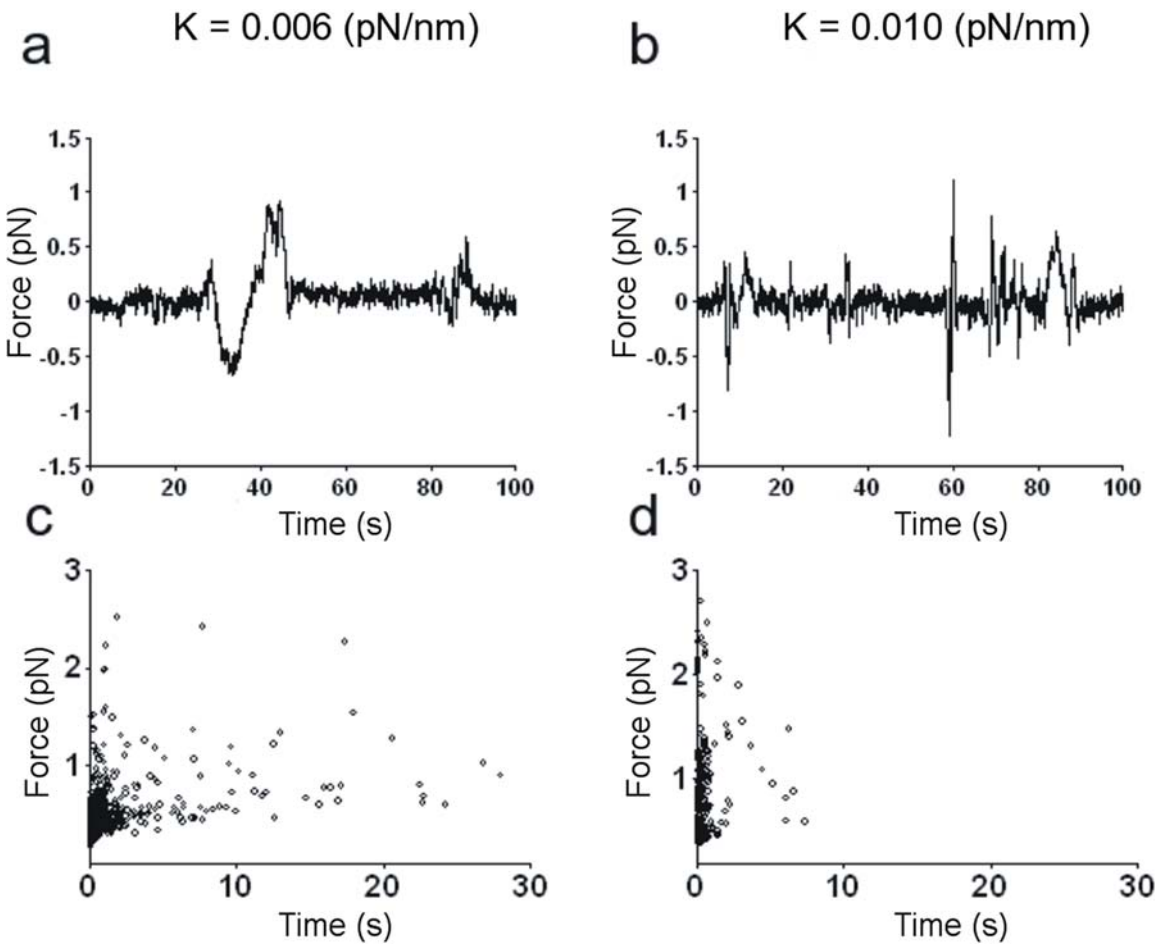

Figure 3. Effect of trap stiffness on force exerted. (a–b) F_x from the QPD during collisions between the same filopodium and the same bead trapped with a stiffness of 0.006 and 0.010 pN nm^{-1}. Traces were filtered at 50 Hz and sub-sampled. **(c–d)** Scatter plot of force duration for collisions between filopodia and beads trapped with a stiffness of 0.006 and 0.010 pN nm^{-1}. Data collected from 15 experiments at each stiffness.
doi:10.1371/journal.pone.0001072.g003

to be displaced from its equilibrium position inside the well only by the force to be measured. When adhesion forces between the bead and the growth cone and/or between the bead and the substrate become dominant, the stiffness of the optical trap is profoundly modified and it is impossible to obtain an accurate force measurement. Therefore, it is necessary to place the bead at 1 micron or so from the substrate where neurons are growing. As exploring filopodia and lamellipodia lift up from the substrate, forces can be reliably measured under these conditions.

Filopodia are composed of bundles of actin filaments and occasional microtubules [5,24]. We observed that the force exerted by a protruding filopodium is in the pN range, not exceeding 3 pN. Its amplitude is of the same order as that measured during polymerization of actin filaments[14,17] and microtubules[16]. This similarity implies that the protrusion force generated by polymerization is minimally counterbalanced by the membrane surrounding actin bundles and microtubules, indicating that the membrane at the filopodia tips has a low stiffness[38,39].

Simple mechanical considerations show that the force exerted by a wandering filopodium during a lateral collision (Fig. 2a–c) can be accounted for by the elastic force expected from its flexural rigidity[19,40] and its bending or buckling. No additional contribution from other force-generating mechanisms is required. The exact mechanisms causing filopodia to bend and/or buckle are not understood. Thermal fluctuations certainly provide a constant driving force, but a variety of other motor proteins[19,29,29] present in the growth cone could intervene, although their relative contribution is still unknown. Indeed, inhibition of myosin II and microtubule polymerization blocked lamellipodia motion and drastically reduced the force produced by growth cones (Fig. 6), while filopodia continued to move and were able to exert forces in the pN range. In contrast, with blockade of actin polymerization, filopodia and lamellipodia produced no measurable forces. Thus, in the absence of actin polymerization, growth cones cannot exert any force, and microtubule polymerization is necessary for development of forces exceeding 3 pN. Therefore, actin filaments and microtubules cooperate and interact in a complex way so as to generate a wide range of forces.

The motion of filopodia and lamellipodia seems to follow stereotyped patterns wherein the stiffness of an obstacle is first probed. Often, an isolated filopodium changed its direction of growth after colliding with a trapped bead. In contrast, lamellipodia could remove an obstacle, often by growing underneath it and lifting it. Exploring filopodia exerted forces in the pN range, whereas migrating cells exert forces in the nN range[18]. A migrating neuron must be able to displace large obstacles; hence, it uses large forces. Filopodia gently explore their environment using only weak forces, and lamellipodia can exert a larger force opening the way for the growth cone. Thus, not only do neurons process information but they are also able to mechanically modify their environment by selecting forces varying from less than 1 pN to 1 nN[18]. Indeed,

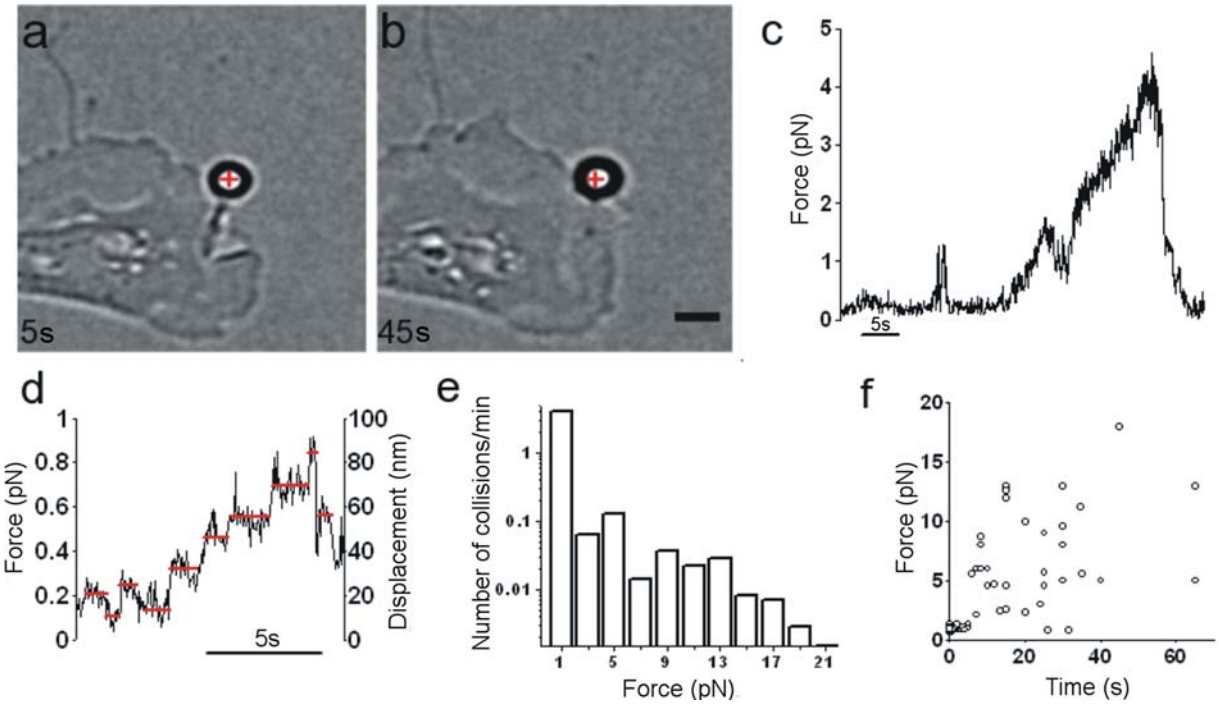

Figure 4. Force exerted by lamellipodia. (a–b) A lamellipodium growing and pushing a trapped bead. The red cross indicates the equilibrium position inside the optical trap. Scale bar, 2 μm. **(c)** F_{neu} in the x,y plane obtained from a QPD recording. Trap stiffness was 0.009 pN nm^{-1}. **(d)** The force exerted by a lamellipodium showing step-like jumps. Red lines, drawn by eye, indicate presumed discrete levels. The QPD recording was sub-sampled and filtered at 50 Hz. After low-pass filtering, the value of σ was reduced to 0.05 pN. Trap stiffness was 0.01 pN nm^{-1}. **(e)** Histogram of forces measured during collisions between lamellipodia and trapped beads. Data reflect 65 experiments, each lasting 2 min. **(f)** Scatter plot of force duration for the collisions shown in (e).
doi:10.1371/journal.pone.0001072.g004

differentiating neurons sense the mechanical and chemical properties of barriers in front of their neurites and appear to have smart molecular motor planning, which guides and modifies the ultimate direction taken by neurites in the developing nervous system. Notably, these capabilities are in sharp contrast with metal and/or silicon components used for commercial information processing, which lack motility and motor planning.

MATERIALS AND METHODS

Rats (P10−12) were anesthetized with CO2 and sacrificed by decapitation in accordance with the Italian Animal Welfare Act. DRGs were incubated with trypsin (0.5 mg/ml), collagenase (1 mg/ml), and DNase (0.1 mg/ml) in 5 ml Neurobasal medium in a shaking bath (37°C, 35–40 min). They were mechanically dissociated, centrifuged at 300 rpm, resuspended in culture medium, and plated on poly-L-lysine-coated (0.5 ug/ml) coverslips. Cells were incubated for 24 to 48 h, and nerve growth factor (50 ng/ml; Alomone, Israel) was added before measurements were obtained.

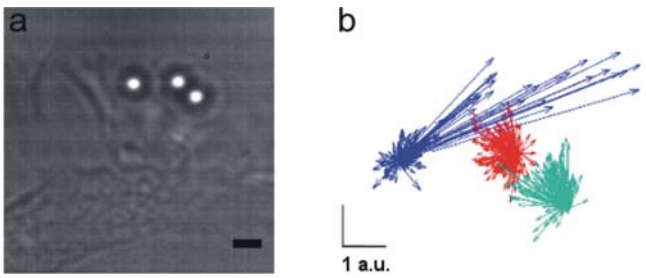

Figure 5. Force field exerted by lamellipodia. (a) A lamellipodium colliding with three trapped beads. **(b)** Direction and amplitude (in arbitrary units, a.u.) of forces exerted on the three beads. Superposition of bead displacements was obtained by video tracking at 5 Hz from a 4-min recording. Scale bar, 2 μm.
doi:10.1371/journal.pone.0001072.g005

The optical tweezers setup was built as previously described.[41] The dish containing the differentiating neurons and the beads (PSI-1.0NH2; G.Kisker GbR, Steinfurt, Germany) was placed on a microscope stage, which could be moved by a 3-axis piezoelectric nanocube (17 MAX 301; Melles Griot Inc., USA). The temperature of the dish was maintained at 37°C using a Peltier device. Bead position was determined in the x,y plane with an accuracy of 10 nm, using back focal plane (BFP) detection which relies on the interference between forward scattered light from the bead and unscattered light[22,42]. The BFP of the condenser was imaged onto a QPD, and the light was converted to differential outputs digitized at 4 kHz and low-pass filtered at 2 kHz. The bead displacement d = (dx,dy) from the equilibrium position inside the optical trap was also determined by video tracking using correlation methods with sub-pixel resolution. The lateral trap stiffness κx,y = (kx,ky) and the detector sensitivity were calibrated using the power spectrum method[22], with voltage signals filtered and digitized at 5 and 20 kHz, respectively. For multiple trapping experiments, computer-generated diffractive optical elements were projected onto the liquid crystal display of the phase-programmable modulator (PPM X8267-11; Hamamatsu Photonics, Japan)[41,43] in order to generate multiple spots in the specimen with a Gaussian intensity profile. For experiments where a single Gaussian beam was required, the PPM was switched off. In multiple trapping experiments, only the direction of the force was determined but not its amplitude.

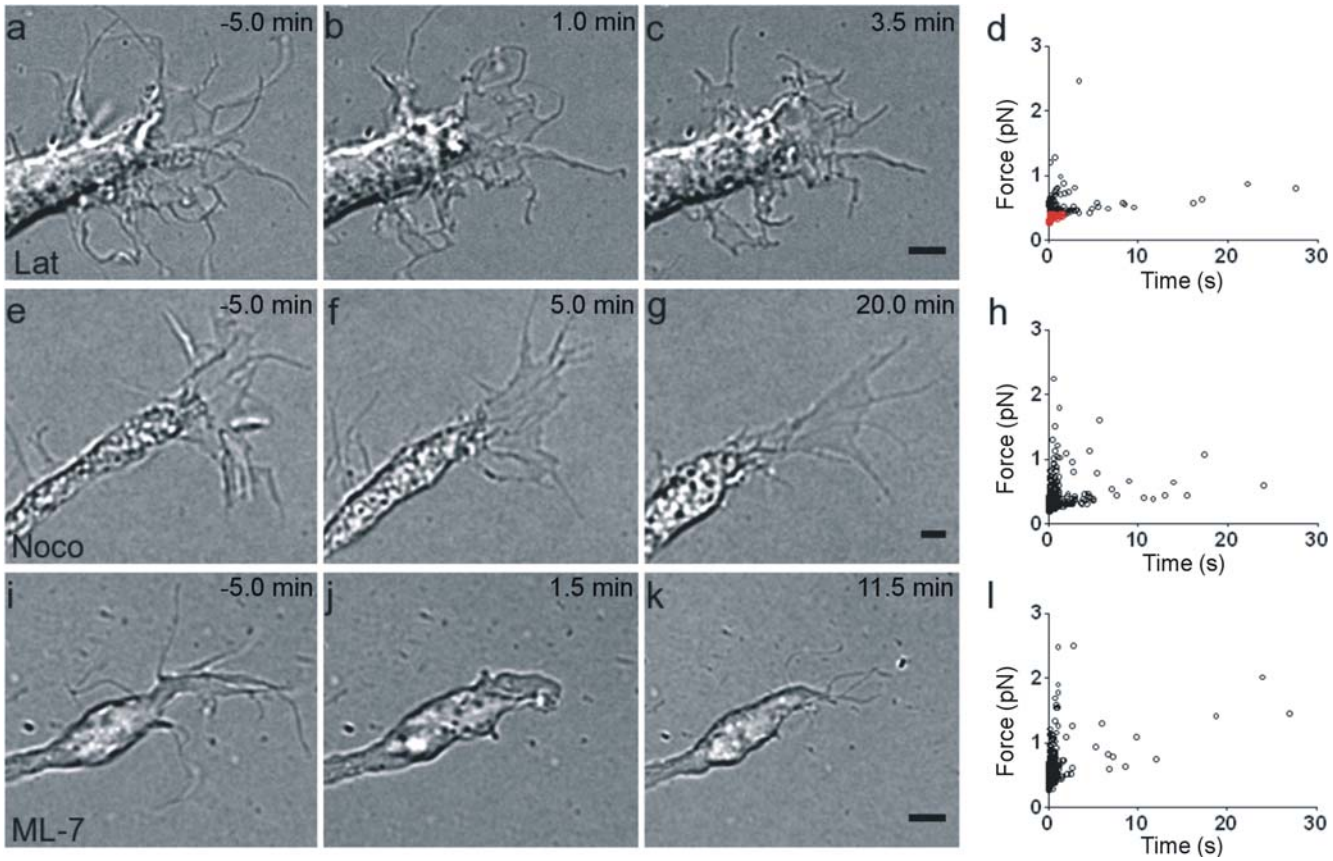

Figure 6. Effect of inhibitors on force exertion. A growth cone before **(a)** and after **(b–c)** application of 100 nM latrunculin A. No motion was observed after 3.5 min of exposure. **(d)** Scatterplot of force duration for collisions after application of 50 nM (black symbols) and 100 nM (red symbols) latrunculin A. A growth cone is shown before **(e)** and after **(f–g)** application of 50 nM nocodazole. The growth cone retracted, but filopodia continued to move for at least 30 min after drug exposure. **(h)** Scatterplot of force duration for collisions after application of 50 nM nocodazole. A growth cone is shown before **(i)** and after **(j–k)** application of 4 μM ML-7. Filopodia quickly retracted but then regrew and moved for at least 20 min after drug application. **(l)** Scatterplot of force duration for collisions after application of 4 μM ML-7. Scale bars, 2 μm. Drugs were added at time 0.
doi:10.1371/journal.pone.0001072.g006

For statistical analysis, QPD traces were low-pass filtered at 50 Hz. Collisions selected for statistical analysis had to satisfy three criteria: 1) maximal amplitude larger than 5σ, 2) duration longer than 100 ms, and 3) presence of a colliding filopodium or lamellipodium in contact with a bead verified by visual inspection of the movie. The collision duration was calculated as the interval between two consecutive crossings of 5σ. The force exerted by the neurite Fneu was calculated as -Ftrap. When the displacement of the bead from its equilibrium position inside the trap was less than 400 nm, Ftrap = (Fx, Fy) was calculated as Fx = dxkx and Fy = dyky[22]. When the bead was also moved along the vertical axis, the lateral displacement measured with the QPD was compared with data obtained from video tracking; the data were discarded if lateral displacements measured with the two methods differed by more than 50%. The axial force along the z axis was not measured.

SUPPORTING INFORMATION

Figure S1 (a–b) Another example of a collision between a protruding filopodium and a trapped bead . The filopodium grows and hits the trapped bead. Trap stiffness was 0.006 pN/nm. c: Fy from the QPD during the protrusion lateral of a–b. Scale bar, 2 μm. Numbers in the lower right corner indicate time in seconds.
Found at: doi:10.1371/journal.pone.0001072.s001 (3.29 MB TIF)

Movie S1 Movie of the motion of a growth cone imaged with time-lapse differential interference contrast (DIC) microscopy on the surface of the coverslip where the growth cone is located and at three focal planes 1, 2 and 3 μm above the coverslip. The four planes were scanned every 5 seconds. Filopodia are often seen in focus at 2 and 3 μm from the coverslip. (Acquisition rate: 5Hz; Scale bar, 2 μm). Numbers in the upper right corner indicate time in seconds.
Found at: doi:10.1371/journal.pone.0001072.s002 (1.97 MB MOV)

Movie S2 Movie of the collision between the growth cone and a trapped bead shown in Fig.1a–c. The trap stiffness was 0.02 pN/nm. The time of image acquisition is indicated in the corresponding frame (Acquisition rate: 5Hz; Scale bar, 2 μm). Numbers in the upper right corner indicate time in seconds.
Found at: doi:10.1371/journal.pone.0001072.s003 (4.95 MB MOV)

Movie S3 Movie of the lateral collision between the filopodium and a trapped bead shown in Fig.2a–b. The trap stiffness was 0.006 pN/nm. (Acquisition rate: 20Hz; Scale bar, 2 μm). Numbers in the upper right corner indicate time in seconds.
Found at: doi:10.1371/journal.pone.0001072.s004 (4.07 MB MOV)

Movie S4 Movie of the collision between the protruding filopodium and a trapped bead shown in Fig.2d–e. The trap stiffness was 0.006 pN/nm. (Acquisition rate: 20Hz; Scale bar, 2 μm). Numbers in the upper right corner indicate time in seconds.
Found at: doi:10.1371/journal.pone.0001072.s005 (4.45 MB MOV)

Movie S5 Movie of the collision between the protruding filopodium and a trapped bead shown in Supplementary Figure 1a–b. The trap stiffness was 0.006 pN/nm. (Acquisition rate: 20Hz; Scale bar, 2 μm). Numbers in upper right corner indicate time in seconds.
Found at: doi:10.1371/journal.pone.0001072.s006 (3.60 MB MOV)

Movie S6 Movie of the collision between the lamellipodium and a trapped bead shown in Fig.4a–b. The trap stiffness was 0.02 pN/nm. (Acquisition rate 20Hz; Scale bar, 2 μm). Numbers in upper right corner indicate time in seconds.
Found at: doi:10.1371/journal.pone.0001072.s007 (3.20 MB MOV)

ACKNOWLEDGMENTS

We thank Walter Vanzella (Glance Vision Technologies) for computational support.

Author Contributions

Conceived and designed the experiments: VT DC ED. Performed the experiments: EF FD RS. Analyzed the data: DC EF FD RS JL. Contributed reagents/materials/analysis tools: RS JL MR. Wrote the paper: VT DC ED.

REFERENCES

1. Solecki DJ, Govek EE, Hatten ME (2006) mPar6 alpha controls neuronal migration. J Neurosci 26: 10624–10625.
2. Ghashghaei HT, Lai C, Anton ES (2007) Neuronal migration in the adult brain: are we there yet? Nat Rev Neurosci 8: 141–151.
3. Goodman CS (1996) Mechanisms and molecules that control growth cone guidance. Annu Rev Neurosci 19: 341–377.
4. Bray D, Thomas C, Shaw G (1978) Growth cone formation in cultures of sensory neurons. Proc Natl Acad Sci U S A 75: 5226–5229.
5. Gordon-Weeks PR (2004) Microtubules and growth cone function. J Neurobiol 58: 70–83.
6. Song H, Poo M (2001) The cell biology of neuronal navigation. Nat Cell Biol 3: E81–E88.
7. Gallo G, Letourneau PC (2000) Neurotrophins and the dynamic regulation of the neuronal cytoskeleton. J Neurobiol 44: 159–173.
8. Aletta JM, Greene LA (1988) Growth cone configuration and advance: a time-lapse study using video-enhanced differential interference contrast microscopy. J Neurosci 8: 1425–1435.
9. Gomez TM, Letourneau PC (1994) Filopodia initiate choices made by sensory neuron growth cones at laminin/fibronectin borders in vitro. J Neurosci 14: 5959–5972.
10. Baker MW, Macagno ER (2007) In vivo imaging of growth cone and filopodial dynamics: evidence for contact-mediated retraction of filopodia leading to the tiling of sibling processes. J Comp Neurol 500: 850–862.
11. Galbraith CG, Yamada KM, Galbraith JA (2007) Polymerizing actin fibers position integrins primed to probe for adhesion sites. Science 315: 992–995.
12. Mongiu AK, Weitzke EL, Chaga OY, Borisy GG (2007) Kinetic-structural analysis of neuronal growth cone veil motility. J Cell Sci 120: 1113–1125.
13. Janson ME, de Dood ME, Dogterom M (2003) Dynamic instability of microtubules is regulated by force. J Cell Biol 161: 1029–1034.
14. Kovar DR, Pollard TD (2004) Insertional assembly of actin filament barbed ends in association with formins produces piconewton forces. Proc Natl Acad Sci U S A 101: 14725–14730.
15. Marcy Y, Prost J, Carlier MF, Sykes C (2004) Forces generated during actin-based propulsion: a direct measurement by micromanipulation. Proc Natl Acad Sci U S A 101: 5992–5997.
16. Kerssemakers JW, Munteanu EL, Laan L, Noetzel TL, Janson ME, et al. (2006) Assembly dynamics of microtubules at molecular resolution. Nature 442: 709–712.
17. Footer MJ, Kerssemakers JW, Theriot JA, Dogterom M (2007) Direct measurement of force generation by actin filament polymerization using an optical trap. Proc Natl Acad Sci U S A 104: 2181–2186.
18. Prass M, Jacobson K, Mogilner A, Radmacher M (2006) Direct measurement of the lamellipodial protrusive force in a migrating cell. J Cell Biol 174: 767–772.
19. Howard J (2001) Mechanics of Motor Proteins and the Cytoskeleton. Sunderland, MA: Sinauer Associates, Inc.
20. Ashkin A (1997) Optical trapping and manipulation of neutral particles using lasers. Proc Natl Acad Sci U S A 94: 4853–4860.
21. Bustamante C, Macosko JC, Wuite GJ (2000) Grabbing the cat by the tail: manipulating molecules one by one. Nat Rev Mol Cell Biol 1: 130–136.
22. Neuman KC, Block SM (2004) Optical trapping. Rev Sci Instrum 75: 2787–2809.
23. Giannone G, Dubin-Thaler BJ, Dobereiner HG, Kieffer N, Bresnick AR, et al. (2004) Periodic lamellipodial contractions correlate with rearward actin waves. Cell 116: 431–443.
24. Dent EW, Kalil K (2001) Axon branching requires interactions between dynamic microtubules and actin filaments. J Neurosci 21: 9757–9769.
25. Pralle A, Prummer M, Florin EL, Stelzer EH, Horber JK (1999) Three-dimensional high-resolution particle tracking for optical tweezers by forward scattered light. Microsc Res Tech 44: 378–386.
26. Bovolenta P, Mason C (1987) Growth cone morphology varies with position in the developing mouse visual pathway from retina to first targets. J Neurosci 7: 1447–1460.
27. Myers KA, He Y, Hasaka TP, Baas PW (2006) Microtubule transport in the axon: Re-thinking a potential role for the actin cytoskeleton. Neuroscientist 12: 107–118.
28. Mogilner A, Oster G (1996) Cell motility driven by actin polymerization. Biophys J 71: 3030–3045.
29. Mogilner A (2006) On the edge: modeling protrusion. Curr Opin Cell Biol 18: 32–39.
30. Raucher D, Sheetz MP (2000) Cell spreading and lamellipodial extension rate is regulated by membrane tension. J Cell Biol 148: 127–136.
31. Mogilner A, Rubinstein B (2005) The physics of filopodial protrusion. Biophys J 89: 782–795.
32. Atilgan E, Wirtz D, Sun SX (2006) Mechanics and dynamics of actin-driven thin membrane protrusions. Biophys J 90: 65–76.
33. Guan KL, Rao Y (2003) Signalling mechanisms mediating neuronal responses to guidance cues. Nat Rev Neurosci 4: 941–956.
34. Pollard TD, Blanchoin L, Mullins RD (2000) Molecular mechanisms controlling actin filament dynamics in nonmuscle cells. Annu Rev Biophys Biomol Struct 29: 545–576.
35. Grunwald IC, Klein R (2002) Axon guidance: receptor complexes and signaling mechanisms. Curr Opin Neurobiol 12: 250–259.
36. Huber AB, Kolodkin AL, Ginty DD, Cloutier JF (2003) Signaling at the growth cone: ligand-receptor complexes and the control of axon growth and guidance. Annu Rev Neurosci 26: 509–563.
37. du Roure O, Saez A, Buguin A, Austin RH, Chavrier P, et al. (2005) Force mapping in epithelial cell migration. Proc Natl Acad Sci U S A 102: 2390–2395.
38. Dai J, Sheetz MP (1995) Mechanical properties of neuronal growth cone membranes studied by tether formation with laser optical tweezers. Biophys J 68: 988–996.
39. Liu AP, Fletcher DA (2006) Actin polymerization serves as a membrane domain switch in model lipid bilayers. Biophys J 91: 4064–4070.
40. Gittes F, Mickey B, Nettleton J, Howard J (1993) Flexural rigidity of microtubules and actin filaments measured from thermal fluctuations in shape. J Cell Biol 120: 923–934.
41. Cojoc D, Emiliani V, Ferrari E, Malureanu R, Cabrini S, et al. (2004) Multiple Optical Trapping by Means of Diffractive Optical Elements. Jpn J Appl Phys 43: 3910–3915.
42. FGittes, Schmidt C (1998) Interference model for back-focal-plane displacement detection in optical tweezers. Opt Lett 23: 7–9.
43. Dufresne ER, Spalding GC, Dearing MT, Sheets SA (2001) Computer-Generated Holographic Optical Tweezer Arrays. Review of Scientific Instruments 72: 1810–1816.

4.2

Force generation in lamellipodia is a probabilistic process with fast growth and retraction events

Shahapure R., Difato F., Laio, A., Cojoc D., Ferrari E. , Laishram J., Bisson G. & Torre V.

Submitted to PNAS

BIOLOGICAL SCIENCES/ BIOPHYSICS

Force generation in lamellipodia is a probabilistic process with fast growth and retraction events

Shahapure R.[*], Difato F.[*,†], Laio, A.[*], Cojoc D.[‡], Ferrari E.[‡], Laishram J.[*], Bisson G.[*] & Torre V.[*,†]

[*]*International School for Advanced Studies (SISSA-ISAS), Trieste, Italy.* [†]*Italian Institute of Technology, ISAS Unit, Italy.* [‡]*CNR-INFM Laboratorio Nazionale TASC, 34012 Trieste, Italy*

Corresponding Author:

Vincent Torre

International School for Advanced Studies (SISSA)

Area Science Park, S.S.14, Q1 Building.

Basovizza,

Trieste-34012

ITALY

Phone: +39 040 3756 513

Fax: +39 040 3756 502

Email: torre@sissa.it

Manuscript information:

Number of text pages (including references and figure legends): 15

Number of figures: 5

Abbreviations:

Bold notations **x**, **v**, and **F** indicate vectorial quantities and x, v and F indicate either the modulus or a component of these vectors.

Abstract

Polymerization of actin filaments is the primary source of motility in lamellipodia and is controlled by a variety of regulatory proteins. The underlying molecular mechanisms are only partially understood and a precise determination of dynamical properties of force generation is necessary. Using optical tweezers we have measured with millisecond temporal resolution and pN sensitivity the force-velocity (Fv) relationship and the power dissipated by lamellipodia of dorsal root ganglia (DRG) neurons. When force and velocity are averaged over 3-5 s, the Fv relationships can be flat. On a finer time scale, random occurrence of fast growths and sub-second retractions become predominant. Maximal power dissipated by lamellipodia over a silica bead with a diameter of 1 μm is 10^{-16} W. Our results clarify the dynamical properties of force generation: i - force generation is a probabilistic process; ii - underlying biological events have a bandwidth up to at least 10 Hz; iii - fast growths of lamellipodia leading edge alternate with local retractions.

Introduction

Neurons are among the most specialized cells in living organisms and are capable to self organize in complex networks, formed by billions of individual cells, at the basis of higher brain functions. In order to develop a network, neurons protrude to form neurites, highly motile structures exploring the environment in search of the appropriate chemical cues necessary for the formation of the correct synaptic connections (1-3). The neurite's search is guided by growth cones (4-6) located at their tip, formed by an extended lamellipodium from which thin filopodia emerge (7). Filopodia tips can move at a speed up to 0.8-1 $\mu m\ s^{-1}$ and their motility is at the basis of the efficient formation of neural networks. Due to its enormous importance, this system has been the object of intense experimental and theoretical investigation. The primary source of motility in growth cones is the polymerization of actin filaments (8, 9), a process controlled by a variety of regulatory proteins (10). The addition of actin polymers to actin filaments in close contact with the membrane pushes the cellular membrane forward exerting a protrusive force (11, 12). The overall dynamics regulating this process is not yet clear and mathematical modeling provides a way to link known molecular events to force generation (1). A key outcome of these models is represented by the so-called Fv relationships, describing how the force F exerted by the actin filament network is related to the velocity v of their growing ends (8, 13-17). Fluctuations of contacts between the tip of actin filaments and the surrounding membrane is an essential feature of Brownian ratchet models (8, 13, 14) leading to Fv relationships in which v decreases exponentially with increasing values of F. In autocatalytic models (17, 18) when an obstacle is encountered the actin network, due to the action of controlling proteins, originates new branches, so that the velocity v can remain constant with increasing values of F. The experimental investigation of the molecular events underlying force generation in growth cones requires a precise measurement of Fv relationships with high temporal resolution and sensitivity. Previous determinations of the Fv relationships (19) with an Atomic Force Microscope (AFM) cantilever (20, 21) had a limited time resolution and were obtained either in vitro or in migrating keratocytes exerting forces in the nN range.

In this work, by using optical tweezers (22-24), we provide an experimental characterization of Fv relationships in neuronal growth cones with a millisecond resolution and pN sensitivity. This experimental technique enabled us to determine the three components of the force $\mathbf{F} = (F_x,F_y,F_z)$ exerted by a lamellipodium from rat dorsal root ganglia (DRG) and of the velocity $\mathbf{v} = (v_x,v_y,v_z)$ of its

leading edge. From these vectorial quantities we have derived several properties of force generation in lamellipodia that have important biological consequences. We find that force generation in lamellipodia is an intrinsically multi-scale process. At a temporal resolution of 3-5 s, the exerted force can increase, maintaining a constant velocity, where the Fv relationships are almost flat. At a millisecond resolution, a much more complex behavior is observed, with random occurrence of fast growths and sub-second retractions. Our results show that autocatalytic models (15, 17, 18) of force generation are correct in a mean approximation. At a higher temporal resolution the network of actin filaments evolves in a much more complex manner that can be characterized only probabilistically. Fast forward motions consuming up to 10^4 molecules of ATP s^{-1} μm^{-2} alternate with local catastrophes, whose duration has a power law distribution. These results provide a precise characterization of the dynamics of force generation in lamellipodia, necessary to understand the biochemical events underlying force generation.

Results

DRG neurons isolated from P10-P12 rats were plated on poly-L-lysine-coated glass coverslips, positioned on the stage of an inverted microscope used for imaging and measuring forces (see Methods). After 1 or 2 days of incubation, neurites emerged from the DRG soma and their motion was analysed. Filopodia and lamellipodia moved rapidly exploring the three dimensional (3D) space in all directions, which, in some occasions, could have a tip velocity as high as 1 $\mu m\ s^{-1}$. DRG lamellipodia were imaged with Atomic Force Microscopy (Fig.1a) and the height of their leading edges varied from 45 to 660 nm (Fig.1b). Silica beads of 1 μm diameter were trapped with a 1064 nm infrared (IR) laser tweezers and positioned in front of the leading edge of a lamellipodium (Fig 1e). When the centre of the bead is located at about 800 nm above the coverslip, a thick lamellipodium can push the bead (Fig.1c). Visual inspection of lamellipodia indicates the existence of four stereotyped behaviours (25): (i) the lamellipodium grows underneath the bead without displacing it (Fig.1d); (ii) the bead seals to the cell membrane and when the lamellipodium retracts the bead is pulled away from the trap; (iii) the lamellipodium grows underneath the bead displacing it upwards and eventually moving it in a "shovel-like" manner (26); (iv) the lamellipodium pushes the bead forward exerting a force in the direction of its growth (Figs.3a and b). Often, two or more of these stereotyped behaviours were observed in the same experiment. In the example illustrated in Fig.1f, initially the lamellipodium pushed the bead

upwards by some hundreds nm (at 68.2 s) and the bead returned into the equilibrium position inside the trap following lamellipodium retraction (at 94 s). After a few seconds, the lamellipodium grew under the bead and, because of the presence of adhesion forces, the bead sealed to the lamellipodium membrane. Finally, when the lamellipodium retracted, it dragged away the bead from the trap (after 100 s). Force velocity relationships were computed only from those experiments in which the lamellipodium pushed the bead and then retracted (events of type iv). In all experiments, the growth cone behaviour was followed with video imaging and the displacement of the bead $\mathbf{x} = (x, y, z)$ was measured with a high temporal resolution using a Quadrant Photo Diode (QPD). The z axis is perpendicular to the coverslip and parallel to the IR laser beam used for optical trapping. By determining the trap stiffness $\mathbf{k} = (k_x, k_y, k_z)$, $\mathbf{F}$ was obtained as $(-x\ k_x, -y\ k_y, -z\ k_z)$ (23, 27).

At a low temporal resolution the force can increase with an almost constant velocity and the Fv relationships can be flat

When lamellipodia pushed the bead upwards, they exerted forces up to 20 pN. In the case of the experiment shown in Fig.1, when the bead displacement was low pass filtered at 0.2 Hz (green trace in Fig.1g) corresponding to a temporal averaging over a time window of 3-5 s, the computed velocity v_z had little oscillations around an almost constant value.

From the smoothed values of F_z and v_z, the Fv relationship (green trace) shown in Fig.1h was obtained. The Fv relationship - following an initial rise – resulted almost flat, indicating that the lamellipodium can increase the exerted force while the velocity of its leading edge remains almost constant. Nearly identical results were obtained when Fv relationships were computed from the modulus of $\mathbf{F}$ and not from a single component (F_z).

An almost flat Fv relationship was observed in other 7/95 experiments but not in all of them. As it will be discussed later, force generation is not a deterministic event but a probabilistic process. The observation that, in some experiments, Fv relationships filtered at 0.2 Hz are flat, indicates that the overall dynamics assumed by autocatalytic models capture basic properties of force generation. These models predict that when the underlying system of actin filaments and controlling proteins have the time to self-reorganize, v becomes independent of F. Almost flat Fv relationships were obtained averaging the values of F and v in a time window of 3-5 s, which could be the time required by the underlying system of actin filaments to reorganize properly, as predicted by these models.

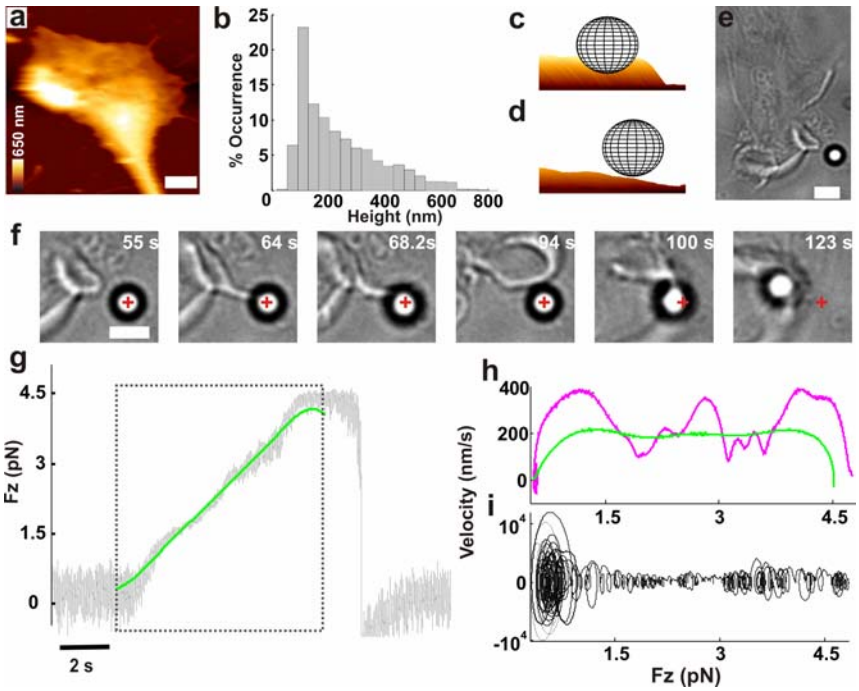

Fig. 1. (a) AFM image of a lamellipodium. The height is coded as in the coloured scale bar and horizontal scale bar (white), 2 µm**. (b)** Occurrence histogram of measured height of lamellipodium leading edges from 7 growth cones. **(c -d)** A 1 µm bead in front of a thick and a thin lamellipodium respectively. **(e)** Low resolution image of a lamellipodium in front of a bead trapped with an infrared laser. Scale bar, 2 µm. **(f)** Successive frames showing the lamellipodium (55 s) growing towards the bead (64 s) and lifting it up (68.2 s). Subsequently, the lamellipodium retracted (94 s) and grew under the bead pulling it out of the trap during retraction (100-123 s). Cross indicates the centre of the optical trap. Scale bar, 2 µm. **(g)** F_z (grey trace) used for computing the Fv relationship. The dotted box indicates the section of force measurement used to compute the Fv relationship after Gaussian filtering at 0.2 Hz (green trace). **(h-i)** Fv relationships obtained after smoothing at 0.2 Hz (green trace in h) at 1 Hz (pink trace in h) and at 10 Hz (i).

At a higher temporal resolution the velocity oscillates and transient periods of negative velocities are observed

Averaging a temporal series over a time window of 3-5 s corresponds to smoothing the data with a low pass filter with a bandwidth up to 0.2 Hz. This is a strong assumption, and, in order to determine if this cut-off frequency is appropriate, we investigated the bandwidth of biological events underlying force generation. We computed and compared the power spectrum density $PSD_{noise}(f)$ of forces measured far from any neuron (red inset in Fig.2a) - originating from Brownian fluctuations and instrumental noise - and the $PSD_{push}(f)$ of forces measured when the leading edge of the lamellipodium pushed the bead (blue inset). $PSD_{noise}(f)$ and $PSD_{push}(f)$ are very similar and almost indistinguishable for $f > 30$ Hz, but at frequencies below 1 Hz the energy of $PSD_{push}(f)$ is at least 30 times larger than that caused by Brownian collisions. The analysis of $PSD_{noise}(f)$ and $PSD_{push}(f)$ in 14 experiments

indicates that the bandwidth of biological events underlying force generation in DRG lamellipodia extends up to 10 Hz. Therefore, events occurring on a time scale of 100 ms cannot be neglected and force generation must be analysed at a temporal resolution higher than in previous investigations. In some experiments, we also observed 5-30 nm jumps of bead position occurring in less than 1 ms, which could constitute the elementary events underlying force generation (26).

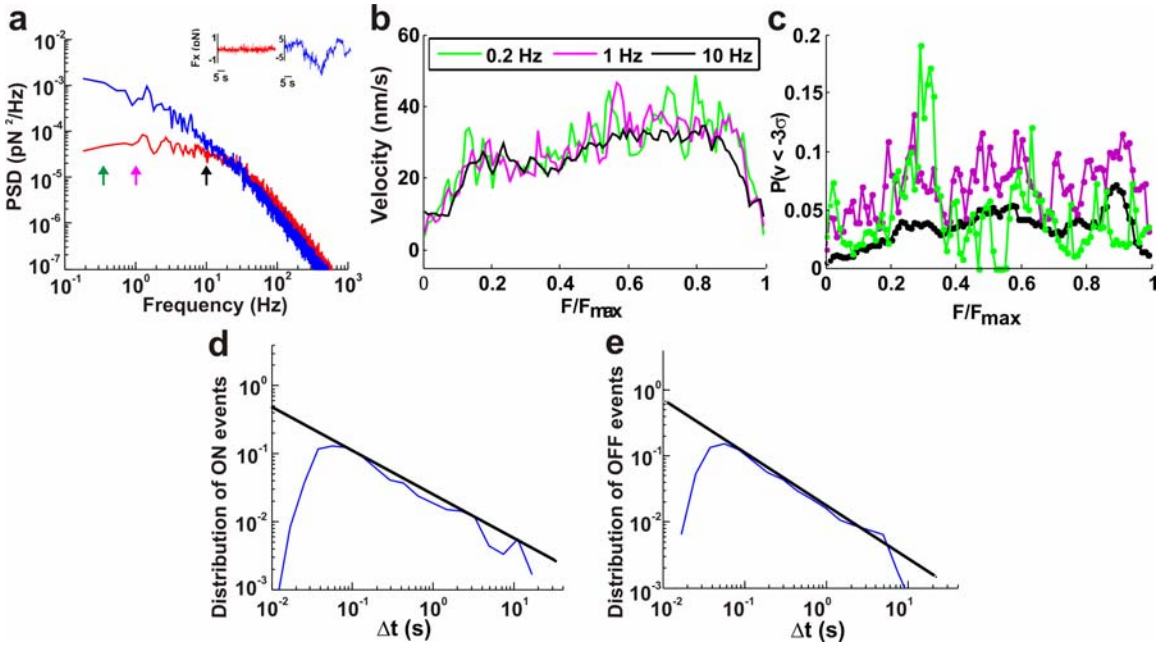

Fig. 2. (a) Power spectrum density of forces measured far from the lamellipodium (red trace) and when the lamellipodium pushed the bead (blue trace), computed from the red and blue traces respectively shown in the inset. Green, pink and, black arrows indicate 0.2, 1 and 10 Hz respectively. **(b)** Average $\langle Fv \rangle_x$ relationships from data filtered up to a bandwidth of X Hz. $\langle Fv \rangle_{0.2}$, (green trace), $\langle Fv \rangle_1$ (pink trace), and $\langle Fv \rangle_{10}$ (black trace). **(c)** Probability distribution p ($v<-3\ \sigma_v | F/F_{max}$) of velocities being less than $-3\sigma_v$ at fixed forces (F/F_{max}). Average Fv relationships from 95 experiments obtained from data filtered with a Gaussian filter at a cut-off frequency of 0.2 (green), 1 (red) and, 10 (blue) normalized to F_{max}. **(d-e)** Distribution of ON and OFF events, respectively. Black straight lines have a slope of -0.6 and -0.78 in (d) and (e) respectively.

We computed Fv relationships from the experiment of Fig.1g after smoothing at 0.2 (green trace in Fig.1h), 1 (pink trace in Fig.1h) and 10 Hz (Fig.1i). When data were smoothed at 1 and 10 Hz the velocity oscillated around an almost constant value of 200 nm s^{-1} reaching occasional peak values up to 1-10 μm s^{-1}. In the majority of the experiments (88/95) the shape of measured Fv relationships was not constant. Two examples are shown in Fig.1 and Fig.3. In some experiments (14/95) the lamellipodium pushed the bead and then retracted repetitively. Also in these cases the maximal force and the shape of Fv relationships measured at different times varied. These results suggest that force generation in lamellipodia is an inherently probabilistic process and does not follow a deterministic

mechanism. In order to characterize this probabilistic dynamics we attempted to determine *average* Fv relationships <Fv>. Forces measured in the individual experiments were normalized to the maximal exerted force F_{max}, defined as the maximal force beyond which the lamellipodium leading edge does not advance and the velocity is consistently negative for at least 10 s. This procedure was repeated for data filtered at 0.2, 1 and 10 Hz. The three average Fv relationships obtained in this manner exhibited the same overall behaviour (Fig.2b), with the velocity increasing together with the force, up to about 30 nm/s, and remaining approximately constant up to F_{max}. Thus, even if in the single events the Fv relationship can vary significantly, the average Fv relationship is flat, consistent with autocatalytic models.

Having observed the existence of periods during which lamellipodia leading edges have negative velocities, we asked whether these periods occurred at random times or occurred more frequently near the maximal measured force F_{max}. We computed the probability distribution of velocities being less than $-3\sigma_v$ at fixed forces F/F_{max}, $p(v < -3\sigma_v | F/F_{max})$, where σ_v is the standard deviation of Brownian fluctuations at a given bandwidth (see next section and Fig.3). This probability distribution was estimated from the 95 experimentally determined Fv relationships. The value of $p(v < -3\sigma_v | F/F_{max})$ varied between 0.05 and 0.1 (Fig.2c) and was nearly identical when it was derived from Fv relationships computed at 0.2, 1 and 10 Hz bandwidth. This result indicates that retractions of the lamellipodium leading edge are not triggered by a strong load but their occurrence is random.

Statistical properties of Fv relationships were characterized by measuring the distribution of time intervals (Δt) with a positive (Fig.2d) and a negative velocity (Fig.2e), representing the ON and OFF events of the lamellipodium leading edge. Detected ON and OFF events were seen using a bandwidth of 0.2 Hz. The distributions of the ON and OFF events obtained at the a bandwidth of 0.2 Hz do not have an exponential behaviour but exhibit a power law distribution of the type $\Delta t^{-0.7}$ (see straight lines in Figs.2d and e) over almost two log units, suggestive of a growth characterized by avalanches (28).

In some experiments, the lamellipodium (Fig.3a) pushed the bead causing a pure lateral displacement (Fig.3b) so that only F_x and F_y changed appreciably (Figs.3c and d), whereas F_z remained constant (Fig.3e). Transient retractions of the lamellipodium leading edge caused the appearance of knots i.e. those periods with a negative velocity in the Fv relationships (Figs.3g and h). Because of the limited spatial and temporal resolution of the CCD camera used, these transient retractions could not be confirmed by video imaging (Fig.3b). Therefore, we asked whether they could originate from

numerical artefacts and noise fluctuations. Indeed, the numerical computation of derivatives from noisy data is ill-conditioned (29) and negative velocities could be produced by the specific method used to compute the velocity from the displacement. Therefore, we compared two alternative methods to obtain the velocity from the displacement, such as Gaussian filtering and Linear regression. In Gaussian filtering the velocity is obtained from the displacement by its convolution with the derivative

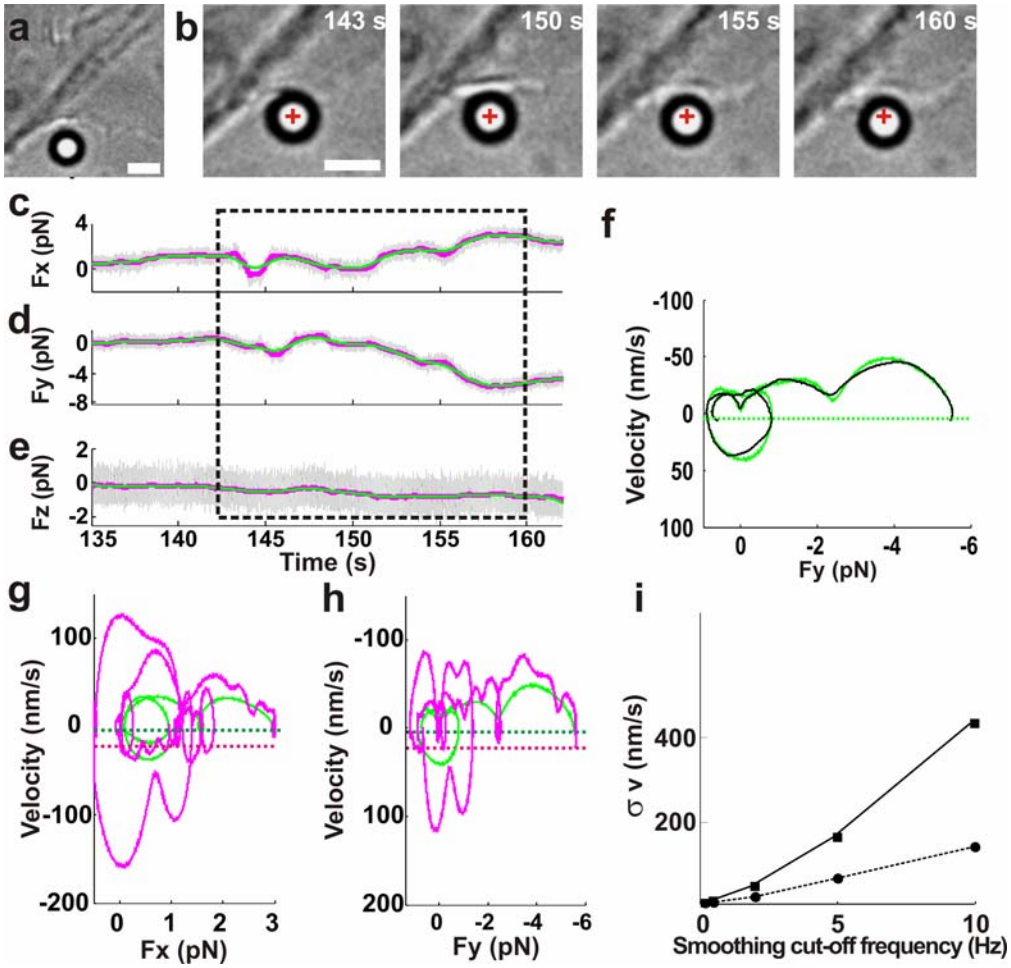

Fig. 3. (a) Low resolution image of a lamellipodium near the trapped bead. Scale bar, 2 µm. **(b)** Micrographs of the lamellipodium pushing the bead laterally during its protrusion. Images taken at different times during force generation as shown in panels c-e. Cross indicates the centre of the optical trap. Scale bar, 2 µm. **(c-e)** The three components F_x, F_y and F_z of force recordings used to compute the Fv relationships (grey trace) and after Gaussian filtering at 0.2 and 1 Hz (green and pink traces). The dotted box indicates the section of the recording used to compute Fv relationships in f-h. **(f)** Green and black Fv relationships computed with Gaussian filtering at 0.2 Hz and Linear regression, respectively. **(g-h)** Fv relationships computed with Gaussian filtering at 0.2 and 1 Hz (green and red traces) from the F_x and F_y component of the force. Dotted red and black lines represent $-3\sigma_v$ at the 0.2 and 1 Hz bandwidths, respectively. During the push F_y becomes negative and therefore, in panel h, transient retractions are associated to positive velocities. **(i)** Relationship between standard deviation of velocity distribution as a function of smoothing and for two trap stiffnesses of 0.005 pN/nm (squares) and 0.045 pN/nm (circles).

of a Gaussian function with a given cut-off frequency, while in the Linear regression method (see Methods) the velocity is obtained from the displacement and a linear interpolation of the data on a window containing W data points. In these two methods the time scale is given by the cut-off frequency of the Gaussian function and by the number of points W in the window, respectively. As shown in Fig.3f (compare green and black traces) the Fv relationships computed by the two methods from F_y had the same shape and number of knots.

However, as shown in Figs.3g and h, the number of knots in the Fv relationships computed for both the F_x and F_y components, increased when the bandwidth of Gaussian filtering increased from 0.2 to 1 Hz (green and pink traces respectively). As numerical differentiation is very sensitive to noise and it amplifies its high frequency components, we investigated at what extent the knots, are caused by Brownian fluctuations. We computed Fv relationships from force measurements obtained far from the lamellipodia. The obtained velocity was Gaussian distributed around 0, with a standard deviation σ_v increasing with the bandwidth of Gaussian filtering, depending also on the trap stiffness (Fig.3i). Periods with a negative velocity, less than $-3\sigma_v$, could not be ascribed to Brownian fluctuations and all negative velocities exceeding $-3\sigma_v$ lines (green and red dotted lines in Figs.3g and h) were caused by interactions with the lamellipodium: the $-3\sigma_v$ line was crossed several times and more often at larger bandwidths.

Lamellipodia dissipate power per unit area up to 10^{-16} W μm^{-2} during force generation

Having determined the Fv relationships and estimated the maximal exerted pressure, we asked how much mechanical work and power lamellipodia exert on encountered obstacles such as beads. In several occasions we have observed that the lamellipodium leading edge (Fig.4a) pushed the bead in an elaborated, non-linear way (Fig.4b) so that its motion was not a simple displacement in one preferred direction. In these experiments F_x, F_y, F_z change almost independently, reaching their maximum amplitude at different times (Fig.4c). In these cases, the bead motion is not a simple upward axial motion as in Fig.1, but the bead moves along a trajectory that often changes its direction (see black trace in Fig.4f). The knots in the Fv relationship described in the previous section are a consequence of these changes of direction. In order to investigate more quantitatively the nature of these events, it is useful to monitor the vectors $\mathbf{F}$ and $\mathbf{v}$, with their modulus and direction. The power dissipated by the lamellipodium is the scalar product $\mathbf{F} \circ \mathbf{v}$. The amplitude of the instantaneous velocity

depends on the bandwidth used for filtering the data and $\mathbf{F} \circ \mathbf{v}$ reaches values up to 4×10^{-18} W, when $\mathbf{v}$ is computed at a bandwidth of 0.2 Hz but up to 10^{-16} W at a bandwidth up to 10 Hz (Fig.4d).

The analysis of the angle ϕ between $\mathbf{F}$ and $\mathbf{v}$ provides useful information to understand the mechanics of collisions between beads and lamellipodia: when ϕ is close to 0 the lamellipodium pushes the bead and develops a positive work, and when ϕ is close to π the lamellipodium retracts. When the angle ϕ is close to $\pi/2$ lamellipodia do not perform any work. A negligible work is performed primarily in two occasions: firstly, when the lamellipodium exerts a force comparable with that caused by Brownian collisions with the surrounding medium molecules; secondly, when the bead slides over the lamellipodium and $\mathbf{F}$ becomes orthogonal to $\mathbf{v}$ and no work is generated. The angle ϕ was determined as $\phi = \text{Arccos}(\mathbf{F} \circ \mathbf{v} / |\mathbf{F}| |\mathbf{v}|)$ (Fig.4e). When the modulus of $\mathbf{F}$ was larger than 2 pN, ϕ was usually close to either 0 or to π (Fig.4h), indicating that $\mathbf{F}$ and $\mathbf{v}$ are parallel or antiparallel with an opposite versus.

In contrast, when the modulus of $\mathbf{F}$ is smaller than 2 pN (Fig.4g) the value of ϕ is most of the time close to $\pi/2$. A sudden change of the bead motion like those shown in Fig.4f could be caused either by a momentary sliding of the bead over the lamellipodium or by a transient retraction of the lamellipodium leading edge. The position of the lamellipodia was followed by video imaging with a CCD camera (see Figs.4a and b) and we could verify by visual inspection that the bead was always in contact with the lamellipodium leading edge. In addition, these two mechanisms can be easily distinguished observing the work: if the bead slides over the lamellipodium no work will be done and ϕ will remain close to $\pi/2$. Instead, if the lamellipodium transiently retracts, the work done by the lamellipodium will be negative and ϕ will remain close to π. With this procedure, we verified that periods with negative velocities analyzed in Fig.2 and Fig.3 were indeed associated to values of ϕ close to π and therefore were not caused by an occasional sliding of the bead but by transient retractions of the lamellipodium leading edge.

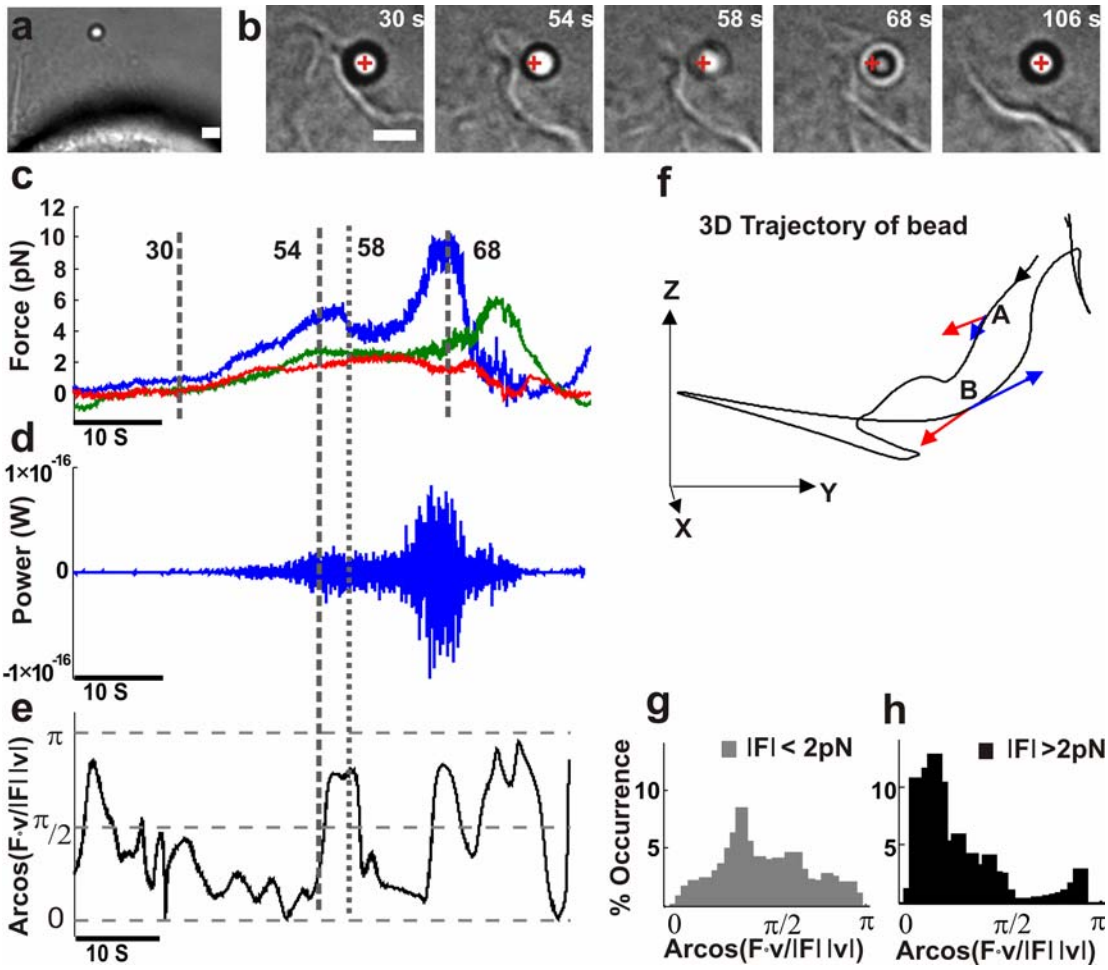

Fig. 4. (a) Low resolution image of a lamellipodium pushing a trapped bead. Scale bar, 2 µm. **(b)** Successive frames taken at different times during the push. Cross indicates the centre of the optical trap. Scale bar, 2 µm. **(c)** Three components of the force F_x (blue), F_y (green) and F_z (red) exerted by a lamellipodium during the push smoothed at 10 Hz. **(d)** Instantaneous power $\mathbf{F}\circ\mathbf{v}$ acting on the bead. **(e)** Time evolution of Arcos($\mathbf{F}\circ\mathbf{v}$ / $|\mathbf{F}|\,|\mathbf{v}|$) during the push. Data obtained after smoothing at 0.2 Hz. **(f)** The trajectory of the bead in a 3D space. The black arrow indicates the direction of the trajectory. Red and blue arrows on A and B indicate the instantaneous **F** and **v** respectively at the two times corresponding to 54 and 58 s in panels b-e. When **F** and **v** are parallel Arcos($\mathbf{F}\circ\mathbf{v}$ / $|\mathbf{F}|\,|\mathbf{v}|$) is close to 0 and when **F** and **v** are antiparallel Arcos($\mathbf{F}\circ\mathbf{v}$ / $|\mathbf{F}|\,|\mathbf{v}|$) is close to π. **(g)** Histogram of the Arcoss ($\mathbf{F}\circ\mathbf{v}$ / $|\mathbf{F}|\,|\mathbf{v}|$) when $|\mathbf{F}|$ was smaller than 2 pN. **(h)** Histogram of the Arcoss ($\mathbf{F}\circ\mathbf{v}$ / $|\mathbf{F}|\,|\mathbf{v}|$) when $|\mathbf{F}|$ was larger than 2 pN.

Discussion

The present manuscript provides a precise characterization of force generation in DRG lamellipodia with millisecond time resolution and pN sensitivity. Previous measurements made with the cantilever of an AFM were restricted to a temporal resolution in the second range and were obtained in migrating keratocytes producing forces in the nN range (21). By using optical tweezers we

measured force generation in DRG growth cones and we could characterize several physical properties of the molecular network underlying force generation. As shown in Fig.2, relevant biological events occur on a time scale of less than 100 ms and different dynamical properties are seen at a time scale of 3-5 s. Our results show that: i - force generation is not a deterministic mechanism but follows a probabilistic process; ii - underlying dynamical events occur on different time scales varying from 100 ms to 5 s; iii - fast growths alternate to local retractions of the lamellipodium leading edge. These results shed a new light on the biochemical network controlling force generation in neuronal growth cone lamellipodia (10, 30, 31).

Physical properties of force generation

The maximal force exerted by pushing lamellipodia on a bead with a diameter of 1 μm was about 20 pN (24). In some experiments this force clearly stopped the lamellipodium growth and could be identified as the stall force F_{stall}, i.e. the force that is able to block protrusion. As very often lamellipodia retract spontaneously, in most experiments F_{stall} was expected to be larger than the maximum force that was measured, F_{max}. The contact area between pushing lamellipodia and beads was determined by the analysis of video images of the event under examination. For all frames i corresponding to a detectable force measured with the QPD, we determined the arc Γ_i of the bead in close contact with the leading edge of the lamellipodium and the corresponding angle $2\theta_i$ on the bead center, as shown in red in Figs.5a-c.

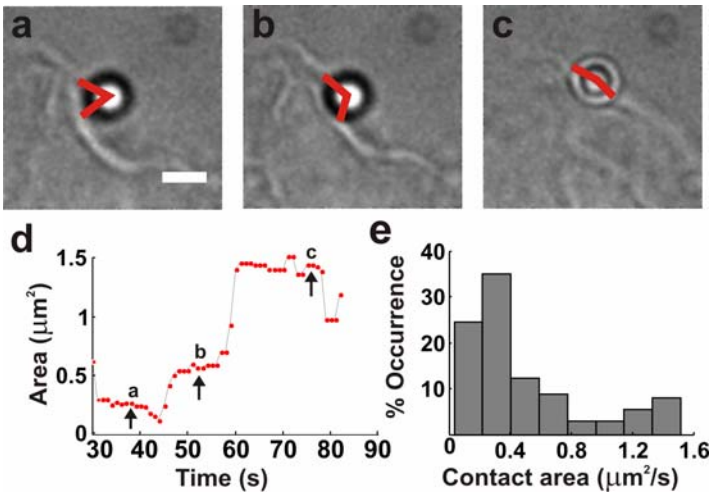

Fig. 5. (a-c) Micrographs of a lamellipodium pushing the bead at different times (see time scale in d). Scale bar, 2 μm. Red angles drawn by eye. (**d**) Evolution of estimated contact area S_c during the push. (**e**) Histograms of the value of S_c obtained from 4 experiments during which lamellipodia pushed the bead.

Then the contact surface at frame i, $S_c(i)$, is assumed to be equal to the corresponding spherical cap of the bead. Simple geometrical formulae indicate that $S_c(i) = 2\,\pi\,(1-\cos\theta_i)\,r^2$, where r is the bead radius. Fig.5d reproduces the time evolution of the estimated value of S_c when a lamellipodium pushed a bead. The value of S_c varied from 0.25 to 1.57 μm^2 (Fig.5e). Therefore, the maximal pressure exerted by DRG lamellipodia was 20-80 pN μm^{-2}. The maximum power per unit area exerted by lamellipodia was estimated to be $1\text{-}4\times10^{-16}$ W μm^{-2}. The hydrolysis of one molecule of ATP provides energy of about 10^{-19} J (32) and, if this energy is converted into work with an efficiency of 60%, the hydrolysis of about $0.25\text{-}1\times10^{4}$ s^{-1} of ATP per μm^2 is necessary to produce the measured power. The number of actin filaments in keratocyte and fibroblast lamellipodia has been estimated to be of the order of 100 per μm^2 (21). Therefore, the number of elementary motors per μm^2 is likely to be of the order of 100, where each elementary motor consumes approximately 25 to 100 ATP per second.

Fv Relationships

When position and force were filtered at 0.2 Hz, in some experiments, the pushing lamellipodia exerted an increasing force maintaining a constant velocity (Fig.1h). In the great majority of the experiments performed, however, force generation was characterized by large fluctuations of the velocity. This shows that force generation in lamellipodia is probabilistic in nature and only *average* <Fv> relationships (Fig.2b) exhibit a flat shape, during which the mean velocity remains constant while the force can increase. Therefore, autocatalytic models correctly describe force generation in a mean approximation. In individual experiments, the velocity does not remain constant but oscillates and can become negative. In these experiments, the same force can be exerted with a positive and negative velocity, a characteristic feature of systems exhibiting hysteresis (20). The time duration of periods with a negative velocity has a power law distribution reminiscent of self-organized systems near criticality (28). During these events, the force exerted on the bead by the lamellipodium acts in the opposite direction of its velocity, indicating that the bead is not simply sliding on the membrane, but that the actin filaments network is retracting, possibly due to local catastrophe or organized depolymerization controlled by cofilin and other severing proteins (10). Therefore, force generation is not a smooth process but it is characterized by a random alternation of fast growths and retractions of the lamellipodia leading edges.

Possible mechanisms underlying local retractions

What could be the mechanism underlying the unstable dynamics responsible for the frequent occurrence of negative velocities of lamellipodia leading edge? Proteins controlling the network of actin filaments, such as cofilin, could randomly sever a large branch of actin filaments leading to a local catastrophe causing a transient retraction of lamellipodium leading edge. Although the occurrence of local catastrophes seems the most likely biological mechanisms underlying local transient retractions, it is possible that instability could originate also from interactions with the cellular membrane. Growing and branching of the actin filaments can also be instable because of the action of membrane tension. Indeed, the maximum measured force F_{max} is approximately 20-100 $pN/\mu m^2$, of the same order of the force exerted by a membrane with a surface tension γ equal to 0.005 k_BT/nm^2 axially deformed by 1 μm (33). The actin filament network is confronted with a membrane exerting a force similar to F_{max}, so that the actin filament network is only marginally stable and its propulsive force is almost counterbalanced by the membrane tension. Growing and retracting in conditions of marginal stability allows fast reactions and could provide lamellipodia the flexibility necessary for its physiological functions.

In conclusion, autocatalytic models (15, 17, 18) capture basic molecular mechanisms underlying force generation in a mean approximation. The network of actin filaments underlying force generation in lamellipodia, besides giving origin almost continuously to new branches of actin filaments, grows in a probabilistic way with fast forward motions consuming up to 10^4 molecules of ATP s^{-1} μm^{-2} alternating with local catastrophes, whose duration have a power law distribution.

Methods

Neuron preparation

Wistar rats (P10−12) were anesthetized with CO_2 and sacrificed by decapitation in accordance with the Italian Animal Welfare Act. DRGs were incubated with trypsin (0.5 mg/ml), collagenase (1 mg/ml), and DNase (0.1 mg/ml) in 5 ml Neurobasal medium in a shaking bath (37º C, 35-40 min). They were mechanically dissociated, centrifuged at 300 rpm, resuspended in culture medium, and plated on poly-L-lysine (PLL)-coated (0.5 μg/ml) 30 mm coverslips in Neurobasal medium containing 10% fetal bovine serum (FBS) at a density of 2.5 x 10^5 cells/cm^2. Cells were incubated for 24 to 48 hours before the measurements. At this stage, filopodia tips and lamellipodia leading edge could move

at a speed of 1 μm s^{-1}. After 2-3 days plated neurons formed a dense network and the growth cones motion was drastically reduced.

AFM imaging

We determined the three dimensional (3D) structure of DRG lamellipodia and filopodia using Atomic Force Microscopy (AFM). Before imaging with AFM, DRG neurons were fixed with Glutaraldehyde. DRG growth cones were imaged using a commercial AFM (Nanowizard II, JPK Berlin) combined with an inverted optical microscope (Zeiss Axiovert 200), and a fluorescence set-up (Zeiss X-cite). Soft tips from VEECO with low force constant (OBL, 0.03N/m) were utilized and forces were kept between 100 pN and 1 nN during scanning.

Optical tweezers set-up

The optical tweezers set-up was built as described in (24). The dish containing the differentiating neurons and the beads (PSI-1.0NH2, G.Kisker GbR, Steinfurt Germany) was placed on the microscope stage which could be moved by a 3 axes piezoelectric nanocube (17 MAX 301, Melles Griot Inc., USA). The temperature of the dish was kept at 37º C by a Peltier device. The dish was maintained in an environment providing a controlled level of CO_2 (5%) and moisture (95%). The bead position $\mathbf{x} = (x,y,z)$ was determined along all the axes (x, y and z) with an accuracy of 10 nm using back focal plane (BFP) detection, which relies on the interference between forward scattered light from the bead and unscattered light (23, 27, 34). The BFP of the condenser was imaged onto a quadrant position detector (QPD; Hamamatsu C5460SPL 6041) and the light intensity was converted to differential outputs digitized at 20 kHz and low pass filtered at 5 kHz. Bead z position was determined using the Gouy phase shift effect (23). The trap stiffness $\mathbf{K}_{x,y,z}=(k_x,k_y,k_z)$ and the detector sensitivity were calibrated using the power spectrum method (23). Detector sensitivity was also checked by measuring voltage signals originating from displacements of a bead stuck to the coverslip obtained with the 3 axis piezoelectric nanocube. The force exerted by the lamellipodium $\mathbf{F}$ was taken as equal to $-\mathbf{F}_{\mathbf{trap}}$. When the displacement of the bead from its equilibrium position inside the trap $\mathbf{d}=(d_x,d_y,d_z)$ was less than 400 nm, $\mathbf{F}_{\mathbf{trap}} = (F_x, F_y, F_z)$ was calculated as $F_x= d_xk_x$, $F_y=d_yk_y$ and $F_z=d_zk_z$ (23). All experiments of force recordings were monitored by video imaging with a CCD camera at a frame rate of 20 Hz. Visual inspection of recorded images allowed to discard from the analysis all

force recordings during which visible debris interfered with the optical determination of the bead position **x**.

Data Analysis

The velocity **v**=(v_x,v_y,v_z) of the bead was obtained by numerical differentiation of its sampled position **x**=(x(n),y(n),z(n)) n=1,…N. Numerical differentiation was computed either by convolution of the position components x(n),y(n) and z(n) with the derivative of a Gaussian filter $1/(\sigma\sqrt{2\pi})$ exp(-t^2/σ^2) (Gaussian filtering) or by Linear regression. In the Linear regression method, the components v_x(n), v_y(n) and v_z(n) of velocity **v** were calculated by a linear least square fit of the equations x(n)= a_x + v_x(n) (i – n)Δt, y(n)= a_y + v_y(n) (i – n)Δt and z(n)= a_z + v_z(n) (i – n)Δt with i = -W,…,W where Δt was the sampling interval. The two parameters a_x and v_x(n) were determined by minimizing the cost function:

$$[v_x, a] = \arg\min_{[v,a]} \left[\sum_{i=n-W}^{n+W} \left(a + v_x (i-n)\Delta t - y(i) \right)^2 \right]$$

and similarly for a_y and v_y(n) and for a_z and v_z(n). The computation of derivatives with the Linear regression method depended on the number of samples W. Fv relationships obtained from the same force measurement sampled at 10 kHz with the Linear regression method with W=2200 (black trace in Fig.3c) and obtained by using a Gaussian filter with a cut-off frequency of 1 Hz (red trace in Fig.3c) had the same number of knots. Similarly, Fv relationships obtained with the Linear regression method with W = 10,000 and by using a Gaussian filter with a cut-off frequency of 0.2 Hz had the same shape. When the number of points, W, considered for Linear regression was increased, it was equivalent to decreasing the band width of the Gaussian filter.

Acknowledgement:

We thank Walter Vanzella (Glance Vision Technologies s.r.l.) for the computational support.

References

1. Fletcher DA, Theriot JA (2004) An introduction to cell motility for the physical scientist. Phys Biol 1:T1-T10

2. Solecki DJ, Govek EE, Hatten ME (2006) mPar6 alpha controls neuronal migration. J Neurosci 26:10624-10625

3. Ghashghaei HT, Lai C, Anton ES (2007) Neuronal migration in the adult brain: are we there yet? Nat Rev Neurosci 8:141-151

4. Bray D, Thomas C, Shaw G (1978) Growth cone formation in cultures of sensory neurons. Proc Natl Acad Sci U S A 75:5226-5229

5. Goodman CS (1996) Mechanisms and molecules that control growth cone guidance. Annu Rev Neurosci 19:341-377

6. Song HJ, Poo MM (2001) The cell biology of neuronal navigation. Nat Cell Biol 3:E81-E88

7. Mongiu AK, Weitzke EL, Chaga OY, Borisy GG (2007) Kinetic-structural analysis of neuronal growth cone veil motility. J Cell Sci 120:1113-1125

8. Mogilner A, Oster G (1996) Cell motility driven by actin polymerization. Biophys J 71:3030-3045

9. Pollard TD, Borisy GG (2003) Cellular motility driven by assembly and disassembly of actin filaments. Cell 112:453-465

10. Pak CW, Flynn KC, Bamburg JR (2008) Actin-binding proteins take the reins in growth cones. Nat Rev Neurosci 9:136-147

11. Howard J (2001) Mechanics of Motor Proteins and the Cytoskeleton. Sinauer Associates, Inc, Sunderland, MA.

12. Raucher D, Sheetz MP (2000) Cell spreading and lamellipodial extension rate is regulated by membrane tension. J Cell Biol 148:127-136

13. Peskin CS, Odell GM, Oster GF (1993) Cellular Motions and Thermal Fluctuations - the Brownian Ratchet. Biophys J 65:316-324

14. Mogilner A, Oster G (2003) Force generation by actin polymerization II: the elastic ratchet and tethered filaments. Biophys J 84:1591-1605

15. Carlsson AE (2003) Growth velocities of branched actin networks. Biophys J 84:2907-2918

16. Dickinson RB, Caro L, Purich DL (2004) Force generation by cytoskeletal filament end-tracking proteins. Biophys J 87:2838-2854

17. Mogilner A (2006) On the edge: modeling protrusion. Curr Opin Cell Biol 18:32-39

18. Carlsson AE (2001) Growth of branched actin networks against obstacles. Biophys J 81:1907-1923

19. Marcy Y, Prost J, Carlier MF, Sykes C (2004) Forces generated during actin-based propulsion: A direct measurement by micromanipulation. Proc Natl Acad Sci U S A 101:5992-5997

20. Parekh SH, Chaudhuri O, Theriot JA, Fletcher DA (2005) Loading history determines the velocity of actin-network growth. Nat Cell Biol 7:1219-1223

21. Prass M, Jacobson K, Mogilner A, Radmacher M (2006) Direct measurement of the lamellipodial protrusive force in a migrating cell. J Cell Biol 174:767-772

22. Bustamante C, Macosko JC, Wuite GJL (2000) Grabbing the cat by the tail: Manipulating molecules one by one. Nat Rev Mol Cell Biol 1:130-136

23. Neuman KC, Block SM (2004) Optical trapping. Rev Sci Instrum 75:2787-2809

24. Cojoc D et al. (2007) Properties of the force exerted by filopodia and lamellipodia and the involvement of cytoskeletal components. PLoS ONE 2(10):e1072. doi:10.1371/journal.pone.0001072

25. Heidemann SR, Lamoureux P, Buxbaum RE (1990) Growth Cone Behavior and Production of Traction Force. J Cell Biol 111:1949-1957

26. Kress H et al. (2007) Filopodia act as phagocytic tentacles and pull with discrete steps and a load-dependent velocity. Proc Natl Acad Sci U S A 104:11633-11638

27. Kress H, Stelzer EHK, Griffiths G, Rohrbach A (2005) Control of relative radiation pressure in optical traps: Application to phagocytic membrane binding studies. Phys Rev E 71:061927-1-061927-10

28. Jensen HJ (1998) Self-Organized Criticality.Cambridge Lecture Notes in Physics. Cambridge University Press.

29. Bertero M, Poggio TA, Torre V (1988) Ill-Posed Problems in Early Vision. Proc IEEE 76:869-889

30. Weiner OD, Marganski WA, Wu LF, Altschuler SJ, Kirschner MW (2007) An actin-based wave generator organizes cell motility. PLoS Biol 5:2053-2063

31. Lacayo CI et al. (2007) Emergence of large-scale cell morphology and movement from local actin filament growth dynamics. PLoS Biol 5:2035-2052

32. Bray D (1992) Cell Movements. Garland Publishing, New York.

33. Atilgan E, Wirtz D, Sun SX (2006) Mechanics and dynamics of actin-driven thin membrane protrusions. Biophys J 90:65-76

34. Gittes F, Schmidt CF (1998) Interference model for back-focal-plane displacement detection in optical tweezers. Opt Lett 23:7-9

4.3
Detection and Characterization of discrete events underlying force generation in lamellipodia of Dorsal Root Ganglia Neurons

Shahapure R., Ercolini E., Amin L., Laio A., Bisson G.& Torre V.

Manuscript in preparation

Detection and Characterization of discrete events underlying force generation in lamellipodia of Dorsal Root Ganglia Neurons

Shahapure R.[1], Ercolini E.[2], Amin L.[1], Laio A.[1], Bisson G.[1]& Torre V.[1,3]

[1]International School for Advanced Studies (SISSA-ISAS), Trieste, Italy. [2] Cluster in Biomedicine (CBM), Area Science Park Basovizza, Trieste, Italy, [3]Italian Institute of Technology, ISAS Unit, Italy.

Corresponding Author:

Vincent Torre

International School for Advanced Studies (SISSA)

Area Science Park, S.S.14, Q1 Building.

Basovizza,

Trieste-34012

ITALY

Phone: +39 040 3756 513

Fax: +39 040 3756 502

Email: torre@sissa.it

Abstract

Force generation in lamellipodia of growth cones is thought to originate by polymerization of actin filaments (1). The progressive addition of actin polymers to the existing network of actin molecules is expected to generate a force on the membrane in the range of 1-20 pN for μm^2 . By using optical tweezers, we have characterized with high temporal resolution and sensitivity the molecular mechanisms by which lamellipodia generate force on encountered obstacles such as silica beads. Because of the presence of adhesion forces, beads in close contact with a lamellipodium can seal on its membrane reducing the amplitude of Brownian fluctuations often by more than 10 times. Under these conditions, when the lamellipodium growths and pushes the bead, fluctuations of bead position increase and discrete jumps varying from about 5 to 50 nm are clearly detected. When the lamellipodium retracts, pulling the beads with it, no discrete events are observed. These discrete events are not observed in the presence of Latrunculin A, a blocker of actin polymerization (2). These jumps could be the elementary events underlying force generation in lamellipodia.

Introduction

The growth of actin filament networks is a fundamental biological process that drives a variety of cellular and intracellular motions (3). In neuronal growth cone lamellipodia, the kinetic force necessary for growth cone motility is a result of the systematic interplay between various processes, such as the actin-based protrusive activity coupled with retrograde actin flow from peripheral to central domain and the attachment of the actin network to both membrane and substrate (5,4). In this study, by using optical tweezers, we have characterized with high temporal resolution and sensitivity the molecular mechanisms by which lamellipodia generate force on optically trapped beads. We observed that the thermal fluctuations of an optically trapped bead were affected when a lamellipodium pushed or pulled the bead. A detailed analysis of this change in noise allowed us to characterize the discrete events underlying force generation in lamellipodia.

Neurons obtained from dorsal root ganglia (DRG) were isolated from P10-P12 rats and plated on poly-L-lysine-coated glass coverslips, positioned on the stage of an inverted microscope used for imaging and measuring forces (see Methods and (6,7)). After 24 to 48 hours of incubation, neurites emerged from the DRG soma and their motion was analysed. Often the leading edge of lamellipodia emerging from the soma of a DRG neuron grew at a speed of 0.1 $\mu m\ sec^{-1}$ and after about one minute lifted up, initiating a three dimensional (3D) shovel like motion, then retracted. In many occasions, during this movement a new lamellipodium protruded underneath. The overall cycle of protrusion, 3D buckling and retraction occurred repeatedly with a period varying from 60 to 150 sec. Lamellipodia not emerging from the soma but originating from growth cones of distal neurites grew and retracted without the large 3D motion observed in lamellipodia emerging from the soma of differentiating DRG neurons.

Results

By using optical tweezers it is possible to record with a temporal resolution in the kHz range the displacement and force exerted by the leading edge of a lamellipodium (6,7). The sensitivity of the recording system is limited by the presence of Brownian fluctuations, which make the detection of forces smaller than 200 fN difficult. In some occasions, however, beads seal onto the lamellipodium, because of the presence of adhesion forces, and Brownian fluctuations almost disappear. Under these conditions it is

possible to record discrete jumps with an amplitude varying from 5 to 100 nm which could be the elementary events underlying force generation in lamellipodia.

Change of noise during push and pull

Silica beads of 1 μm in diameter were trapped with a 1064 nm infrared (IR) optical tweezers in front of lamellipodia of differentiating DRG neurons (Fig.1a). The centre of the bead was positioned at a height of about 700 nm from the coverslip so that the protruding lamellipodium could push it. The position of the bead, $\boldsymbol{x} = (x,y,z)$, was measured with a quadrant position detector (QPD) from which, by knowing the trap stiffness $\boldsymbol{k} = (k_x,k_y,k_z)$, the force exerted on the bead (8,9) $\boldsymbol{F} = (F_x,F_y,F_z)$ is obtained as $\boldsymbol{F} = - \boldsymbol{k} . (\boldsymbol{x} - \boldsymbol{x_{eq}})$, where $\boldsymbol{x_{eq}}$ is the equilibrium position inside the optical trap (9).When the protruding lamellipodium grew, it pushed the bead (Fig.1b and c) displacing it both laterally and axially.

Under these conditions, recordings of bead displacements - and of exerted forces – obtained with the QPD (Fig.1f) exhibited a clear increase of noise on the three components. In contrast, when the lamellipodium retracted (Fig.1d and e) pulling the bead with it, no increase of noise was observed (Fig.1f) and instead a clear reduction of the amplitude of Brownian fluctuations was observed. Under these conditions adhesion forces between the bead and the lamellipodium caused the bead to seal on the membrane leading to a drastic reduction of the amplitude of Brownian fluctuations. Given the presence of these adhesion forces when the lamellipodium retracted it could pull the bead away from the optical trap.

Observed changes of noise could be caused by modifications of the properties of the optical trap following bead displacement from its equilibrium position, fluctuations of adhesion forces between the bead and the neuronal membrane or by the random superposition of elementary events underlying force generation. If the observed increase of noise is caused by the elementary events of force generation, in the presence of drugs interfering with actin polymerization this noise is expected to be altered but it will be the same if it originates from changes of trap properties. When differentiating neurons are treated with 100 nM of the depolymerising agent Latrunculin A, lamellipodia and filopodia stop moving (6).Under these conditions, if the laser beam trapping the bead is moved towards the neuron, the bead can be displaced from its equilibrium position as when it is pushed by a protruding lamellipodium. No significant increase of noise was observed when the bead was displaced by less than 500 nm from the equilibrium position inside the optical trap (Fig.1g). When the bead is lifted up by more than 600 nm, properties of the optical trap and of the sensitivity of the detection system of the bead position change, affecting measured displacements. In

several occasions, the bead could seal onto the membrane of lamellipodia treated with Latrunculin A and Brownian fluctuations drastically decreased but no subsequent increase of noise could be observed. These observations suggest that the increase of noise observed during force generation (Fig.1f) for displacements less than 300 nm, is associated to the dynamics of the actin filaments network and its analysis can reveal properties of elementary events underlying force generation.

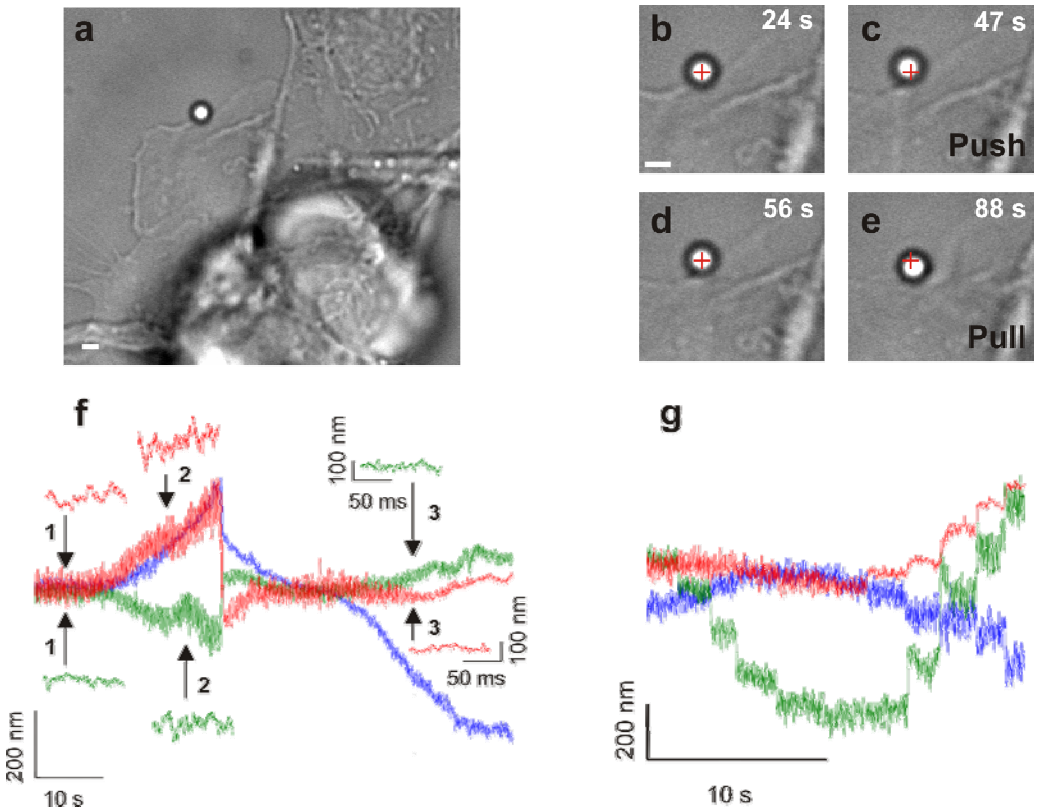

Fig.1. (a) Low resolution image of a lamellipodium protruding from the DRG neuron soma. The bead is trapped in front of the lamellipodium leading edge by an IR laser. Scale bar, 1 µm. **(b-c)** Successive high resolution frames of the lamellipodium during a push. At 24 s the bead is in its equilibrium position in front of the leading edge of the lamellipodium (b). Subsequently, the lamellipodium grows and pushes the bead (47 s) displacing it both laterally and axially (c). The cross indicates the equilibrium position of the optical trap. Scale bar, 1 µm. **(d-e)** Successive high resolution frames of the lamellipodium during a pull. The lamellipodium retracted, pulling the bead back into its equilibrium position (56 s). Then, it continues retracting (88 s) pulling further the bead. The cross indicates the equilibrium position of the optical trap. Scale bar, 1 µm. **(f)** The three components of the bead displacement x (blue), y (green), and z (red). Insets highlight the increase of noise during the push (2), the decrease of noise during pull (3) with respect to the amplitude of the Brownian fluctuations of the trapped bead in the equilibrium position (1) for the axial (red) and one of the lateral components (green). **(g)** The three components of the bead displacement x (blue), y (green), and z (red) recorded while moving the laser beam trapping the bead towards the neuron, after treatment with 100 nM Latrunculin A.

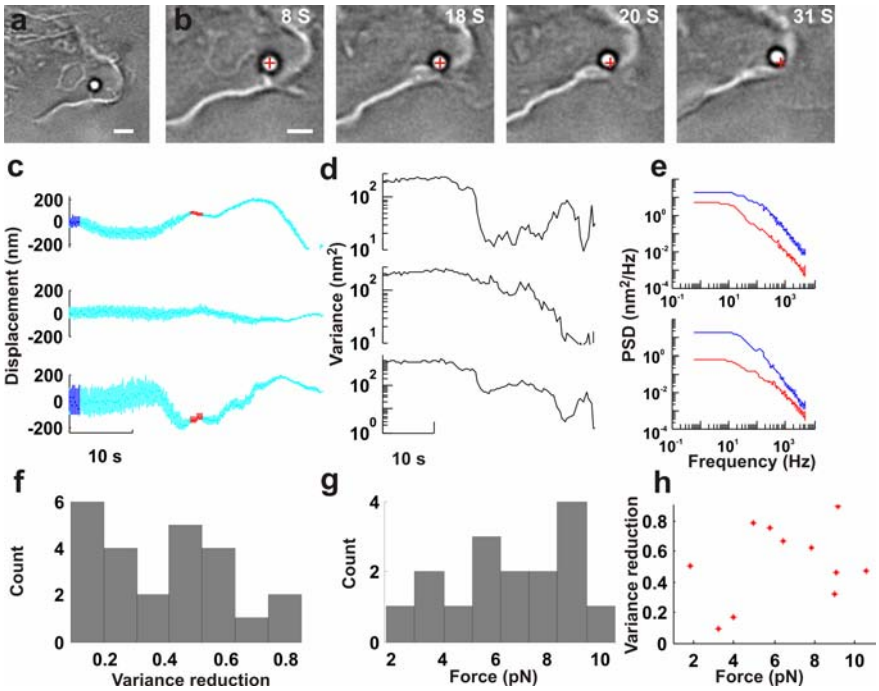

Fig.2. (a) Low resolution image showing the trapped bead sealed on the lamellipodium membrane. Scale bar, 1 μm. **(b)** Four subsequent microimages depicting the lamellipodium while it retracts and pulls the bead which happens to be sealed to the lamellipodium membrane. The cross indicates the equilibrium position of the optical trap. Scale bar, 1 μm. **(c)** From top to bottom: the three components of the bead displacement (x, y, and z respectively) during the pull of the bead performed by the retracting lamellipodium. All the components show a clear reduction of the amplitude of the Brownian fluctuations due to the adhesion of the bead to the membrane of the retracting lamellipodium. Blue and red parts of the traces correspond respectively to Brownian motion and adhesion considered for the analysis of the power spectrum density (PSD) shown in (e). **(d)** Variance of the bead displacement for the three components in (c) vs time. **(e)** Top: power spectrum density (PSD) of the bead displacement during Brownian fluctuations (blue trace) and during adhesion (red trace) for the x component of the bead displacement shown in (c). Bottom: power spectrum density (PSD) of the bead displacement during Brownian fluctuations (blue trace) and during adhesion (red trace) for the z component of the bead displacement shown in (c). **(f)** Histogram of the variance reduction of the Brownian fluctuations during adhesion. **(g)** Histogram of the modulus of the adhesion force $\boldsymbol{F_{ad}}$. **(h)** Relation between the variance reduction of displacement fluctuations and the modulus of the adhesion force.

Adhesion properties

Electrical recordings from single channels (10) provide a major experimental tool for understanding molecular mechanisms underlying electrical signals in neurons. In single channel recordings the recorded noise is reduced when the tip of patch electrodes seals on the membrane patch (10) as a consequence of the development of adhesion forces between the membrane and the electrode glass. When the silica bead seals (Fig.2a) on the membrane and is pulled by the retracting lamellipodium (Fig.2b), the Brownian noise affecting force and displacement recordings is drastically reduced on the three components *x,y* and *z* (Fig.2c). In several experiments, the variance of lateral and axial fluctuations of displacement far

from the lamellipodium was about 200 and 1000 nm^2, respectively, but during adhesion it could decrease by more than 10 times (Fig.2d). In several occasions, the bead was attracted towards the lamellipodium (lower trace in Fig.2c) and its axial position *z* decreases by 100-300 nm (10) and, simultaneously, Brownian fluctuations greatly reduced and often their variance σ_z^2 decreased to less than 5 nm^2 (Fig.2d). The power spectrum density (PSD) of Brownian fluctuations far from the lamellipodium, $S_{FF}(f)$, had a Lorentzian distribution of the type (9):

$$S_{FF}(f) = K_B T / \pi^2 \beta (f_c^2 + f^2) \qquad (1)$$

where K_B, and T are the Boltzmann's constant and the absolute temperature, respectively, β is the hydrodynamic drag coefficient of the bead and f_c is equal to $\kappa/2\pi\beta$, where κ is the trap stiffness. In our experiments f_c varied from 80 to 120 Hz. The PSD of position fluctuations during the establishment of adhesion could be fitted by the same Lorentzian distribution but with a higher value of drag coefficient β (Fig.2e), presumably because of the formation of bonds between the lamellipodium membrane and the bead. The amplitude distribution of Brownian fluctuations in the three coordinates *x*,*y* and *z* during the establishment of adhesion had always a normal distribution with a progressively smaller variance. During adhesion, the variance of Brownian fluctuations could decrease by 20 up to 80 % (Fig.2f). After establishment of adhesion, in many experiments when the lamellipodium retracted it pulled the bead away from the optical trap and the modulus of adhesion force $\boldsymbol{F_{ad}}$ was larger than the maximum trapping force $\boldsymbol{F_{max}}$, which in our experiments varied from 5 to 20 pN. In these circumstances adhesion forces (12,11) - exceeding the maximal trapping force – hold the bead anchored to the lamellipodium (12,14,13). Often, during retraction the bead returned abruptly inside the trap and the maximum measured force provided a good measure of the modulus of $\boldsymbol{F_{ad}}$. Collected values from 16 experiments show that the modulus of $\boldsymbol{F_{ad}}$ varied from just 2 pN to 10 pN (Fig.2g). The analysis of the relation between estimated modulus of $\boldsymbol{F_{ad}}$ and decrease of the standard deviation of displacement fluctuations indicate that larger adhesion forces are associated on average to a larger decrease of noise (Fig.2h).

Increase of noise during push

Often adhesion of the bead reduced drastically the amplitude of Brownian fluctuations so that the standard deviation, σ_z, could be less than 5-10 nm (lower traces Fig.2c) and, in the presence of this reduced noise, when the lamellipodium pushed the bead, a different kind of noise was observed, in which discrete

jumps in displacement and force recordings could be observed. In several experiments, during the establishment of adhesion the amplitude of Brownian fluctuations decreased and when the lamellipodium pushed the bead, the variance of recorded displacements increased (Fig.3a and e). Changes in noise are better analysed when the slow component was removed, leaving unaltered all frequencies above 0.1 Hz (Fig.3b and 3f). The autocorrelation function $\rho_x(t)$, $\rho_y(t)$ and $\rho_z(t)$ of Brownian fluctuations along the three components *x*, *y* and z, measured before adhesion, as expected were delta functions $\delta(t)$ (blue traces in panels of Fig.3c and g). However, the autocorrelation functions during the pushing phase following adhesion, were not anymore delta functions, but exhibited an exponential behaviour $e^{-t/\lambda}$ with a value of λ varying between 10 and 40 msec (red traces in Fig.3c and g). Similarly, the cross-correlation functions $\rho_{x,y}(t)$, $\rho_{x,z}(t)$ and $\rho_{y,z}(t)$ before adhesion were $\delta(t)$ functions, but exhibited a clear cross-correlation when lamellipodia pushed the bead (Fig.3d and h). In these experiments the bead remained within 700 nm from the center of the optical trap, and changes of stiffness and sensitivity were less than 20 % (9) and measured forces were corrected for these changes. This new kind of noise is not observed when growth cones were treated with Latrunculin A (Fig.1g) and is referred as Latrunculin-sensitive noise.

Detection of discrete jumps

Visual inspection of the Latrunculin-sensitive noise shows the presence of discrete jumps with variable amplitude ranging from just 3-5 nm to about 50 nm, corresponding to force jumps varying from some tens of fN to 100-200 fN. These fluctuations were significantly larger than those observed during the initial phase of bead adhesion and were different from Brownian fluctuations observed when the bead was far from the lamellipodium.

Visually observed discrete jumps were detected by appropriate algorithms. Discrete jumps with varying amplitude were detected using well known tools from signal processing.

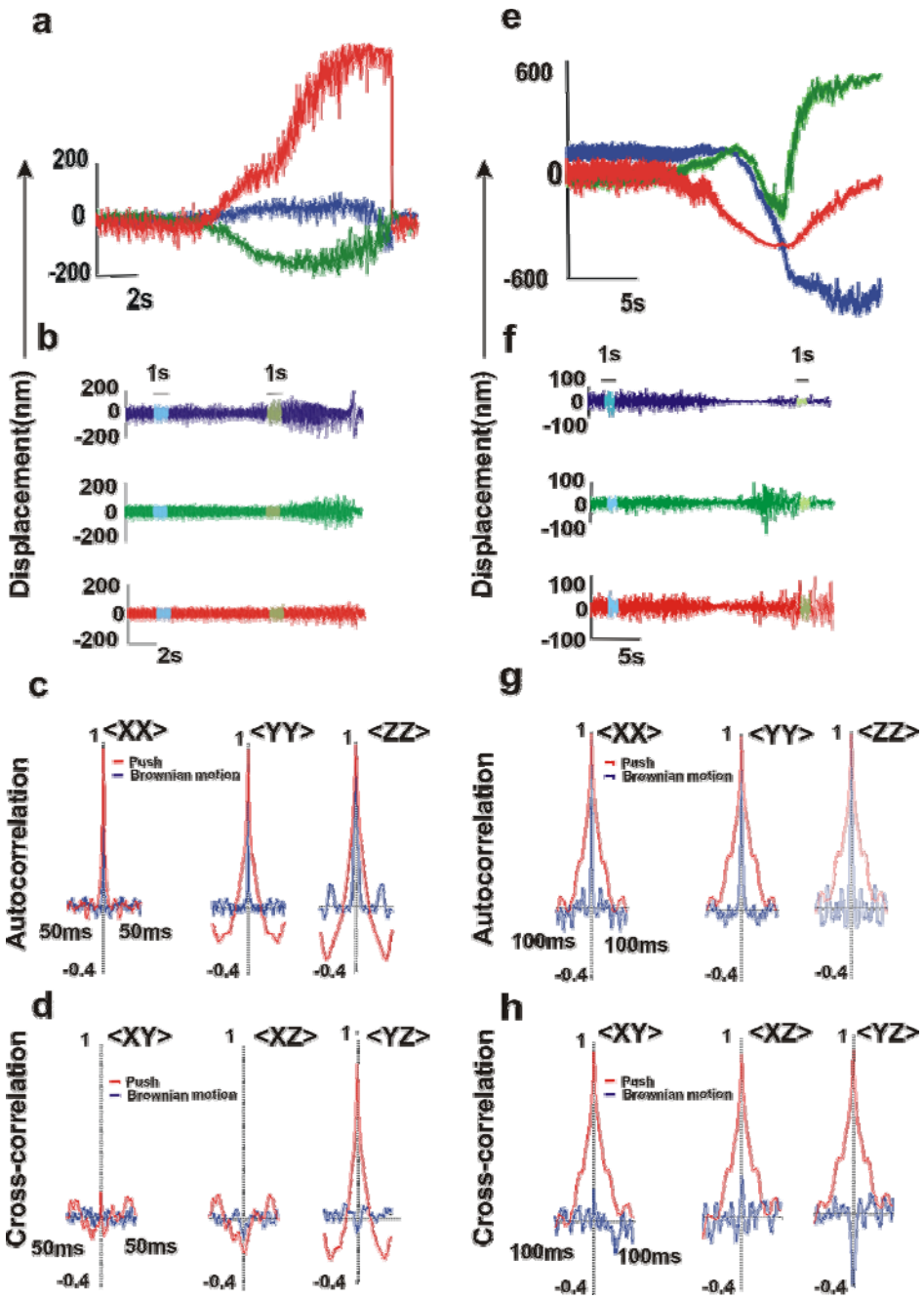

Fig.3. (a) The three components of the bead displacement x (blue), y (green), and z (red) during a mainly vertical push. **(b)** From top to bottom: the three components in (a) after removal of the slow component. The colored parts of each trace were considered for the calculation of the autocorrelation (see panels (c) and (g)) and cross-correlation (see panels (d) and (h)) in the region of Brownian fluctuations (light blue) and push (light green), respectively. **(c)** From left to right: autocorrelation functions $\rho_x(t)=\langle x \cdot x \rangle$, $\rho_y(t)=\langle y \cdot y \rangle$, and $\rho_z(t)=\langle z \cdot z \rangle$, respectively, calculated for Brownian fluctuations (in blue) and push (in red), for the parts of the traces in panel (b) colored in light blue and light green. **(d)** From left to right: cross-correlation functions $\rho_{xy}(t)=\langle x \cdot y \rangle$, $\rho_{xz}(t)=\langle x \cdot z \rangle$, and $\rho_{yz}(t)=\langle y \cdot z \rangle$, respectively, calculated for Brownian fluctuations (in blue) and push (in red), for the parts of the traces in panel (b) colored in light blue and light green. **(e)** The three components of the bead displacement x (blue), y (green), and z (red) during a mainly lateral push. **(f)-(h)** Same as panels (b)-(d) for the displacement in (e).

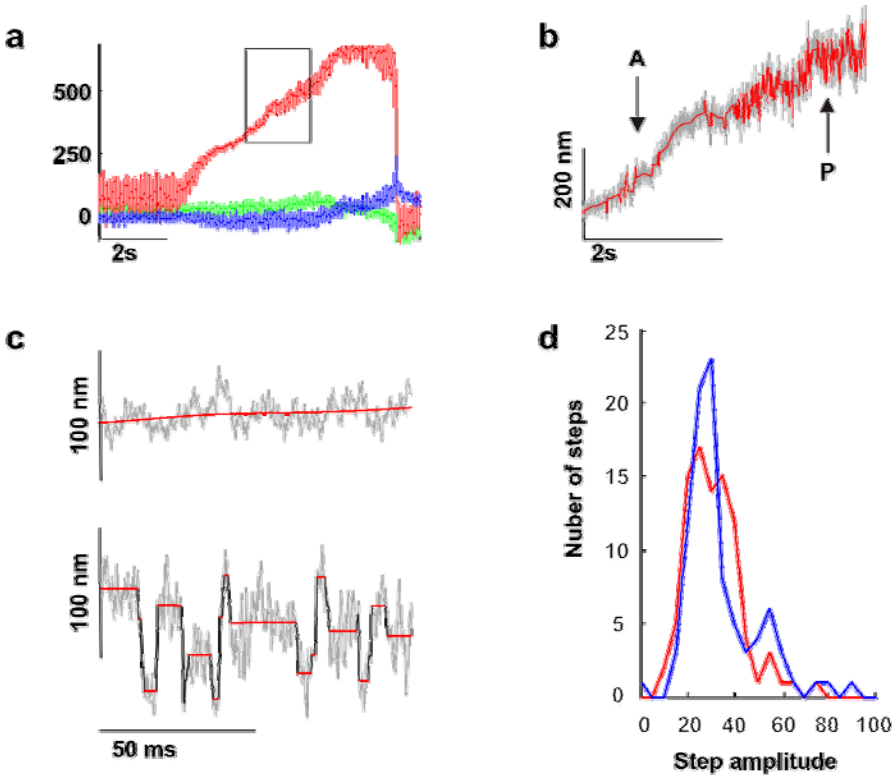

Fig.4. (a) The three components of the bead displacement x (blue), y (green), and z (red). The Latrunculin sensitive noise can be visually detected in the part of the trace contained in the black rectangle. **(b)** The original trace contained in the black rectangle in (a) is here shown in gray with superimposed the regularized trace in red (see text for more details). "A" and "P" stand for "adhesion" and "push", respectively. **(c)** Top: No jumps are detected during the adhesion phase (indicated with "A" in panel (b)). Bottom: jumps detected during the exertion of the force by the lamellipodium leading edge (indicated with "P" in panel (b)) **(d)** Distribution of upward (blue) and downward (red) jumps.

We used a nonlinear diffusion filtering (15) in which two parameters s and γ are used to fix a threshold for the detection of jumps (minimal length detected, 5 nm) and for their bandwidth (up to 5 kHz), described in Supplementary Information 1. This procedure allowed the original data (Fig.4a and grey trace in Fig.4b) to be approximated with a smooth piece-wise function (red trace in Fig.4b) interrupted by discrete jumps or discontinuities. Almost no jumps were detected during the adhesion phase (Fig.4c, upper panel), but jumps became evident only when the exerted force increased (Fig.4c, lower panel). The distributions of upward and downward jumps were very similar (Fig.4d), but more upward jumps were detected.

Shape of the elementary events

We superimposed large discrete events by aligning the steepest portion of the rising phase, so to obtain a representative profile of these jumps. A good fit of the profile of these jumps is obtained with the simple equation $A\ t\ e^{-t/a}$, with a value of a corresponding to 2.5 msec. These observations suggest that force

generation could originate from the superposition of discrete events with a profile similar to $A\ t\ e^{-t/a}$. In order to test this possibility, we developed a procedure (see Supplementary Information 2) to detect events of this shape during recordings of displacement when lamellipodia pushed the bead (Fig.5a).

Many events with this shape were detected (Fig.5b) and indeed entire recordings during pushing could be fitted as the superposition of events of this kind, but with a variable amplitude (A) and time constant (a). The majority of best fit (red curves) is found during the push (Fig.5b and 5c).

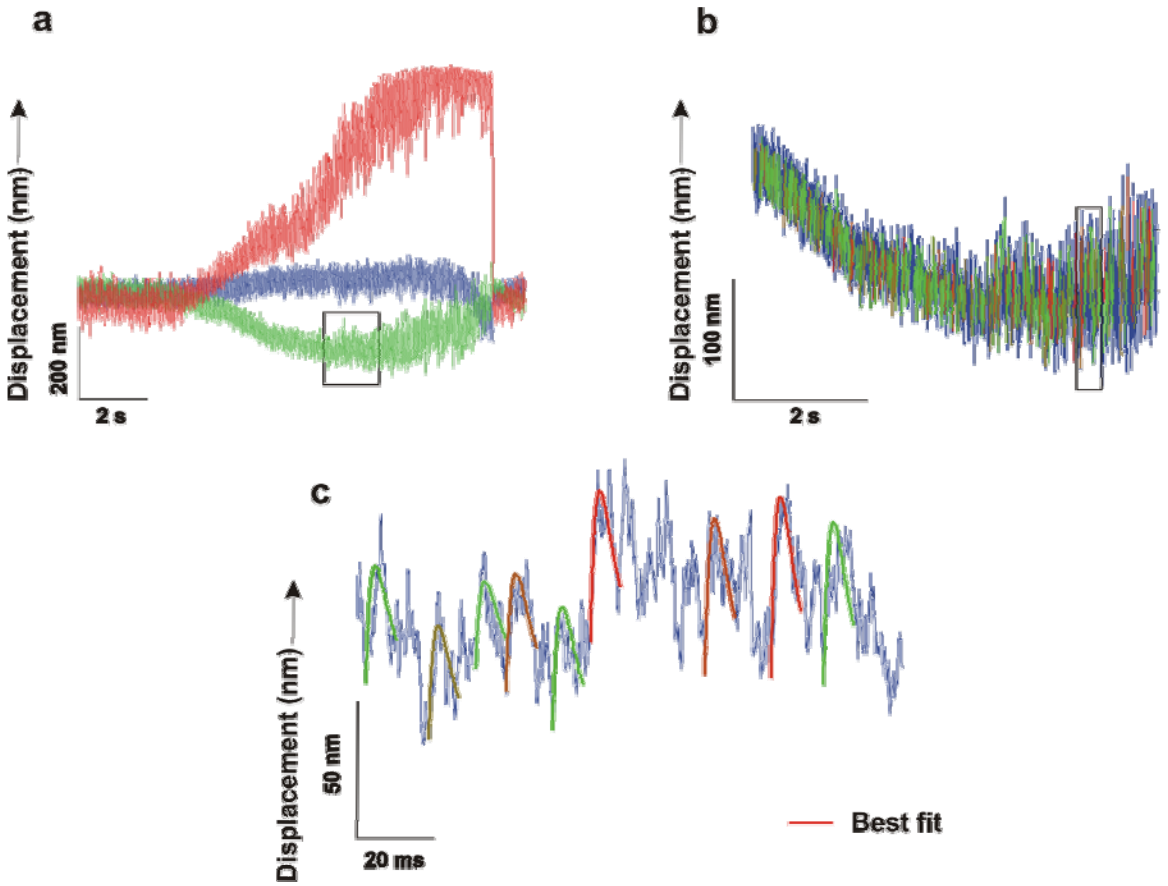

Fig.5. (a) The three components of the bead displacement x (blue), y (green), and z (red) during a push performed by the growing lamellipodium. The black rectangle corresponds to the part of the lateral trace considered in (b). **(b)** The lateral trace delimited by the black rectangle in (a) is here depicted in blue and shown superimposed with the events of the type $A\ t\ e^{-t/a}$. The rectangle indicates the part of the trace which is shown in (c). **(c)** Zoom of the trace in (a) showing the original trace and superimposed the fit to the step with functions of the type $A\ t\ e^{-t/a}$ having different values of the amplitude A. The color of the fitting curve indicates how well the fit approach the original signal. Red curves correspond to best agreement.

Discussion

The present manuscript shows that when a lamellipodium exerts a force on a silica bead confined in an optical trap, measurements of bead position are affected by a noise different from that originating from Brownian fluctuations (Fig.1 and Fig.3). This noise is characterized by the presence of discrete jumps with amplitude varying from 5 to 30 nm (Fig.4), corresponding to forces from 40 to 200 fN and it is not observed when growth cones were treated with 100 nM Latrunculin A. In contrast, when lamellipodia pull away silica beads which have sealed onto the cellular membrane no additional noise is observed (Fig.1 and Fig.2). As a consequence of bead adhesion on the membrane, often the amplitude of Brownian fluctuations decreases by 80 % and if the lamellipodium pushes the bead it is possible to observed putative elementary events (Fig.5) underlying force generation. This experimental procedure is reminiscent to the detection of single channel currents in electrophysiological experiments, when single discrete current are detected after the pipette sealed on the membrane and Brownian noise is consequently decreased (10).

Adhesion forces between a bead and living cells are usually dominated by non specific adhesions caused by electrostatic and Vander Waals forces (12) with an amplitude of less than 40 pN. Stronger forces are produced by the formation of chemical bonds between adhesion molecules such as integrins and the bead, leading to larger forces (12,14,13). By anchoring the bead to the lamellipodium membrane, these forces reduce the Brownian fluctuations of bead (Fig.2) and this fact is likely to be caused by multiple concomitant mechanisms. The establishment of adhesion forces between beads and lamellipodia is a necessary event for pulling.

The increase of noise observed when lamellipodia push the bead is abolished by Latrunculin A and therefore its orgin could be attributed to polymerization and depolymerisation dynamics of the network of actin filaments present at lamellipodia leading edge. Although our results do not establish a causal link between the actin filaments dynamics and the observed noise, it is useful to consider this possibility and evaluate its implication on the notion that actin filaments polymerization is the mechanism underlying force generation at lamellipodia leading edge. Observed discrete jumps have an amplitude from just some nm up to 40-60 nm, with most frequent values around 25-30 nm (Fig.4d). As the dimension of a single actin monomer is 2.7 nm, observed discrete jumps could be caused by a burst of polymerization and/or by the insertion of an actin polymer constituted by some tens of actin molecules. These discrete jumps correspond

to force increases varying from 40 to 200 fN, which could be caused by the elementary motors inside lamellipodia. Prass *et al* 2006 have recently estimated that about 100 active actin filaments impinge on 1 μm of the leading edge of a keratocyte lamellipodium. Abraham et al 1999 have estimated the number of actin filaments in fibroblast lamellipodia to be about 240 in a frontal area of 176 nm x 1 μm. Therefore, the estimated density of actin filaments, possibly constituting the elementary motors impinging on the leading edge of a lamellipodium, is between 100 and 200 per μm^2. If each elementary motor exert a force varying from 40 to 200 fN, the maximal force per μm^2 varies from 4 to 40 pN, in agreement with the maximal force measured by lamellipodia with beads with a diameter of 1 μm (6).

By monitoring filament buckling with fluorescent microscopy, the force exerted by polymerization of single actin filaments was estimated to be in the order of 1 pN (16). Direct measurement with optical tweezers of the force exerted by a bundle of about 8 parallel actin filaments provides an estimate of about 1 pN (17) corresponding to approximately 125 fN per single actin filament. The force exerted by a polymerizing actin filament on a silica bead positioned on the other side of the membrane, as in our experimental conditions, will depend on geometrical and physical properties of the growth cone. This force depends on the incidence angle between the filament and the membrane and it will be maximal when the actin filament will be normal, i.e. at 90 degrees, to the membrane and when actin filaments are not normal to the membrane, the net force will be lower. The force exerted by isolated polymerizing actin filaments is expected to be larger than that observed when actin filaments are in lamellipodia: when actin filaments push on a membrane, the force exerted on an extracellular object, such as a bead, depends on the elastic properties of the membrane. A rigid membrane will damp the protrusion force exerted by polymerizing actin filaments and, therefore, we expect that the transmitted force to be attenuated at some extent. These considerations suggest that the force exerted by single polymerizing actin filaments across the membrane on an external object, such a silica bead used in our experiments, is expected to have a broad range of values not exceeding 125-200 fN, consistently with the distribution of forces measured during detected jumps.

The analysis of the shape of detected discrete events suggests a profile of the elementary push of the type $A\ t\ e^{-t/a}$, consistent with a sudden jump followed by two low pass stages with a time constant in the msec range. As the cellular membrane is expected to dump any sudden protrusion from the cytoplasmic side, one of these time constants could be indeed caused by the membrane.

Conclusions and perspectives

The present manuscript shows that force generation in DRG lamellipodia is characterized by the presence of discrete jumps occurring in a millisecond window with amplitude varying from some nm up to 60 nm, corresponding to forces from 40 to 200 fN. These sudden jumps have a stereotyped shape approximately similar to $A\ t\ e^{-t/a}$ with a in the millisecond range. These jumps could be the putative elementary events underlying force generation. Future work will consist in performing a statistical analysis of these jumps, and in treating the differentiating neurons with drugs that will change the membrane rigidity/fluidity, in order to explore changes in the characteristics of the jumps and of their shape. Moreover, we envisage the study of theoretical mechanisms for the generation of elementary events with a certain shape.

Supplementary Information 1

Non linear diffusion filtering In order to detect discrete jumps (discontinuities), an algorithm based on the theory of anisotropic diffusion (a branch of non linear diffusion filtering) (15) was implemented. After selection of the part of the trace of interest, the original signal was smoothed in order to obtain a smooth piece-wise trace where the discrete jumps were enhanced. The discrete jump detection was an iterative process which rested on the choice of two parameters: the contrast λ, related to the detection sensitivity, i.e. the minimal jump amplitude detected (5 nm in our case), and the scale τ, which sets the amplitude of the temporal window where the steps were searched (in our case, 10 ms).

Supplementary Information 2

Shape of the elementary events The study of the shape of the putative elementary events was performed by using a custom made algorithm (Matlab 7.0.1, http://www.mathworks.com). This algorithm spans the whole signal of the bead displacement, searching for events having the shape $f(t)=A\ t\ e^{-t/a}$, with a variable amplitude A, time constant a equal to 2.5 msec, within a time window of 10 ms. The curves which best fit the original signal are chosen among those which minimize the distance between the curve and the original data, taking into account a similarity threshold which is set by the user.

Methods

Rats (P10−12) were anaesthetised with CO_2 and sacrificed by decapitation in accordance with the Italian Animal Welfare Act. DRGs were incubated with trypsin (0.5 mg/ml), collagenase (1 mg/ml), and

DNase (0.1 mg/ml) in 5 ml Neurobasal medium in a shaking bath (37 °C, 35-40 minutes). DRGs were mechanically dissociated, centrifuged at 300 rpm, resuspended in culture medium and plated on poly-L-lysine-coated (0.5 ug/ml) coverslips. Cells were incubated for 24 to 48 hours followed by the addition of nerve growth factor (50 ng/ml; Alomone, Israel) before the measurements.

The optical tweezers setup was built as previously described (6). The dish containing the differentiating neurons and the beads (PSI-1.0NH2, G.Kisker GbR, Steinfurt Germany) was placed on the microscope stage which could be moved by a 3 axis piezoelectric nanocube (17 MAX 301, Melles Griot Inc., USA). The temperature of the dish was kept at 37^{o}C by a Peltier device. Bead position was determined in the x,y and z plane with an accuracy of 10 nm using back focal plane (BFP) detection, which relies on the interference between forward scattered light from the bead and unscattered light (9,18). The BFP of the condenser was imaged onto a QPD and the light was converted to differential outputs digitized at 10 kHz and low pass filtered at 5 kHz. Both the lateral and axial trap stiffness, $\boldsymbol{\kappa}_{x,y}=(k_x,k_y)$ and k_z, respectively, as well as the detector sensitivity were calibrated using the power spectrum method (9)with voltage signals filtered and digitized at 5 and 20 kHz respectively. The force exerted by the neurite $\mathbf{F_{neu}}$ was taken as equal to $\mathbf{-F_{trap}}$. When the bead displacement of the bead from its equilibrium position inside the trap was less than 400 nm, $\boldsymbol{F_{trap}} = (F_x, F_y, F_z)$ was calculated as $F_x= k_x d_x$, $F_y=k_y d_y$, and $F_z=k_z d_z$, respectively (9).

Acknowledgements We thank Walter Vanzella (Glance Vision Technologies s.r.l.) for computational support. Correspondence and requests for materials should be addressed to Vincent Torre (torre@sissa.it).

References

1. Pollard TD, Borisy GG (2003) Cellular motility driven by assembly and disassembly of actin filaments. *Cell* 112:453-465

2. Dent EW, Kalil K (2001) Axon branching requires interactions between dynamic microtubules and actin filaments. *Journal of Neuroscience* 21:9757-9769

3. Howard J (2001) Mechanics of Motor Proteins and the Cytoskeleton.

4. Lin CH, Thompson CA, Forscher P (1994) Cytoskeletal reorganization underlying growth cone motility. *Curr.Opin.Neurobiol.* 4:640-647

5. Suter DM, Forscher P (2000) Substrate-cytoskeletal coupling as a mechanism for the regulation of growth cone motility and guidance. *J.Neurobiol.* 44:97-113

6. Cojoc D et al. (2007) Properties of the force exerted by filopodia and lamellipodia and the involvement of cytoskeletal components. *PLoS ONE* 2:e1072-

7. Shahapure R. et al. (2009) Force generation in lamellipodia is a probabilistic process with fast growth and retraction events. *submitted*

8. Kress H, Stelzer EH, Griffiths G, Rohrbach A (2005) Control of relative radiation pressure in optical traps: application to phagocytic membrane binding studies. *Phys.Rev.E.Stat.Nonlin.Soft.Matter Phys.* 71:061927-

9. Neuman KC, Block SM (2004) Optical trapping. *Rev Sci Instrum* 75:2787-2809

10. Neher E, Sakmann B (1976) Single-channel currents recorded from membrane of denervated frog muscle fibres. *Nature* 260:799-802

11. Safran SA, Gov N, Nicolas A, Schwarz US, Tlusty T (2005) Physics of cell elasticity, shape and adhesion. *Physica A-Statistical Mechanics and Its Applications* 352:171-201

12. Knoner G et al. (2006) Mechanics of cellular adhesion to artificial artery templates. *Biophysical Journal* 91:3085-3096

13. Simpson KH, Bowden G, Hook M, Anvari B (2003) Measurement of adhesive forces between individual Staphylococcus aureus MSCRAMMs and protein-coated surfaces by use of optical tweezers. *J.Bacteriol.* 185:2031-2035

14. Jass J et al. (2004) Physical properties of Escherichia coli P pili measured by optical tweezers. *Biophysical Journal* 87:4271-4283

15. J.WEICKERT (2001) Applications of nonlinear diffusion in image processing and computer vision. *ACTA MATHEMATICA UNIVERSITATIS COMENIANAE* 70:33-50

16. Kovar DR, Pollard TD (2004) Insertional assembly of actin filament barbed ends in association with formins produces piconewton forces. *Proc Natl Acad Sci U S A* 101:14725-14730

17. Footer MJ, Kerssemakers JWJ, Theriot JA, Dogterom M (2007) Direct measurement of force generation by actin filament polymerization using an optical trap. *Proc Natl Acad Sci U S A* 104:2181-2186

18. Gittes F, Schmidt CF (1998) Interference model for back-focal-plane displacement detection in optical tweezers. *Opt.Lett.* 23:7-9

5. Discussion and conclusions

With sequencing the complete genome, we are starting to have an exhaustive picture of all the proteins present in an organism, yet in many cases we still have little understanding of how these proteins function. Irrespective of cell type, all biochemical processes where the cytoskeleton plays an important role involve understanding forces and motion, questions for which *in vivo* optical traps are ideal tools (Gross, 2003). The main outcome of my thesis is the development of an experimental system for force measurements in living cells under appropriate physiological conditions in both lateral as well as axial direction. We developed high temporal resolution (10 KHz) and force sensitivity (1 pN), optical tweezers setup to perform accurate measurements on living neurons without causing any photodamage. To the best of our knowledge this thesis presents the first quantitative determination of force exerted by filopodia and lamellipodia of neuronal growth cone during neuronal differentiation (Cojoc et al., 2007).

The advancing growth cone is undoubtedly subjected to a rich chemical environment in the developing nervous system, different molecular cues guiding growth cone to the proper target but there is a growing evidence that mechanical signal also plays important role in growth cone guidance (Anava et al., 2009;Heidemann and Buxbaum, 1994;Heidemann et al., 1995). Quantitative characterization of the force exerted by lamellipodia and filopodia during neuronal differentiation could help to elucidate how neurons sense the environment and process mechanical information. The maximum force exerted by filopodia during their exploratory motion (lateral collision) was 2 pN and during growth (protrusion) 3 pN. The diameter of filopodia tips is approximately 100 nm, i.e. 10 times smaller than the diameter of the beads we used, therefore the maximal force measured for filopodia is expected to be a reliable upper limit of the force exerted by these structures. Its amplitude is of the same order as that measured during *in vitro* actin filament (Kovar and Pollard, 2004;Footer et al., 2007) and microtubule growth (Kerssemakers et al., 2006), this similarity with *in vitro* measurement implies that filopodial protrusion is minimally counterbalanced by the membrane surrounding actin bundles and microtubules (occasional), indicating that the membrane at the filopodia tips has a low stiffness (Dai and Sheetz, 1995;Kwik et al., 2003;Liu and Fletcher, 2006) Filopodia appeared to modulate their mechanical response by sensing the mechanical properties of the environment. The duration of the collision was decreased when filopodia encountered a stiffer obstacle.

Lamellipodia exerted a force of up to 20 pN and possibly more, which could increase in discrete steps of approximately 0.2 pN. The measured forces were smaller than forces involved in cellular traction force or measured in migrating keratocytes (Marcy et al., 2004). Maximum force reported here, may not fully represent the ability that lamellipodia have because, at least in some cases, only a fraction of the forces exerted is picked up by the beads, as the contact area between bead and lamellipodium leading edge changes dynamically. The contact area between pushing lamellipodia and beads was determined by the analysis of video images of the event under examination and was observed to vary from 0.25 to 1.57 μm^2 (Shahapure R. et al., 2009). Indeed, we expect lamellipodia to exert larger forces, possibly up to hundreds of pN, as in migrating epithelial cells (du Roure et al., 2005). Therefore, the maximal pressure exerted by DRG lamellipodia was 20-80 pN μm^{-2}. The maximum power per unit area exerted by lamellipodia was estimated to be $1\text{-}4\times10^{-16}$ W μm^{-2}. The hydrolysis of one molecule of ATP provides energy of about 10-19 J (Bray, 1992) and, if this energy is converted into work with an efficiency of 60%, the hydrolysis of about $0.25\text{-}1\times104$ s^{-1} of ATP per μm^2 is necessary to produce the measured power. The number of actin filaments in keratocyte and fibroblast lamellipodia has been estimated to be of the order of 100 per μm^2 (Prass et al., 2006).Therefore, the number of elementary motors per μm^2 is likely to be of the order of 100, where each elementary motor consumes approximately 25 to 100 ATP per second.

Inhibition of myosin II and microtubule polymerization blocked lamellipodia motion and drastically reduced the force produced by growth cones, while filopodia continued to move and were able to exert forces in the pN range (Cojoc et al., 2007). In contrast, with the blockade of actin polymerization, filopodia and lamellipodia produced no measurable forces. Thus, in the absence of actin polymerization, growth cones cannot exert any force, and microtubule polymerization is necessary for development of forces exceeding 3 pN at the leading edge of filopodia and lamellipodia. Therefore, actin filaments and microtubules cooperate and interact in a complex way so as to generate a wide range of forces.

We provided an experimental characterization of Fv relationships in neuronal growth cones with millisecond resolution. We found that force generation in lamellipodia is an intrinsically multi-scale process. At a temporal resolution of 3-5 s, the exerted force can increase, maintaining a constant velocity, where the Fv relationships are almost flat (Shahapure R. et al., 2009). At a millisecond resolution, a much more complex behavior is observed, with random occurrence of fast growths and sub-second retractions (Shahapure R. et al., 2009). Our results show that autocatalytic models of force generation (Carlsson, 2003;Carlsson, 2001;Mogilner, 2006)are correct in a mean

approximation. At a higher temporal resolution the network of actin filaments evolves in a much more complex manner that can be characterized only probabilistically. Fast forward motions consuming up to 10^4 molecules of ATP s^{-1} μm^{-2} alternate with local catastrophes, whose duration has a power law distribution. These results provide a precise characterization of the dynamics of force generation in lamellipodia, necessary to understand the biochemical events underlying force generation. Occurrence of local catastrophes seems the most likely biological mechanisms underlying local transient retractions such as proteins controlling the network of actin filaments, e.g. cofilin, could randomly sever a large branch of actin (Pollard and Borisy, 2003) or transient increase in rate of retrograde actin flow over protrusion rate at leading edge (Lin and Forscher, 1995) causing a transient retraction of lamellipodium leading edge. It is possible that instability could originate also from interactions with the cellular membrane. Growing and branching of the actin filaments can also be instable because of the action of membrane tension. Indeed, the maximum measured force F_{max} is approximately 20-100 $pN/\mu m^2$, of the same order of the force exerted by a membrane with a surface tension γ equal to 0.005 k_BT/nm^2 axially deformed by 1 μm (Atilgan et al., 2006). The actin filament network is confronted with a membrane exerting a force similar to F_{max}, so that the actin filament network is only marginally stable and its propulsive force is almost counterbalanced by the membrane tension. Growing and retracting in conditions of marginal stability allows fast reactions and could provide lamellipodia the flexibility necessary for their physiological functions.

A detailed analysis of fluctuations in biochemical processes can provide insights into the underlying kinetics beyond what can be inferred from studies of average rates alone (Shaevitz et al., 2005). Thermal fluctuations of optically trapped bead were affected when lamellipodia pushed the bead, producing different type of noise other than Brownian motion. This noise is characterized by the presence of discrete jumps with amplitude varying from 5 to 50 nm, corresponding to forces from 40 to 200 fN and it is not observed when growth cones were treated with 100 nM Latrunculin A. In contrast, when lamellipodia pulled away silica beads which have sealed onto the cellular membrane no additional noise was observed. As a consequence of bead adhesion on the membrane, often the amplitude of Brownian fluctuations decreases by 80 % and, when the lamellipodium pushes the bead it is possible to observed putative elementary events underlying force generation. This experimental procedure is reminiscent to the detection of single channel currents in electrophysiological experiments, when single discrete current are detected after the pipette sealed on the membrane and Brownian noise is consequently decreased (Neher and Sakmann, 1976) .

In future it will be interesting to perform detailed statistical analysis of these jumps, and by pharmacologically altering membrane rigidity, explore changes in the characteristics of these jumps and their shape. With respect to the physiological significance it would be important to examine the growth cones subject to different adhesion substrates or extracellular factors that can either accelerate or inhibit growth cone motility. Furthermore, it would be extremely interesting if the beads are coated with certain guidance molecules and examine the mechanic responses.

References

1. Anava,S., A.Greenbaum, E.Ben Jacob, Y.Hanein, and A.Ayali. 2009. The regulative role of neurite mechanical tension in network development. *Biophys. J.* 96:1661-1670.

2. Atilgan,E., D.Wirtz, and S.X.Sun. 2006. Mechanics and dynamics of actin-driven thin membrane protrusions. *Biophys J* 90:65-76.

3. Bray,D. 1992. Cell Movements. Garland Publishing, New York.

4. Carlsson,A.E. 2001. Growth of branched actin networks against obstacles. *Biophys J* 81:1907-1923.

5. Carlsson,A.E. 2003. Growth velocities of branched actin networks. *Biophysical Journal* 84:2907-2918.

6. Cojoc,D., F.Difato, E.Ferrari, R.B.Shahapure, J.Laishram, M.Righi, E.M.Di Fabrizio, and V.Torre. 2007. Properties of the force exerted by filopodia and lamellipodia and the involvement of cytoskeletal components. *PLoS ONE* 2:e1072.

7. Dai,J. and M.P.Sheetz. 1995. Mechanical properties of neuronal growth cone membranes studied by tether formation with laser optical tweezers. *Biophys. J.* 68:988-996.

8. du Roure,O., A.Saez, A.Buguin, R.H.Austin, P.Chavrier, P.Siberzan, and B.Ladoux. 2005. Force mapping in epithelial cell migration. *Proceedings of the National Academy of Sciences of the United States of America* 102:2390-2395.

9. Footer,M.J., J.W.Kerssemakers, J.A.Theriot, and M.Dogterom. 2007. Direct measurement of force generation by actin filament polymerization using an optical trap. *Proc. Natl. Acad. Sci. U. S. A* 104:2181-2186.

10. Gross,S.P. 2003. Application of optical traps in vivo. *Biophotonics, Pt B* 361:162-174.

11. Heidemann,S.R. and R.E.Buxbaum. 1994. Mechanical tension as a regulator of axonal development. *Neurotoxicology* 15:95-107.

12. Heidemann,S.R., P.Lamoureux, and R.E.Buxbaum. 1995. Cytomechanics of axonal development. *Cell Biochem. Biophys.* 27:135-155.

13. Kerssemakers,J.W., E.L.Munteanu, L.Laan, T.L.Noetzel, M.E.Janson, and M.Dogterom. 2006. Assembly dynamics of microtubules at molecular resolution. *Nature* 442:709-712.

14. Kovar,D.R. and T.D.Pollard. 2004. Insertional assembly of actin filament barbed ends in association with formins produces piconewton forces. *Proc. Natl. Acad. Sci. U. S. A* 101:14725-14730.

15. Kwik,J., S.Boyle, D.Fooksman, L.Margolis, M.P.Sheetz, and M.Edidin. 2003. Membrane cholesterol, lateral mobility, and the phosphatidylinositol 4,5-bisphosphate-dependent organization of cell actin. *Proc. Natl. Acad. Sci. U. S. A* 100:13964-13969.

16. Lin,C.H. and P.Forscher. 1995. Growth Cone Advance Is Inversely Proportional to Retrograde F-Actin Flow. *Neuron* 14:763-771.

17. Liu,A.P. and D.A.Fletcher. 2006. Actin polymerization serves as a membrane domain switch in model lipid bilayers. *Biophysical Journal* 91:4064-4070.

18. Marcy,Y., J.Prost, M.F.Carlier, and C.Sykes. 2004. Forces generated during actin-based propulsion: A direct measurement by micromanipulation. *Proceedings of the National Academy of Sciences of the United States of America* 101:5992-5997.

19. Mogilner,A. 2006. On the edge: modeling protrusion. *Curr Opin Cell Biol* 18:32-39.

20. Neher,E. and B.Sakmann. 1976. Single-channel currents recorded from membrane of denervated frog muscle fibres. *Nature* 260:799-802.

21. Pollard,T.D. and G.G.Borisy. 2003. Cellular motility driven by assembly and disassembly of actin filaments. *Cell* 112:453-465.

22. Prass,M., K.Jacobson, A.Mogilner, and M.Radmacher. 2006. Direct measurement of the lamellipodial protrusive force in a migrating cell. *Journal of Cell Biology* 174:767-772.

23. Shaevitz,J.W., S.M.Block, and M.J.Schnitzer. 2005. Statistical kinetics of macromolecular dynamics. *Biophys. J.* 89:2277-2285.

24. Shahapure R., Difato F., Laio A., Cojoc D., Ferrari E., Laishram J., Bisson G., and Torre V. 2009. Force generation in lamellipodia is a probabilistic process with fast growth and retraction events. *submitted*.

6. Acknowledgements

I would like to express my deep and sincere gratitude to my supervisor, Prof Vincent Torre, who greatly supported me during this entire period of my PhD. I thank him for all the hours of valuable discussion, his never ending patience and indulgence. He has taught me the right attitude towards science.

I am deeply grateful to Francesco Difato without whose support it was impossible to accomplish this work. I am deeply indebted to Dr. Dan Cojoc, and Enrico Ferrari for their collaboration and for introducing me to this new technique of optical tweezers.

I wish to express my sincere thanks to my current experimental team members Erika Ercolini and Ladan Amin. I would like to specially acknowledge Erika for critical reading of my thesis and for her comments and suggestions to improve it.

My special gratitude to Jummi, who was always there to support me for carrying out experiments, whenever I was in need.

I would like to give special thanks to Giacomo, Shripad and Walter, who brought *kuch jada hi* MatLab in my poor Biologist's life.

I would like to acknowledge Dr Allesandro Laio, for his valuabale suggestions for the data analysis presented in this work and Massimo Righi for teaching me to prepare DRG neuron cell culture.

I would like to thank Daniela for answering my queries related to biological part of this project and teaching me immunohistochemistry.

I would like to thank all my lab mates Fredric (western Guru whose filopod-ish hand would appear on my side of the desk from his side), Paolo (coolest man), Diana (logical lady), Anil (the complete man), Jelena, Giulietta, Elisabetta and Monica who were directly or indirectly helped me during four years of my stay in the lab. I would like to remember Jacobo, Valentina, Arin & Lin for their silent encouragement.

My sincere thanks to Manuela, who was always ready to assist me whenever I needed her.

It gives me great pleasure to acknowledge Vikas, Fauzia, and Shyju, who supported and encouraged me in the final stage of my PhD.

I owe my loving thanks to my family whose patience and love enabled me to complete this work. They have lost a lot due to my research far from home. Without their encouragement and understanding it would have been impossible for me to finish this work. Last but not the least, I would like to thank the most important person in my life, Cecilia, who is always there for me.